NOAA Technical Memorandum ERL ETL-287

# EVALUATION OF THE CAPABILITY OF THE EXPERIMENTAL OCEANOGRAPHIC FISHERIES LIDAR (FLOE) FOR TUNA DETECTION IN THE EASTERN TROPICAL PACIFIC

J.H. Churnside
J.J. Wilson
C.W. Oliver

Environmental Technology Laboratory
Boulder, Colorado
March 1998

noaa NATIONAL OCEANIC AND ATMOSPHERIC ADMINISTRATION / Environmental Research Laboratories

NOAA Technical Memorandum ERL ETL-287

# EVALUATION OF THE CAPABILITY OF THE EXPERIMENTAL OCEANOGRAPHIC FISHERIES LIDAR (FLOE) FOR TUNA DETECTION IN THE EASTERN TROPICAL PACIFIC

James H. Churnside
James J. Wilson

Environmental Technology Laboratory

Charles W. Oliver

LaJolla Laboratory, NOAA National Marine Fisheries Service

Environmental Technology Laboratory
Boulder, Colorado
March 1998

**UNITED STATES DEPARTMENT OF COMMERCE**

**William M. Daley**
**Secretary**

NATIONAL OCEANIC AND ATMOSPHERIC ADMINISTRATION

D. JAMES BAKER
Under Secretary for Oceans and Atmosphere/Administrator

Environmental Research Laboratories

James L. Rasmussen
Director

## NOTICE



For sale by the National Technical Information Service, 5285 Port Royal Road
Springfield, VA 22061

# Contents

## Explanatory Note

This report is one in a series on the potential for technology applications to enhance efficiency in commercial fisheries, reduce the catch of non-targeted species, and provide new tools for fishery assessments in support of the NMFS strategic goals to build sustainable fisheries and recover protected species. A report synthesizing the results of this series of studies is planned. We hope the distribution of this report will facilitate further discussion and research into the application's potential usefulness, but should not be construed as an endorsement of the application by NMFS.

Pursuant to changes in the Marine Mammal Protection Act in 1988, the NMFS' SWFSC began another series of ETP-related studies in 1990, focused on developing and evaluating methods of capturing yellowfin tuna which do not involve dolphins. This series of studies has been conducted within the SWFSC's Dolphin-Safe Research Program. Studies on the potential use of airborne lidar (LIght Detection And Ranging) systems began in 1991, and studies on low-frequency acoustic systems to detect fish schools at ranges much greater than currently possible were initiated during 1995. In addition to their use as an alternative to fishing on dolphins, these systems have potential to increase the efficiency of the fishing operations by locating fish schools not detectable by customary visual means, and as a fishery-independent tool to conduct population assessments on pelagic fish. They also have potential to adversely impact marine animals.

The Dolphin-Safe Research Program is investigating, through a series of contracts and grants, five airborne lidars: 1) the NMFS-developed "Osprey" lidar (Oliver et al. 1994), 2) the Kaman Aerospace Corporation's FISHEYE imaging lidar (Oliver and Edwards 1996), 3) **the NOAA Environmental Technology Laboratory's Experimental Oceanographic Fisheries Lidar (Churnside et al. 1998)**, 4) the Arete Associates 3D Streak-Tube Imaging Lidar, and 5) the Detection Limited's lidar . An initial study on the potential effects of airborne lidars on marine mammals will be completed during 1998 (Zorn et al. 1998).

The Dolphin-Safe Research Program has completed, through a series of contracts and grants, acoustic system studies on 1) the acoustic target strength of large yellowfin tuna schools (Nero 1996), 2) acoustic detection parameters and potential in the eastern tropical Pacific Ocean (Rees 1996), 3) the design of two towed acoustic systems (Rees 1998, Denny et al. 1998) and, 4) the potential effects of low-frequency sound on marine mammals (Ketten 1998). Studies are in progress to measure swimbladder volumes from large yellowfin tuna and to determine experimentally the effects of blast and acoustic trauma on marine mammals. During 1998, the SWFSC plans to measure the acoustic sound field produced by tuna seiners (and possibly a research vessel) and to obtain direct measurements of the acoustic target strength of tuna schools.

Chuck Oliver
Dolphin-Safe Research Program
Southwest Fisheries Science Center
P.O. Box 271
La Jolla, California 92037

Dolphin-Safe Research Program Detection Technology Reports


**Churnside, J.H., J.J. Wilson, and C.W. Oliver. 1998. Evaluation of the capability of the experimental oceanographic fisheries lidar (FLOE) for tuna detection in the eastern tropical Pacific. Environmental Technology Laboratory, Boulder, CO.**

Denny, G.F., K.E. deVilleroy, and P.K. Simpson. 1998. Long-range tuna school detection sonar system design specification. Grant (NA77FD0044) report. Scientific Fishery Systems, Inc., Anchorage, AK., 38 p.

Ketten, D. 1998. Marine mammal auditory systems: a summary of audiometric and anatomical data and its implications for underwater acoustic impacts. Contract (40JBNF600312) report. Harvard Medical School, Boston, MA., 97 p.

Nero, R. W. 1996. Model estimates of acoustic scattering from schools of large yellowfin tuna. Contract (40ABNF510351) report NRL/MR/774-95-7708. Naval Research Lab. Stennis Space Center, MS. 21p

Oliver, C., W. Armstrong, and J. Young 1994. "Development of an airborne LIDAR system to detect tunas in the eastern tropical Pacific purse-seine fishery" NOAA-TM-NMFS-SWFSC-204. 65 p.

Oliver, C.W. and Edwards, E.F. 1996. Dolphin-Safe Research Program Progress Report II (1992-1996). Southwest Fisheries Science Center Admin. Rpt. LJ-96-13. 91p.

Rees, C. D. 1996. Modeling of acoustic detection of yellowfin tuna in the eastern tropical Pacific fishery area. Contract (40ABNF510351) report. NCCOSC Code 541, San Diego, CA. 83p plus appendices.

Rees, C. D. 1998. Active towed-array acoustic system design study for yellowfin tuna in the eastern tropical Pacific fishery area. Contract (43ABNF61572) report. NCCOSC Code 541, San Diego, CA. 58p plus appendices

Zorn, H.M., J.H. Churnside, and C.W. Oliver. 1998 (in review). Laser safety thresholds for cetaceans and pinnipeds. Environmental Technology Laboratory, Boulder, CO.

# Evaluation of the Capability of the Experimental Oceanographic Fisheries Lidar (FLOE) for Tuna Detection in the Eastern Tropical Pacific

James H. Churnside
James J. Wilson
NOAA Environmental Technology Laboratory
325 Broadway
Boulder, CO  80303

Charles W. Oliver
La Jolla Laboratory, SWFSC
National Marine Fisheries Service, NOAA
P.O. Box 271
La Jolla, California 92038-0271

Abstract A simple computer model is used to investigate the capability of a lidar to detect tuna in the eastern tropical Pacific. The lidar is similar to the Experimental Oceanographic Fisheries Lidar (FLOE) system developed by the National Oceanographic and Atmospheric Administration. It is an inexpensive device using commercially available components. The model predicts a detection depth of 40 m for the specified system under typical conditions and a maximum detection depth of 60 m under ideal conditions. The effects of changes in the lidar design and of changes in conditions are described in a series of figures of signal-to-noise ratio (SNR) and maximum detection depth $z_{max}$. For the various cases, peak irradiance values are compared with the recommended maximum irradiance on the human eye.

## 1. Introduction

The National Oceanic and Atmospheric Administration (NOAA) is currently developing an Experimental Oceanographic Fisheries Lidar (FLOE) through a cooperative program of the Environmental Technology Laboratory and the Southwest Fisheries Science Center. This report presents the results of a study into the capabilities of this lidar or a modified version of this lidar for detection of yellowfin tuna in the tropical eastern Pacific. Currently, the tuna fishing fleet finds fish by a combination of techniques that include visual observations from helicopters and exploitation of the association of tuna with dolphins. The objective is to determine how effectively an inexpensive lidar on the helicopters would increase the direct detection capabilities to the point where ensnaring dolphins would no longer be necessary. Tuna detection by a similar lidar, the Osprey system, has been demonstrated (Grams and Wyman, 1993; Oliver, et al., 1994).

Section 2 describes the operating characteristics of the FLOE. The device was designed to be inexpensive and to operate on small aircraft. Thus, the cost of reproducing this lidar would be under \$100K. The weight is under 100 kg, and the power consumption is less than 1 kW. It has been operated on a four-passenger Cessna 177 and on a six-passenger Partenavia Observer. This system has been used to detect sardines in the Southern California Bight (Churnside, et al., 1997).

Section 3 describes the model that was used in the calculations. It is a relatively simple model that was written with a commercial spreadsheet program (Quattro Pro). Despite its simplicity, we feel that this model works fairly well based on comparisons with actual measurements. The simplifying assumptions that were used to develop the model are described in Section 3. One of the biggest areas of uncertainty lies in the physical characteristics of the fish school that was modeled. More research is needed on the cumulative contributions of fish size, fish reflectivity, fish distribution with depth, the number of fish in a school, and the packing density of the school to the sensitivity of sensors.

The results of the model calculations are presented in Section 4. Three types of results were calculated. The first is a calculation of the signal-to-noise ratio of the lidar return as a function of depth.  The second type is a calculation of the maximum detectable depth of a school of fish for various combinations of lidar, water, and fish parameters.  The last is a calculation of the maximum irradiance as a function of depth for various lidar and water parameters.

A description of the QuattroPro spreadsheet program "FiLM" is included as an appendix. Formulas, parameter values, and both numeric and graphical results are described along with instructions on how to change values to investigate other configurations.

## 2. FLOE

FLOE is a very simple lidar system with no scanning or imaging capabilities.  The laser is a frequency-doubled, Q-switched Nd:YAG laser, linearly polarized parallel to the plane of incidence.  A negative lens in front of the laser increases the beam divergence.  The laser is mounted beside the receiver telescope, and the diverged beam is directed by one mirror to a second mirror in the center of the front of the telescope.  This mirror is used to direct the beam to the water so that it is coaxial with the receiver.

The receiver consists of a lens that collects the scattered light onto a photomultiplier tube detector.  An interference filter is placed in front of the detector to limit interference from background light.  A rotatable polarizer in front of the receiver is used to control the polarization of the return signal to be co-polarized, cross-polarized, or un-polarized with the transmitted light. The detector output is passed through a logarithmic amplifier, and this signal is digitized and stored in the computer.  The lidar parameters are presented in Table 1.

## 3. Lidar Model

The lidar model was developed to perform engineering tradeoffs quickly and easily.  For this reason, it uses a standard commercial spreadsheet (Quattro Pro).  Input parameters and lidar components can be changed quickly, and the program automatically calculates all of the affected quantities.  Plots can be quickly generated within the program to allow the results to be immediately viewed.  The lidar system was assumed to be similar to the NOAA FLOE.

Three water types characteristic of the eastern tropical Pacific were used.  These are the Jerlov types I, IA, and IB.  These specify only the diffuse attenuation coefficient $K_D$.  To get an estimate of lidar attenuation, we need to have an estimate of the volume scattering function $\beta(\theta)$, where $\theta$ is the scattering angle. We will use the general functional form of Petzhold, with the exact values scaled by the value of the scattering coefficient inferred from the different values for $K_D$. We first note that

$$K_D = a + 2\pi b \int_{\frac{\pi}{2}}^{\pi} \frac{\beta(\Theta)}{b} \sin(\Theta) d\Theta, \tag{1}$$

where $a$ is the absorption coefficient of sea water, $b$ is the scattering coefficient, and $\beta(\theta)/b$ is the normalized scattering function of Petzhold. From this expression, we obtain the scattering coefficient for each of the Jerlov water types. The beam attenuation coefficient is given by

$$c = a + b. \tag{2}$$

The lidar attenuation coefficient lies somewhere in between the diffuse attenuation coefficient and the beam attenuation coefficient in a way that depends on the beam divergence of the lidar and on the spot size at the surface. The details of this dependence are not completely understood, and we will make what we hope are reasonable estimates. Following Feigels and Kopilevich (1994), we estimate the divergence angle effect for a beam of negligible size by assuming that photons scattered at angles greater than the lidar divergence angle $\phi/2$ are lost. We then apply a correction to this value for the finite size of the spot at the surface based on a curve fit to the results of Gordon (1982). The final result is an estimate for the lidar attenuation coefficient given by

$$\alpha = K_D + 2\pi b \exp(-0.8 c \phi h) \int_{\frac{\phi}{2}}^{\frac{\pi}{2}} \frac{\beta(\Theta)}{b} \sin(\Theta) d\Theta, \tag{3}$$

where $h$ is the height of the lidar above the surface.

To completely define the fish and the fish schools would require a large number of parameters. To investigate the effects of variations in each of these parameters would take much more time than was available. For this reason, we will define typical values for most of them, and vary only those that seem to have the most effect on lidar performance. The characteristics of the individual fish will not be varied. Yellowfin tuna were modeled as 100-cm long, 10 cm wide, and 20 cm deep, with a mass of 20 kg. Their average reflectivity and depolarization are assumed, for lack of any hard data, to be similar to those of sardines — 13% and 30%, respectively.

Our generic school of tuna is assumed to be 16.5 tons of fish (~750 fish). It is 10 m thick and located at a depth of 50 m. The nominal packing density is 0.125 fish per cubic meter, which is about 2-body length spacing. The school depth, thickness, and packing density were varied. The diameter of the school was adjusted for the packing density to maintain a constant school mass of 16.5 tons. Thus, in some cases, the school diameter is larger than the beam diameter, and, in others, it is smaller.

**a. Signal-to-Noise Ratio**

The signal and noise levels can be defined at any one of a number of points in the receiver, including optical power on the detector, current out of the detector, the voltage generated by that current through a standard 50 Ω resistance, the output of the log-amplifier, or the integer value that this produces when digitized. We will consistently use the voltage across 50 Ω, which is the input voltage to the log-amplifier. For an infinitesimally short laser pulse, this signal varies in time as the pulse propagates through the water. We can relate this time to the depth at which the light was scattered back to the receiver since we know the speed at which light travels through water. Therefore, we can write the signal as a function of depth as:

$$S'(z) = \frac{P(z)\pi d^2 R\beta(z)}{4(z+nh)^2}\exp(-2\alpha z), \qquad \textbf{(4)}$$

where $S'$ is the received signal per unit depth at depth $z$, $P$ is the laser power, $R$ is the responsivity of the detector and load in V/W, $\beta(z)$ is the backscatter coefficient of the water plus any fish present at that depth, $h$ is the height of the lidar above the surface, $n$ is the index of refraction of water (1.33), and $\alpha$ is the lidar attenuation coefficient.

To get the actual signal voltage, we must integrate Eq. (4) over the finite duration of the laser pulse. To get the short pulses desired, it is necessary to use Q-switching. In this technique, the laser resonator is blocked electro-optically while the energy is stored in the lasing medium. The cavity is then quickly opened. Lasing begins rapidly, and the output power quickly builds to a high value. As the energy in the lasing medium is depleted, the output power decreases back to zero. This technique produces a characteristic pulse shape that can be approximated by

$$P(t) = \frac{Et}{\tau^2}\exp\left(-\frac{t}{\tau}\right), \qquad (5)$$

where $E$ is the total pulse energy, and $\tau$ is 0.408 times the full width of the pulse at one half of its maximum value. We convert this time to distance through the speed of light, and integrate Eq. (4) over depth.

These equations suggest several ways in which the signal from a particular depth might be increased. One can increase the laser energy, the telescope diameter, or the detector responsivity. One can decrease the height of the platform above the surface. One can also decrease the attenuation either by finding clearer water or by moving to a laser wavelength with less absorption (blue instead of green). However, because of the technology involved, using laser wavelengths with less attenuation than the one we have chosen is difficult. Available lasers in the blue tend to be much more expensive, larger, less efficient, and less reliable. A great deal of research has been done for the US Navy on laser development, but a commercially viable solution has yet to be found. One promising candidate for a blue laser is being developed at the University of Arizona. This laser is being marketed at a price of about $100K, or about four times the cost of a green laser of similar capability. The attenuation also depends to a certain extent on both the size of the laser spot on the surface and on the divergence of the lidar; for large spots with large divergence, the attenuation is minimized.

Noise in the signal causes fluctuations that can be mistaken for fish. Several sources are present, although one of these will usually dominate the performance for any particular set of conditions. The most fundamental source of noise is the so-called “shot noise” caused by the quantum fluctuations in the light field reaching the detector. To this is added receiver noise that is caused by thermal fluctuations within the receiver electronics. Finally, background light (e.g., scattered sunlight) can add to the fluctuations. The average value of the background is not directly a noise source, because we can measure this value and subtract it from our measured signal. However, random fluctuations of this background are a direct source of noise. These fluctuations arise because of the random motions of the surface under the influence of the wind. The final noise source is caused by the variability of the optical properties of the water with depth.

These noise components are affected differently by the different parameters that affect the signal level. An increase in the laser energy increases the shot noise, but only as the square root of the energy, so there is a net gain in SNR. It does not affect the receiver noise or the background noise at all. An increase in the telescope diameter affects the shot noise in the same way as an increase in energy — as the square root of the increase in received energy — so there is a gain in SNR. An increase in telescope diameter does not affect receiver noise, so the SNR can increase dramatically. It affects the background noise in the same way that it affects the signal so there is no gain in SNR by increasing the telescope diameter in a background-limited situation. An increase in detector responsivity affects both shot noise and background noise in the same way as it affects the signal, so there is no gain in SNR. It may or may not affect receiver noise, depending on the exact source of the noise.

Decreasing the height of the platform increases the shot noise as the square root of the increase in received energy. It does not affect receiver noise or background noise at all. Decreasing the absorption coefficient can have a number of effects, depending on how it is accomplished. If it is accomplished by finding cleaner water or moving to a blue wavelength, the effect is the same as an increase in laser energy or a decrease in operating height. If it is accomplished by increasing the divergence of the lidar, it will not affect shot noise or receiver noise. It will, however, lead to an increase in the background noise. Variability in the water column is not affected by changes in any of the above parameters. Numerical model results of these various tradeoffs are presented in Section 4.

While it would appear that SNR can be increased to any desired value by increasing laser power, telescope diameter, etc., there are practical limitations. The amount of light that can be collected is limited by the capabilities of the detector, typically a photomultiplier tube. Trying to extract too much signal current from the detector will result in detector damage. Even before the damage threshold is reached, the output will not be linear, making detection difficult. To avoid damage to the detector, we will set the detector supply voltage so that in the standard lidar configuration the peak current output of the detector is 0.5 of its maximum.

**b. Maximum Depth Penetration**

We can rewrite the signal level of a lidar system as

$$S(z) = S_0 \frac{\beta_w(z) + \beta_f(z)}{\beta_0} \exp(-2\alpha z), \tag{6}$$

where $S_0$ is the signal level at the surface, $\beta_w$ is the clear-water backscatter coefficient, $\beta_f$ is the backscatter coefficient of a school of fish, and $\beta_0$ is the backscatter coefficient at the surface, where it is assumed that there are no fish. The backscatter coefficients, $\beta$, have units of $m^{-1}$ and represent the fraction of the energy that would be scattered upward by a 1-m layer of either clear water or fish. By clear water, we mean natural seawater with its attendant load of yellow substance, plankton, silt, etc., but without fish. The lidar attenuation coefficient is related to the absorption and scattering coefficients of the water in a way that is not completely understood, but that depends on the field of view of the lidar. A very narrowly collimated system will have an attenuation that is very close to the sum of the absorption and scattering. A wide field of view collects multiple, scattered photons, and the attenuation is closer to the absorption coefficient.

As we have described, the noise in a lidar system can come from several different processes, one of which is likely to predominate in any particular set of circumstances. The thermal noise in the receiver is an additive noise that is independent of signal level. It is Gaussian with zero mean. The shot noise from the sum of the signal current, background-light-generated current, and detector dark current is a Poisson process that depends on the total detector current. However, except for very low illumination levels, the Poisson distribution is nearly Gaussian, and we will make this approximation. Also, we note that if the signal from the fish school is very large, the detection probability is nearly unity, and accurate modeling of the noise distribution is not critical. If the fish signal is small, the shot-noise variance will be very nearly the same whether fish are present or not. This is the situation that must be treated accurately, and so we can assume that shot noise can be approximated by a signal-independent, additive Gaussian process for the purposes of this paper.

Background fluctuations are related to variations in the slope of the surface, which has been shown to be nearly Gaussian. We can therefore assume that the optical fluctuations themselves will be very nearly Gaussian. The final noise source is caused by variations of the optical properties of the water with depth. Variations that are slow compared with the depth resolution of the lidar can be estimated and eliminated. However, more rapid fluctuations will be indistinguishable from noise. In the absence of a better model for these fluctuations, we will also assume that they are Gaussian. Thus, an additive, signal-independent Gaussian noise will be considered, and the source of this noise will not be considered further.

The probability-density function of the instantaneous signal can therefore by approximated by

$$p(s) = \frac{1}{\sqrt{2\pi}N}\exp\left[-\frac{(s-S)^2}{2N^2}\right], \qquad (7)$$

where $s$ is the instantaneous signal at some depth and $N$ is the noise variance. For illustration, we will assume that $N$ is not depth dependent, although $S$ clearly is.

Detection is accomplished by setting a threshold signal level above which we will assert that fish are present. The detection probability is the probability that the instantaneous signal is above this threshold when fish are present (i.e., when $\beta_f > 0$). Thus,

$$P(DETECTION) = \int_T^\infty \frac{1}{\sqrt{2\pi}N}\exp\left[-\frac{(s-S_f)^2}{2N^2}\right]ds, \qquad (8)$$

where $T$ is the threshold level and $S_f$ is the signal level with fish present. Specifying that fish are present whenever the received signal exceeds some threshold value entails some probability of a "false alarm." This probability can be calculated from

$$P(FALSE\ ALARM) = \int_T^\infty \frac{1}{\sqrt{2\pi}N}\exp\left[-\frac{(s-S_w)^2}{2N^2}\right]ds, \qquad (9)$$

where $S_w$ is the signal from clear water.

To reduce the number of free parameters, we can normalize everything by the noise level. Thus, we define a signal-to-noise ratio, $SNR = (S_f - S_w)/N$ and a threshold-to-noise ratio $TNR = (T - S_w)/N$. Then,

$$P(FALSE\ ALARM) = \int_{TNR}^\infty \frac{1}{\sqrt{2\pi}}\exp\left[-\frac{1}{2}s^2\right]ds \qquad (10)$$

and

$$P(DETECTION) = \int_{TNR}^{\infty} \frac{1}{\sqrt{2\pi}} \exp\left[-\frac{1}{2}(s - SNR)^2\right] ds. \qquad \textbf{(11)}$$

The performance of this system depends on both the *SNR* and the *TNR*. One convenient way to summarize the performance is to fix an acceptable false alarm rate, use that to determine the threshold level, and then calculate the detection probability. The results of such a calculation are presented in Figure 1, which is a plot of detection probability as a function of false alarm probability for signal-to-noise ratios of 1 and 3. The two limits of the plot correspond to a very high threshold and to a very low threshold. In the first instance, we never determine that fish are present, and P(false alarm) and P(detection) are both zero. In the second, we always say that fish are present, and P(false alarm) and P(detection) are both unity.

It is also instructive to select an allowable false-alarm rate and a signal-to-noise ratio at the surface, and calculate the detection probability as a function of depth. This was done for a false-alarm probability of 1% and a lidar attenuation coefficient of 0.1 $m^{-1}$, and the results are plotted in Figure 2 for several values of the surface signal-to-noise ratio. There are several interesting features of these results. The first is that the detection probability goes quickly from nearly unity to nearly zero when some depth is reached. Because of this sharp transition, we can define as maximum detection depth $z_{max}$ as the depth at which the detection probability is 0.5. This depth depends logarithmically on signal level because of the exponential attenuation of the signal with depth. Thus, an order-of-magnitude increase in signal level provides an increase of just over 10 m in depth. This is just about 1 lidar attenuation depth, defined as $\alpha^{-1}$. If the attenuation coefficient is different from the value used here, these depth values scale linearly with lidar attenuation depth.

The sensitivity to the false-alarm rate was investigated by calculating the maximum detection depth as a function of the selected false-alarm probability for the same values of the surface signal-to-noise ratio. The results are presented in Figure 3. We note that there is only a slight dependence on false-alarm rate. This implies that we can select a fairly low rate of false alarms for a system without degrading the detection performance seriously. It also implies that we can select a nominal threshold level and obtain a simple expression for the maximum detection depth. A value of *TNR* = 3 results in a false-alarm probability of just above 0.1%. Using this value, we can calculate that

$$z_{max} \approx -\frac{1}{2\alpha}\ln\left(\frac{3}{SNR_0}\right). \tag{12}$$

The detection probability can be approximated by unity for depths above this value and zero for depths below it.

Because of the interference with the surface, it is difficult to actually calculate $SNR_0$. Instead, we note that

$$SNR_0 = SNR_z \exp(2\alpha z), \tag{13}$$

where z is any arbitrary depth, and $SNR_z$ is the signal-to-noise ratio at that depth. The calculations were actually done with a fish school deep enough that the surface effects did not contribute.

### c. Peak Irradiance

The peak irradiance at any depth can be estimated by dividing the power reaching that depth by the area of the beam at that depth. The simplest expression is

$$I_p(z) = \frac{P_p \exp(-\alpha z)}{\pi\left[\frac{\gamma(h + z/n)}{2}\right]^2}, \tag{14}$$

where $P_p$ is the peak transmitted laser power and $\gamma$ is the lidar divergence. This expression does not take into account the additional spreading of the beam because of multiple forward scattering of light. Because of this, it is higher than the actual value at large depths, and overestimates the ocular hazard by an amount that is a complicated function of the water parameters.

Eq. (11) uses a simplified model of the initial irradiance distribution. The assumption is that the total laser power is uniformly distributed within a circular area defined by the laser beam divergence times the distance from the laser. The laser actually produces a Gaussian irradiance distribution, where the reported beam divergence angle is the point where the irradiance has dropped to exp(-2) of its peak value. It is straightforward to show that the peak power for the actual Gaussian beam is twice the average power calculated assuming a uniform distribution. Therefore, we will use the higher value in the peak irradiance calculations.

**d. Eye Safety**

The laser is a pulsed laser and delivers most of its energy in about 10 ns. If a laser transmits 0.067 joules of energy in 10 ns, that corresponds to a peak power of 67 MW. The laser transmits a Gaussian shaped intensity pattern, and it can be shown that the center of the beam has the highest intensity and that intensity is twice the peak power. So for eye safety calculations we use twice the peak power. As the beam propagates away from the laser it diverges and covers an area that can be calculated in $m^2$. We divide the peak power by the area of the beam and get power density ($W/m^2$).

The maximum recommended exposure for this type of laser (i.e., short pulses in the green region of the spectrum) is about 300 $kW/m^2$. This level is noted in the plots as “Eye Safe”. For this type of laser, the light is focused by the lens of the eye onto the retina, where damage occurs at higher light levels.

The mechanism for laser eye damage depends on the pulse length and the wavelength; for the range of pulse lengths and wavelengths considered here, it is a thermo-acoustic mechanism that only depends on the optical irradiance on the retina. This is not true for much longer pulses where thermal dissipation becomes important and the size of the spot on the retina is also important. The worst possible case is where all of the laser light incident on the pupil of the eye is collected into a spot determined by the resolution limit of the eye. In this case, the irradiance on the retina is

$$I_{retina} = \frac{I_{pupil} D_{pupil}^2}{(\alpha_{res} f)^2}, \tag{15}$$

where $D_{pupil}$ is the diameter of the pupil, $\alpha_{res}$ is the angular resolution of the eye, and $f$ is the focal distance. The maximum diameter of the pupil will be about 1/3 of the diameter of the eye for humans or for cetaceans. The focal distance is about the same as the diameter. Thus, we have the approximate formula

$$I_{retina} = 0.1 \frac{I_{pupil}}{\alpha_{res}^2} \tag{16}$$

for either humans or cetaceans. Although it varies from individual to individual, the angular resolution of the human eye is generally accepted to be about 1 minute of arc, or about 0.3 mrad. Measured values of angular resolution for cetaceans are poorer than this (Mobley 1990), with typical values of 1.60 to 1.80 mrad. From this, we conclude that acceptable irradiance levels for cetaceans are 30 to 40 times that for humans. Clearly, the maximum recommended exposure limits for humans are also safe for cetaceans.

## 4. Results

The general philosophy in performing the calculations was to define a baseline system that is very similar to the current FLOE. The actual baseline parameters are presented in Table 2. Parameters were varied from this baseline value, and three calculations were made. These were SNR, maximum detectable depth, $z_{max}$, and peak irradiance as described in Section 3.

Figures 4 through 17 are plots of SNR vs depth with various lidar parameters. Figures 18 through 27 are plots of maximum detectable depth, $z_{max}$ vs various lidar parameters and Figures 28 through 32 are plots of laser power density vs depth for different lidar parameters. Note also that all of the "bumps" that occur at 50 m depth are due to a fish school being there.

**a. Signal-to-Noise Ratio**

The signal-to-noise ratio of the lidar return for the various cases is plotted as a function of depth in Figures 4 through 17. Unless explicitly stated, all parameter values are the baseline case from Table 2. The curves in these plots are very similar to the actual signals that would be received with two important differences. First, the received signal will not be so smooth; it will include random fluctuations because of noise processes. Second, it will not decrease indefinitely with depth; it will decrease to the background level and remain constant thereafter.

**b. Maximum Detectable Depth $z_{max}$**

here are 10 graphs (Figures 18-27) that show $z_{max}$ as a function of other lidar parameters. $z_{max}$ is the maximum depth of detection of fish. We see that detection to a depth of about 40 m is generally possible. Under unfavorable conditions this can decrease to about 30 m, and under favorable conditions it can increase to as deep as 60 m.

**c. Peak Power Density**.

Figures 28 through 32 are peak power density vs depth plots for various water and lidar parameters. Note that almost all cases are eye safe for humans, even at the surface.

## 5. Conclusions

We have presented a standard fish detection lidar system that will detect our modeled, 16.5-ton school (~750 fish) of yellowfin tuna down to a maximum depth of about 40 m. Because the maximum area of the laser beam is only 32% of the area occupied by our modeled fish school, detection to 40 meters is actually predicted for smaller schools (~250 fish). Conversely, if a fish school contains more fish or, is packed greater than 2 body lengths or, is at shallower depth or, in clearer water or, is more reflective, then detention is also predicted. For lack of better information we assumed that the reflectivity and depolarization of tuna were same as sardines (13% and 30%, respectively). This may or may not be a valid assumption. More work must be done to improve our knowledge of the reflection and depolarization characteristics of fish. The lidar system has many places where it could be improved as technology gets better. For instance, a 446 nm wavelength laser looks like it could give general improvement in $z_{max}$ and a variable gain detector that could handle the surface reflection and have sufficient gain for detecting the deep fish signal would be a real improvement. A logarithmic amplifier that matches the large dynamic range of the detector would also help extend the fish detection depth. Automatic receiver FOV adjustment for best SNR for the current background light conditions would also be an improvement.

## References


Oliver, C.W., W.A. Armstrong, and J.A. Young (1994), Development of an Airborne Lidar System to Detect Tunas in the Eastern Tropical Pacific Purse-Seine Fishery, NOAA Tech. Memo. NOAA-TM-NMFS-SWFSC-204, 67 p.

Churnside, J.H., V.V. Tatarskii, and J.J. Wilson (1997), "Lidar Profiles of Fish Schools," Appl. Opt. 36, 6011-6020.

Feigels, V.I. and Yu.I. Kopilevich (1994), "Applicability of Lidar Remote Sensing Methods for Vertical Structure Investigation of Ocean Optical Properties Distribution," in *Ocean Optics XII*, Jules Jaffe, Editor, Proc. SPIE 2258, 413-421.

Gordon, H.R. (1982), "Interpretation of Airborne Oceanic Lidar: Effects of Multiple Scattering," Appl. Opt. 21, 2996-3001.

Grams, G.W. and C.M. Wyman (1993), Extended Field Tests of an Airborne Lidar During Tuna Purse-Seine Fishing Operations in the Eastern Tropical Pacific Ocean, Final Report, NOAA Purchase Order No. 41ABNF2-01797, 252 p.

Mobley, J.R. and D.A. Helweg (1990), "Visual ecology and cognition in cetacean", In: Sensory Abilities of Cetaceans. (Eds: Thomas, J and R. Kastelein) Plenum Press, New York, 519-536.

Table 1. FLOE Lidar Transmitter and Receiver Parameters.

| Parameter | Value |
|---|---|
| Transmitter | |
| Wavelength | 532 nm (green) |
| Pulse length | 15 nsec |
| Pulse energy | 67 mJ |
| Pulse repetition rate | 10 Hz |
| Beam divergence | 43 mrad |
| Receiver | |
| Aperture diameter | 17 cm |
| Focal length | 37 cm |
| Field of view | 26 mrad |
| Optical bandwidth | 10 nm |
| Electronic bandwidth | 100 MHz |
| Sample rate | 1 GHz |

Table 2. Baseline Model Parameters.

| Parameter | Baseline Value | Variations |
|---|---|---|
| Transmitter | | |
| Wavelength | 532 nm | 446 nm, 588 nm |
| Pulse length | 15 nsec | |
| Pulse energy | 100 mJ | 20 mJ, 500 mJ |
| Pulse repetition rate | 10 Hz | |
| Height above surface | 300 m | 100 m |
| Beam divergence | 25 mrad | 10 mrad, 50 mrad, 100 mrad |
| Receiver | | |
| Aperture diameter | 20 cm | 5 cm, 50 cm |
| Field of view | same as transmitter divergence | |
| Optical bandwidth | 10 nm | |
| Electronic bandwidth | 100 MHZ | |
| Sample rate | 1 GHz | |
| Receiver Noise | 140 microvolts | 100 microvolts, 200 microvolts |
| Detector Type | R5800 | R647, MCP (MicroChannel plate) |
| Polarization | Un-Pol | Co-pol, Cross-Pol |
| Water Column | | |
| Water Type | IA | I, IB |
| Background light | 1/4 moon | full sun, full dark |
| Background Light Fluctuations | 2 percent | 0.5 percent, 1 percent, 5 percent |
| Fish School | | |
| Fish Type | Yellowfin Tuna | |
| School Size | 16.5 tons | |
| Packing Density | 0.125 $m^{-3}$ | 0.008, 1 $m^{-3}$ |
| School Depth | 50 m | 10 m, 100 m |
| School Thickness | 10 m | 5 m, 20 m |
| School Reflectivity | 13% | |
| School Depolarization | 30% | |

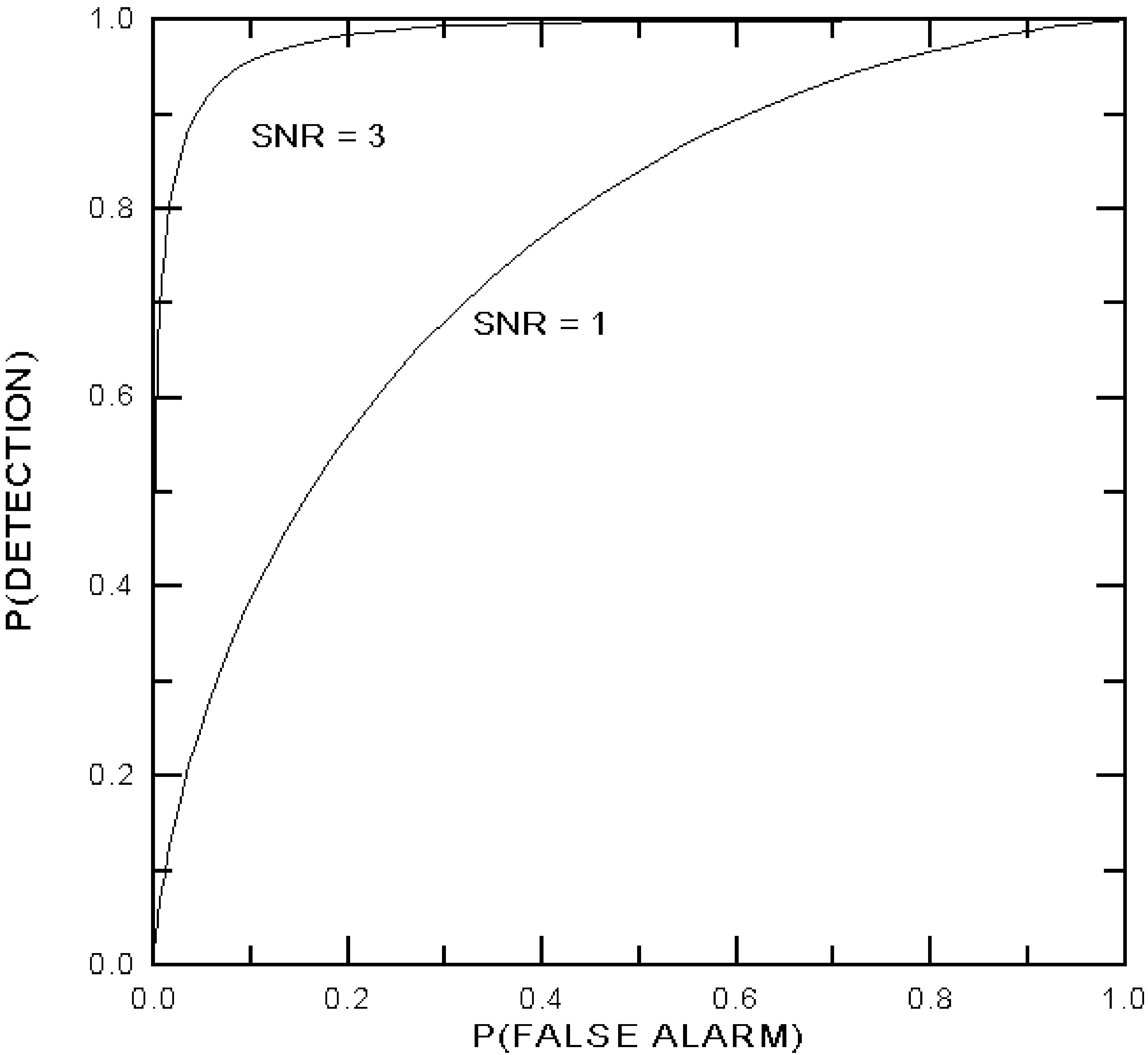


**Figure 1**. Detection probability as a function of the false-alarm probability for lidar systems with signal-to-noise ratios of 1 and 3.

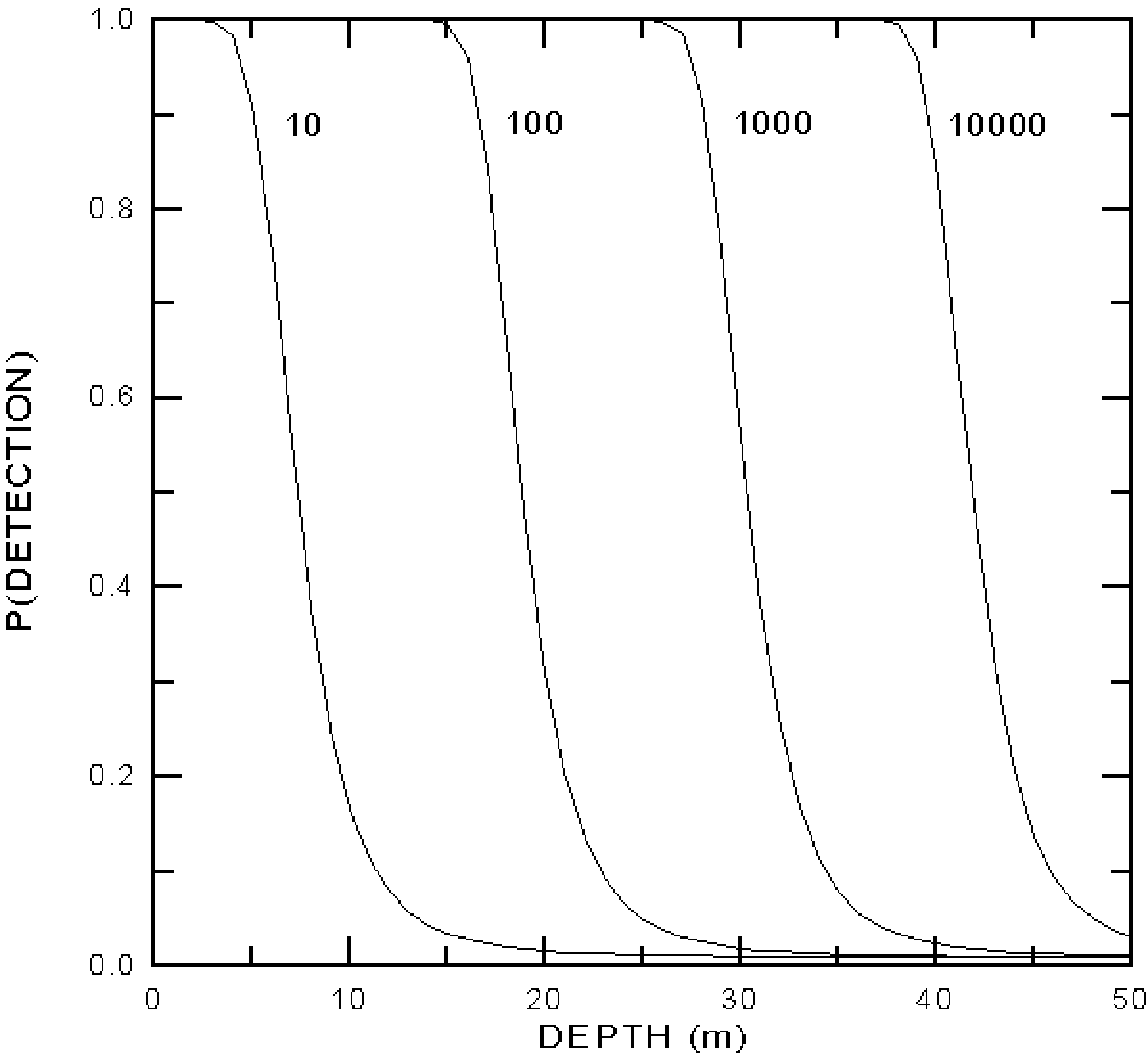


**Figure 2** Detection probability as a function of depth for a lidar system with a false-alarm probability of 0.01 operating in water with an attenuation coefficient of 0.1 $m^{-1}$. Curves are labeled by the value of the signal-to-noise ratio at the surface.

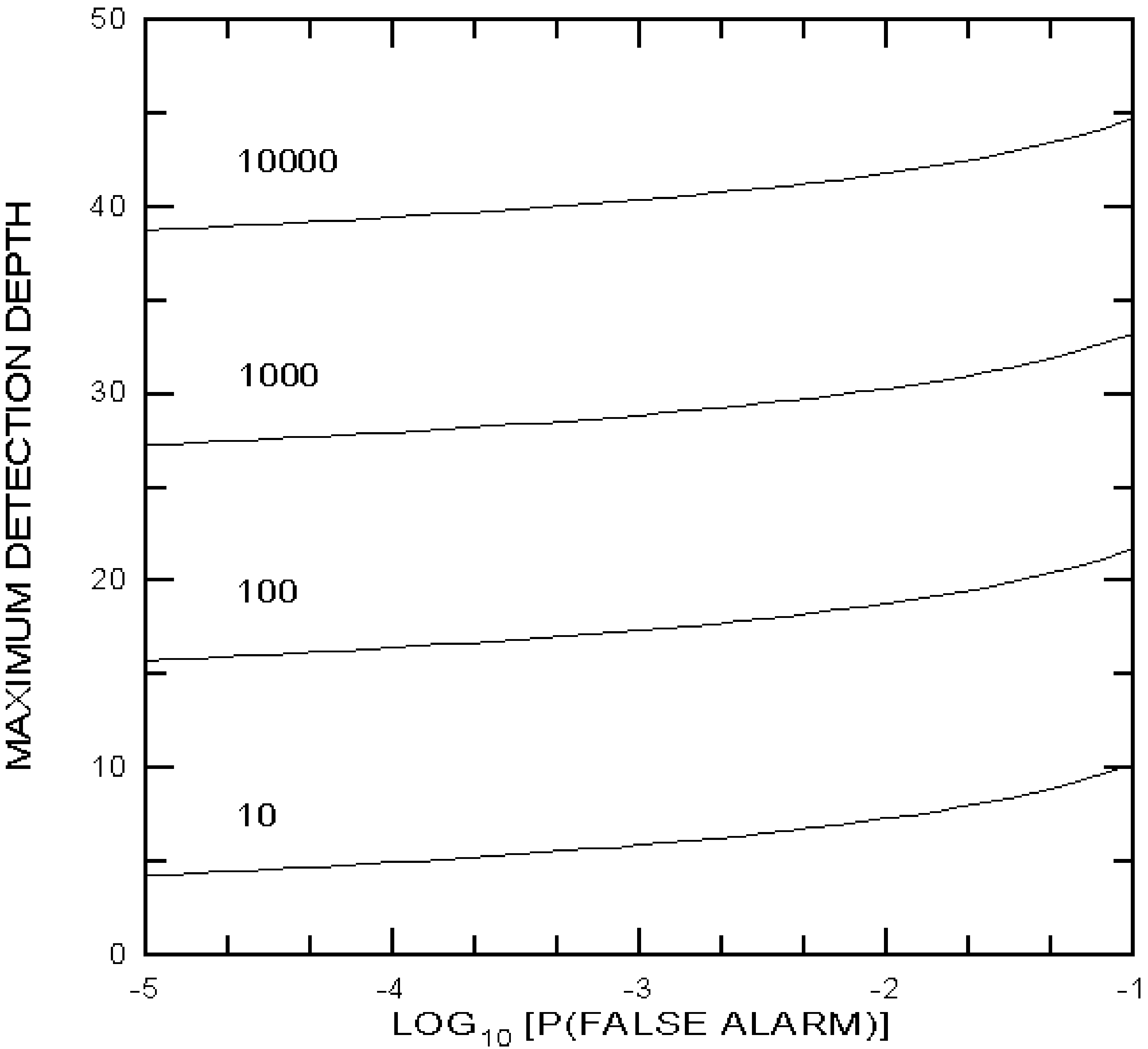


**Figure 3** Maximum detection depth as a function of the false-alarm probability for a lidar system operating in water with an attenuation coefficient of 0.1 $m^{-1}$. Curves are labeled by the value of the signal-to-noise ratio at the surface.

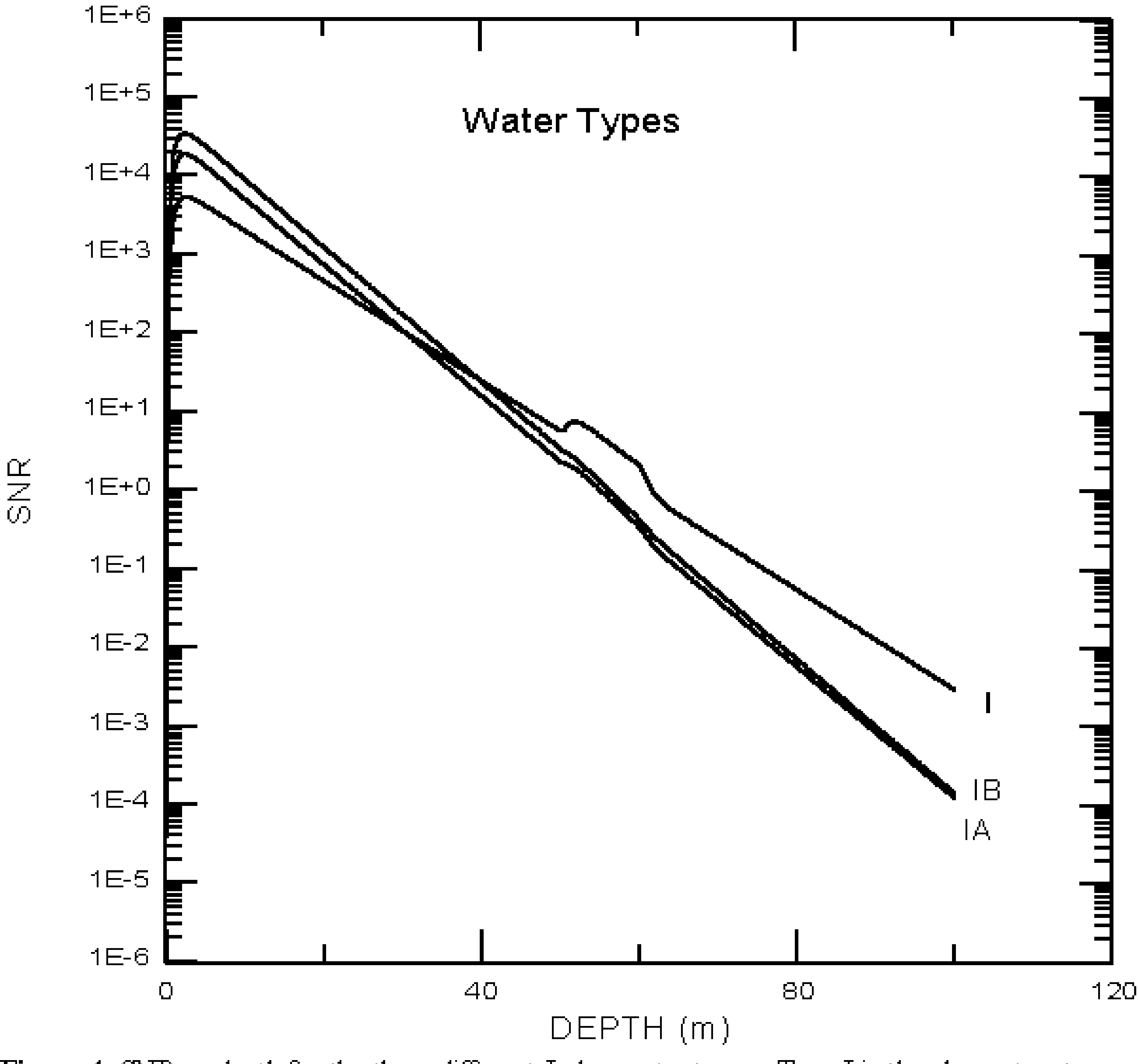


**Figure 4** SNR vs depth for the three different Jerlov water types. Type I is the cleanest water and type IB is the dirtiest. Type I water has fewer particles to scatter light back to the receiver, but also has a smaller lidar attenuation coefficient so that more energy is available to scatter back to the receiver from greater depths.

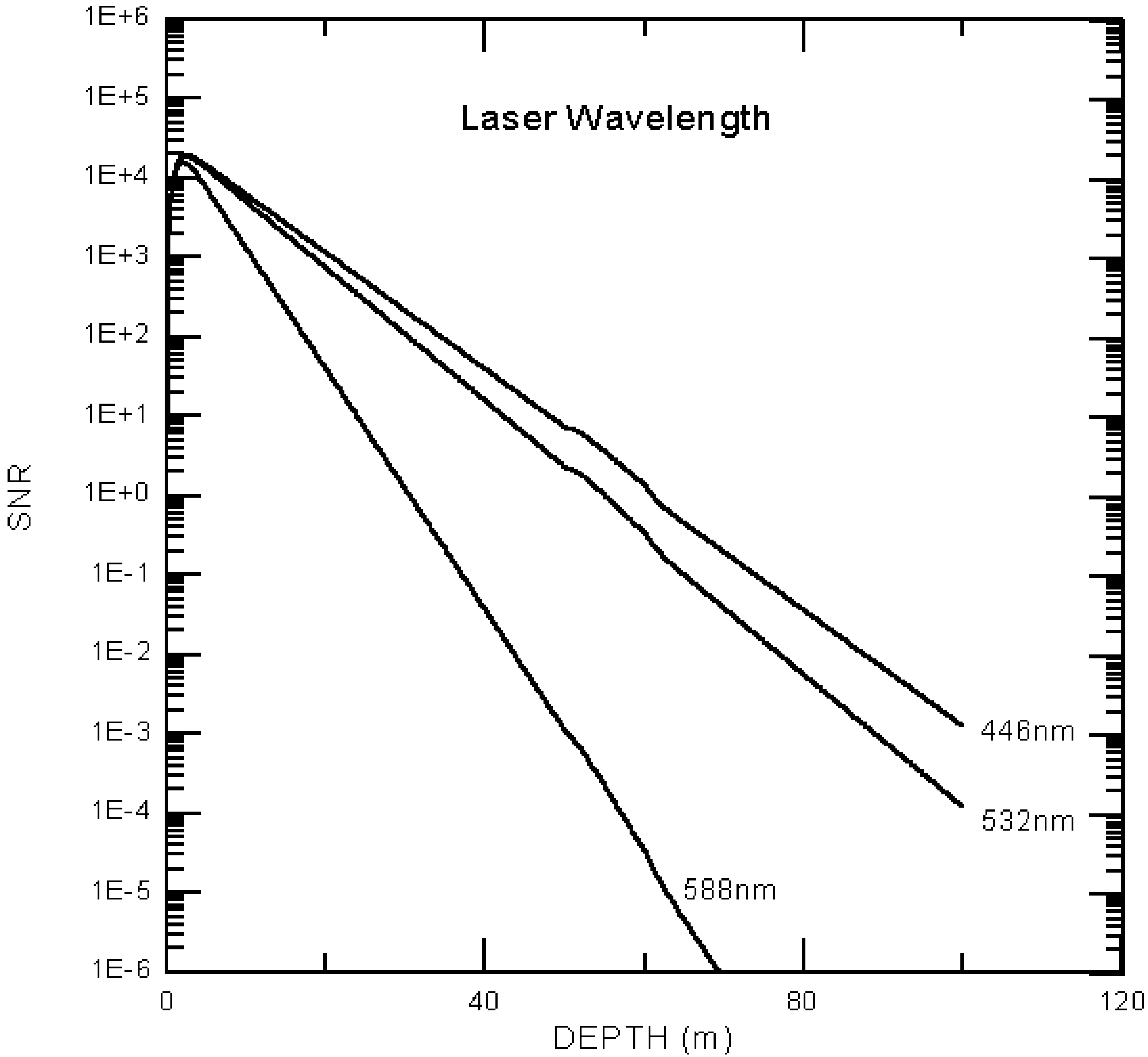


**Figure 5** SNR vs depth for three laser wavelengths. A choice of 446 nm produces the best SNR which is slightly better than 532 nm and is quite a bit better than 588 nm. The major problem with going to the 446 nm wavelength as discussed earlier is the cost. A 446 nm laser costs about $100K compared with $25K for the 532 nm.

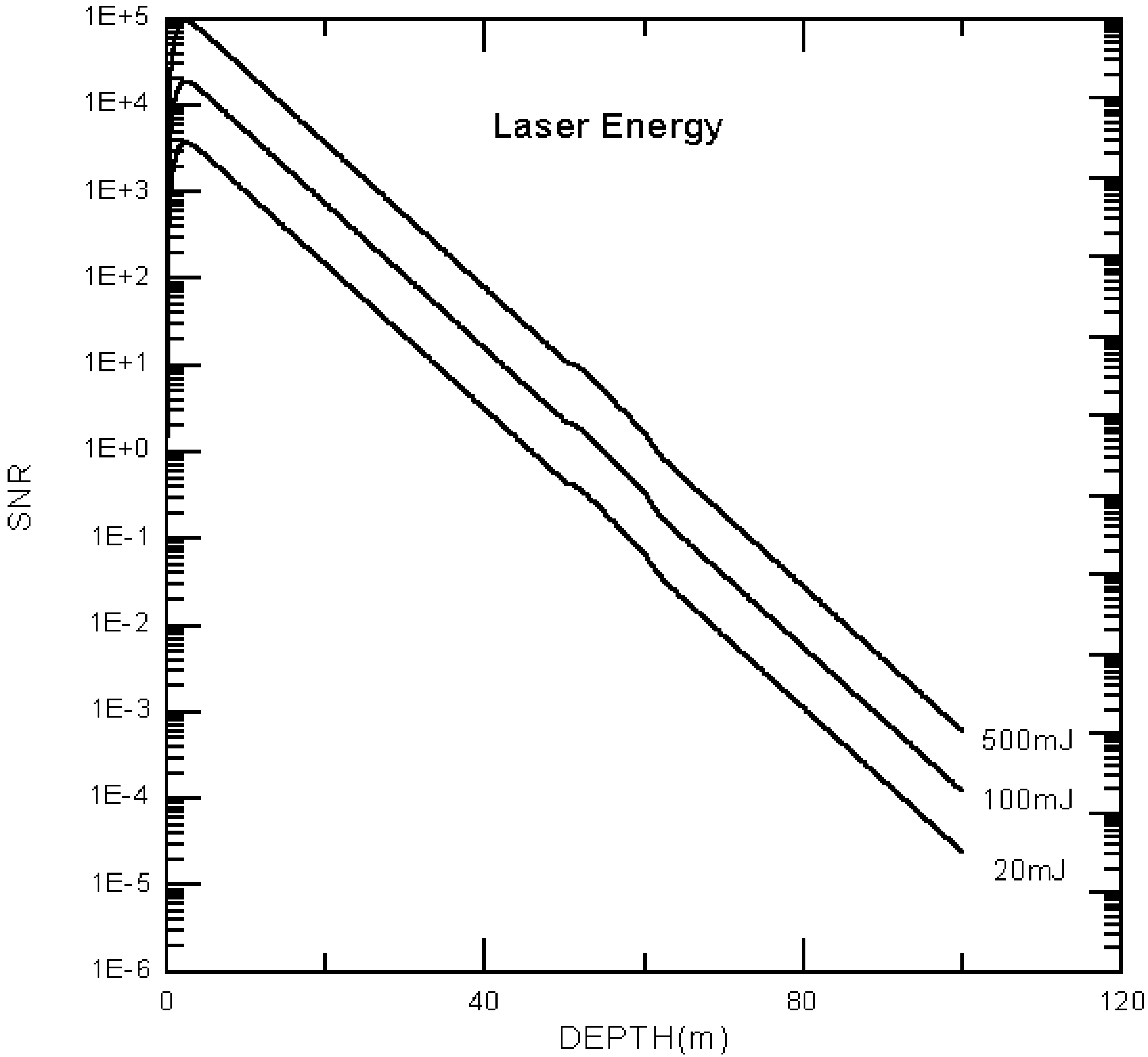


**Figure 6** SNR vs depth for three laser energies. This shows that increasing the laser power by a factor of five increases the SNR by about half a decade. This translates to an increase of about 10 m in depth for the same SNR.

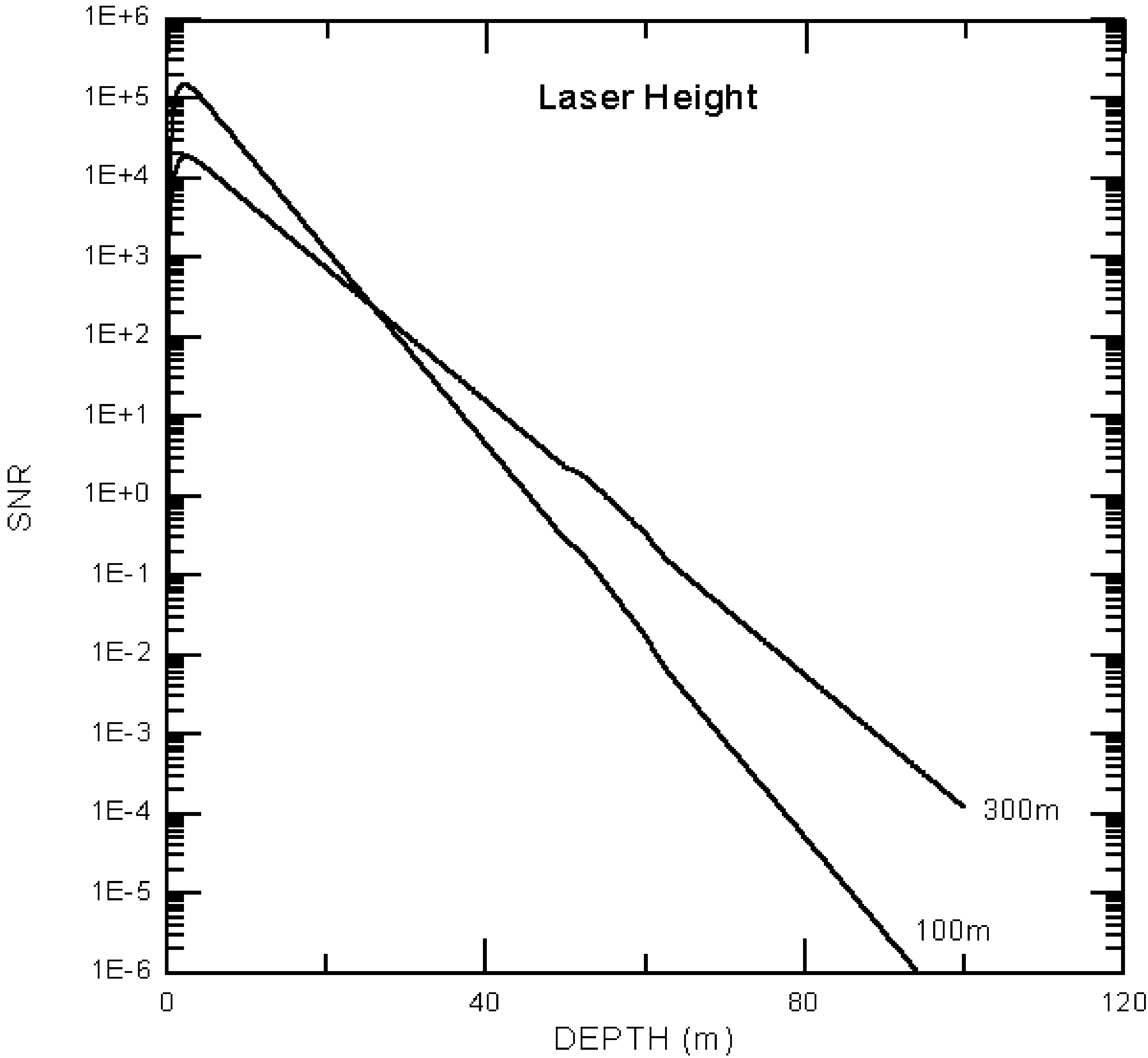


**Figure 7** SNR vs depth for two laser heights with a fixed divergence. The default transmitter divergence is 25 mrad. This translates to a spot size on the surface of 2.5 m for a laser height of 100 m and a spot size of 7.5 m for a laser height of 300 m. The lidar attenuation coefficient is partially determined by the laser spot size on the surface. Generally, the larger the spot on the surface, the closer the lidar attenuation coefficient is to the diffuse attenuation coefficient. The slopes of the lines are the lidar attenuation coefficients.

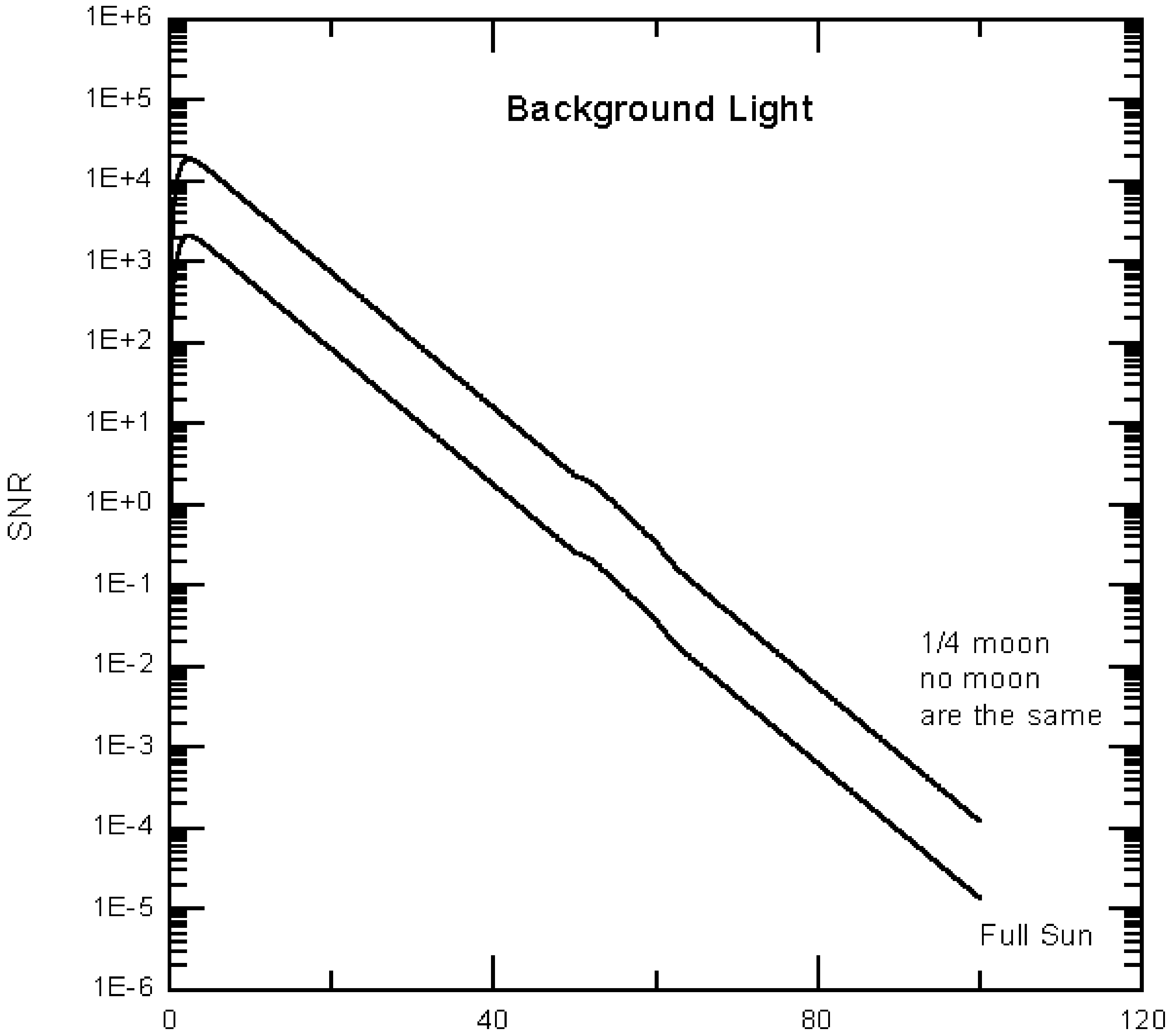


**Figure 8** SNR vs depth for different background light conditions. For a given SNR we can see about 15 m deeper at night than we can see during full daylight.

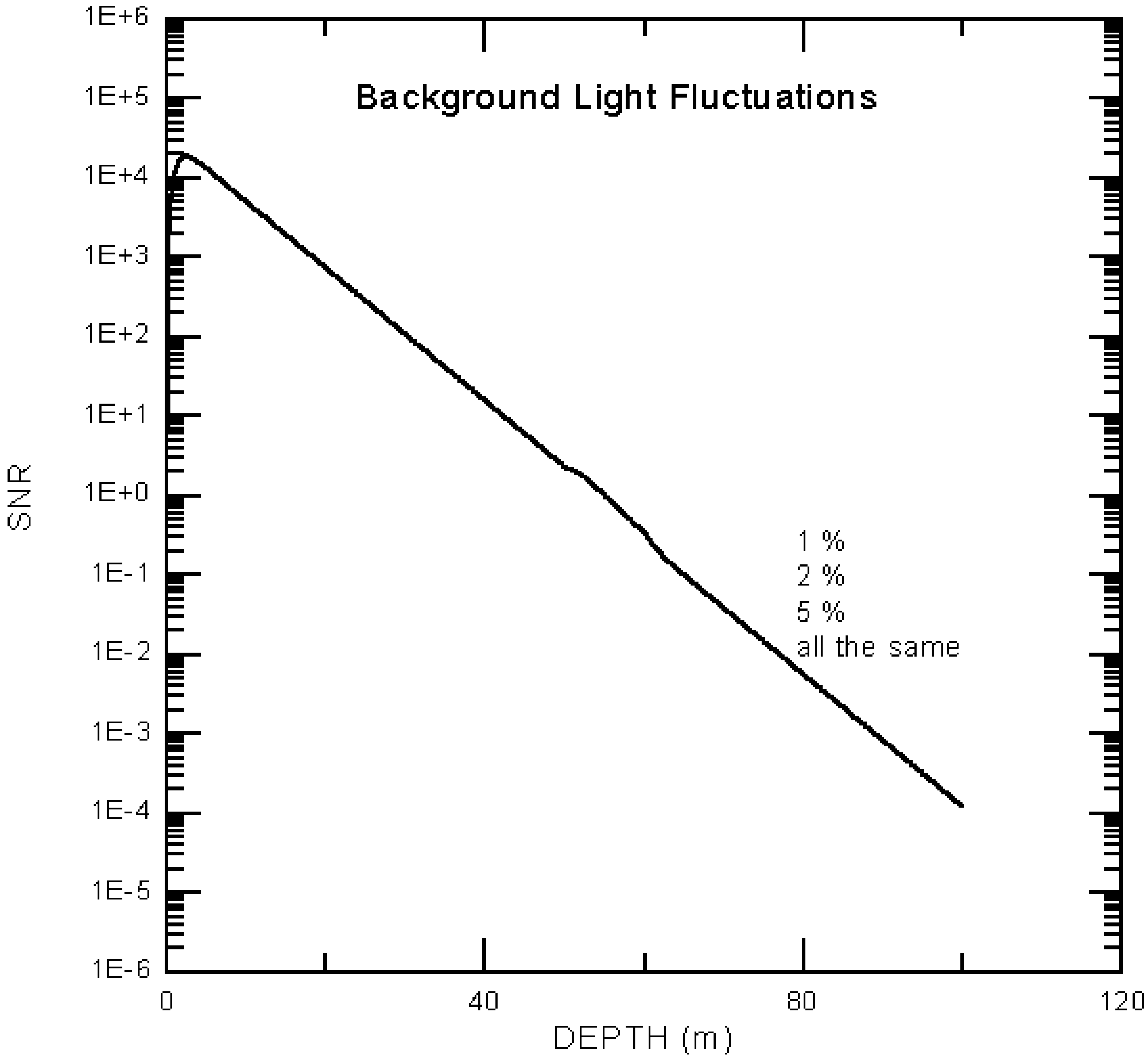


**Figure 9** SNR vs depth for different background light fluctuation levels. In the baseline system, background light is not the dominant noise source, so changes in this parameter do not affect performance.

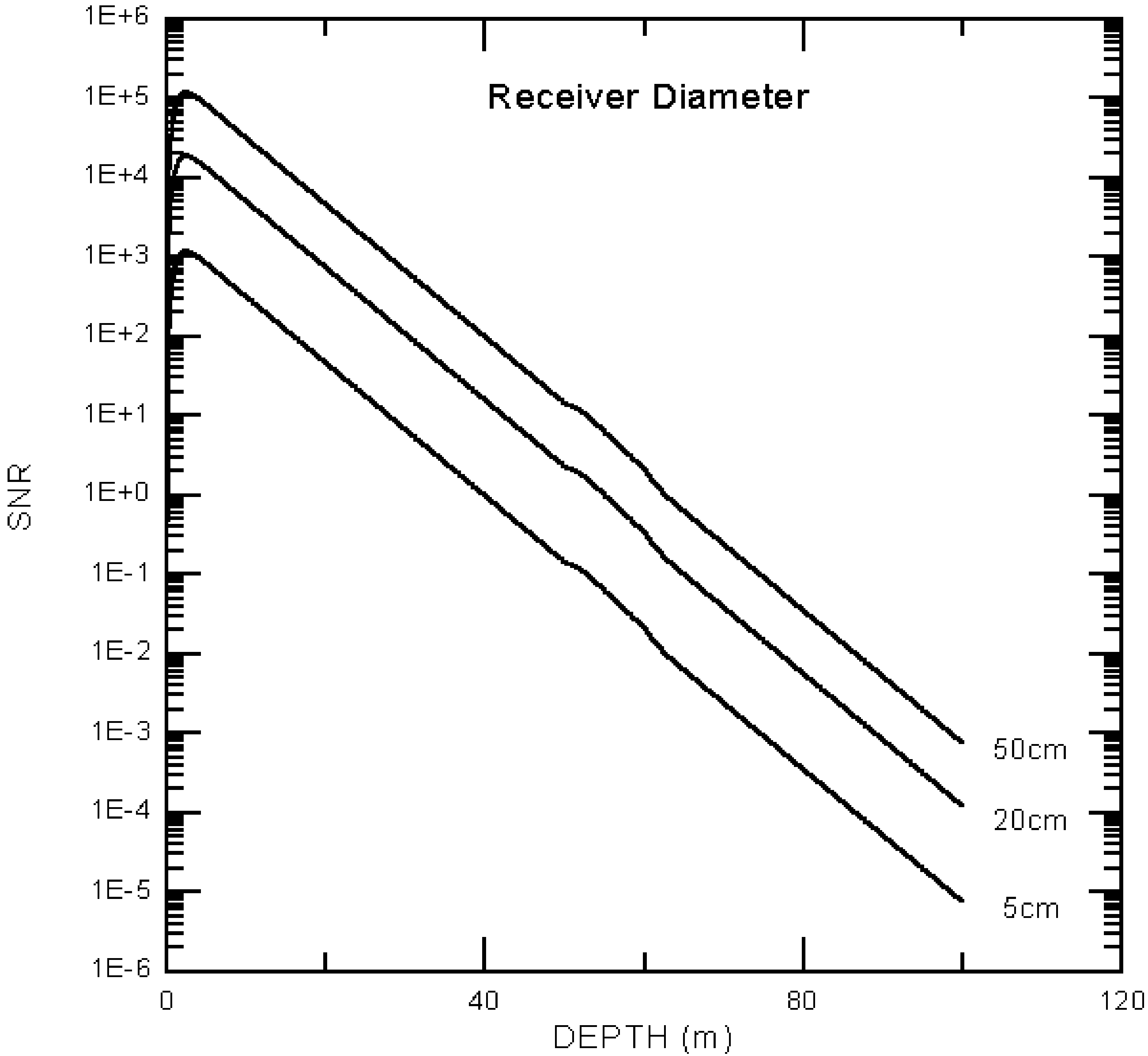


**Figure 10** SNR vs depth for three receiver diameters. Generally bigger is better within the constraints of cost, size, and detector saturation limit.

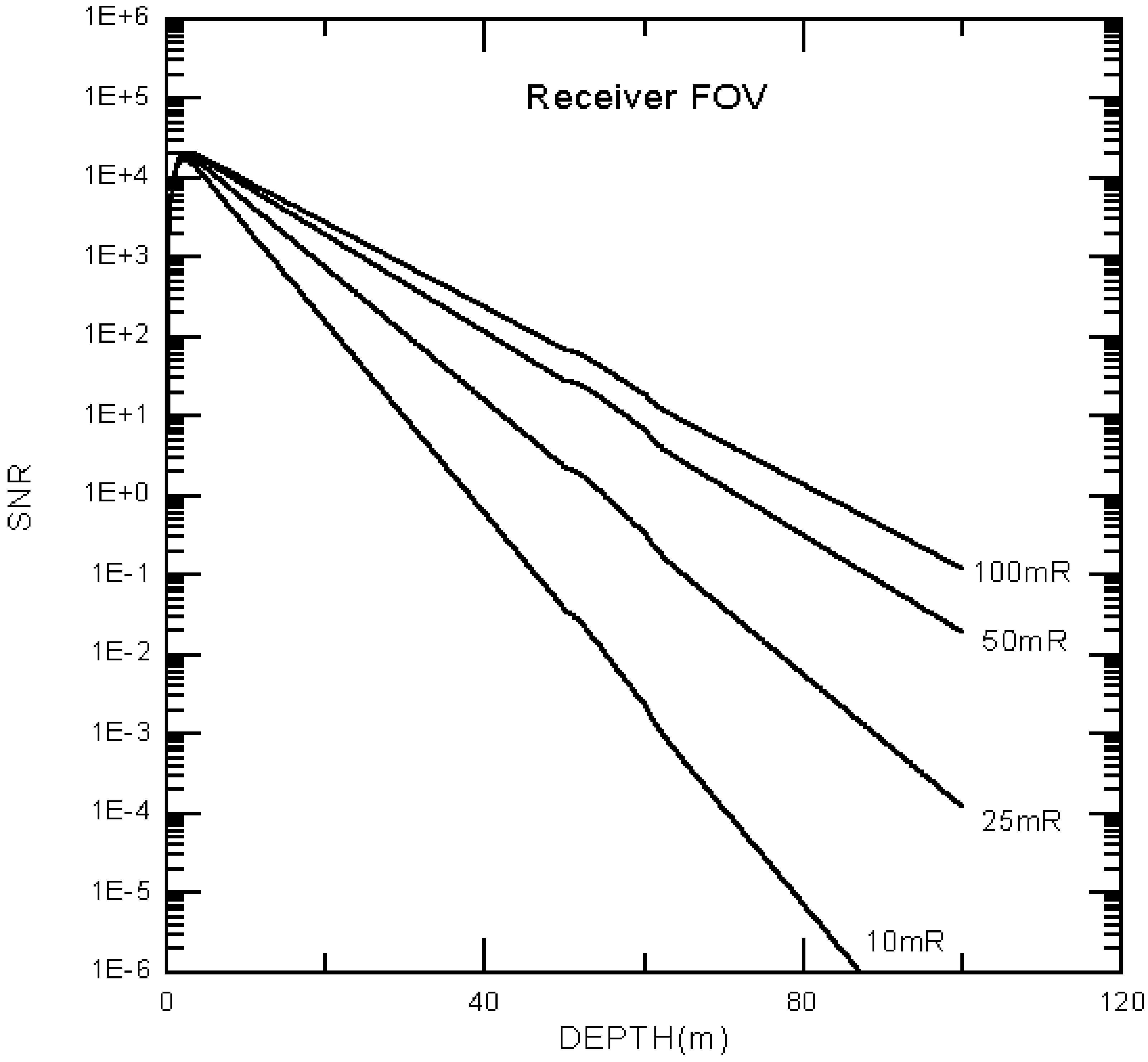


**Figure 11** SNR vs depth for four receiver fields of view (FOV). Generally, wider is better up to the point where background light starts becoming a problem. As the FOV becomes wider, more of the scattered photons remain within the receiver FOV, and the lidar attenuation coefficient approaches the diffuse attenuation coefficient. However, during the day, a large FOV will allow more background light to enter the receiver. Optimization of the FOV under all conditions is an area of active research.

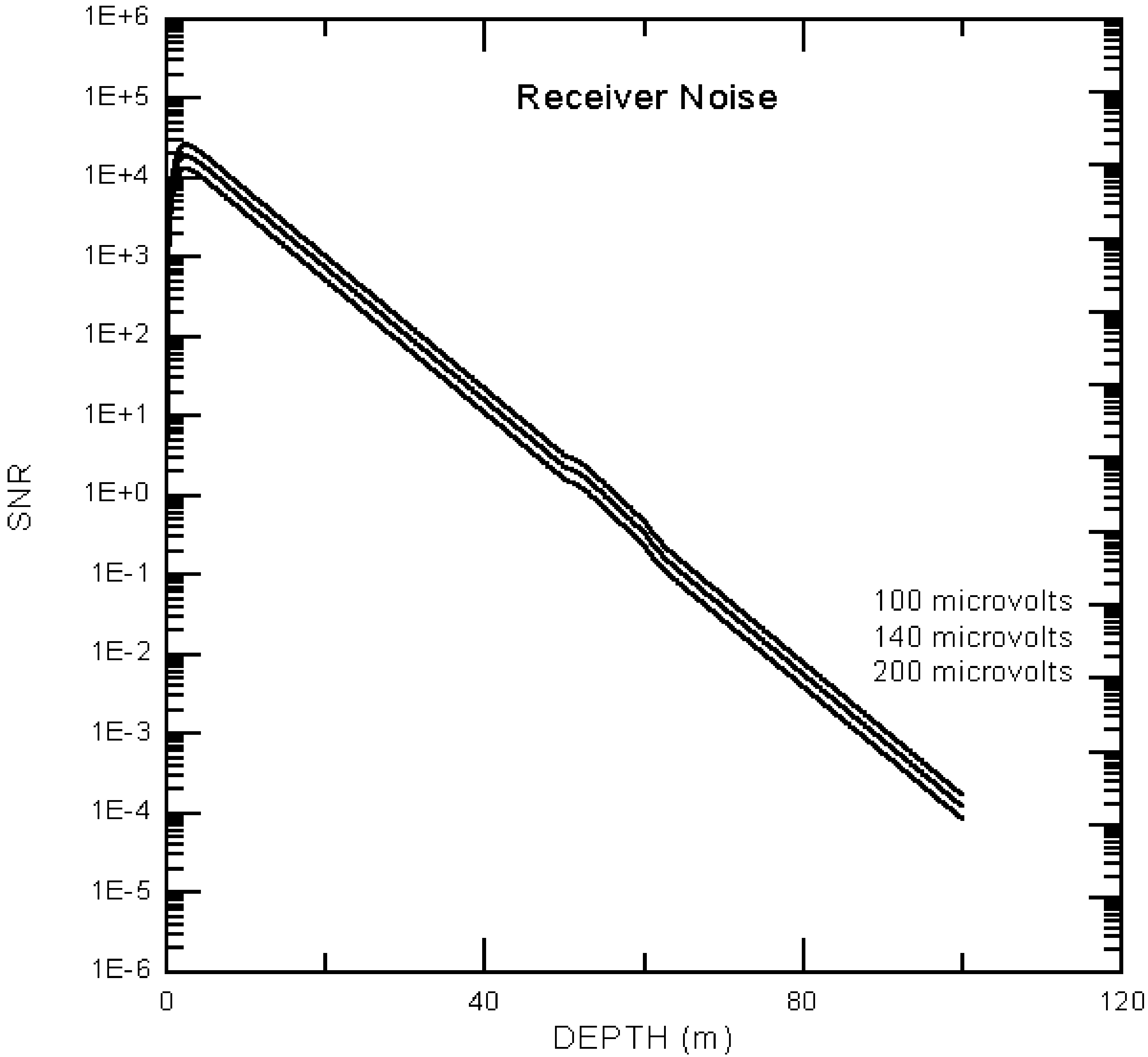


**Figure 12** SNR vs depth for three receiver noise values. Receiver noise, for the values shown, has a fairly small effect on SNR. If you double the receiver noise, you lose about 4 m in depth for the same SNR.

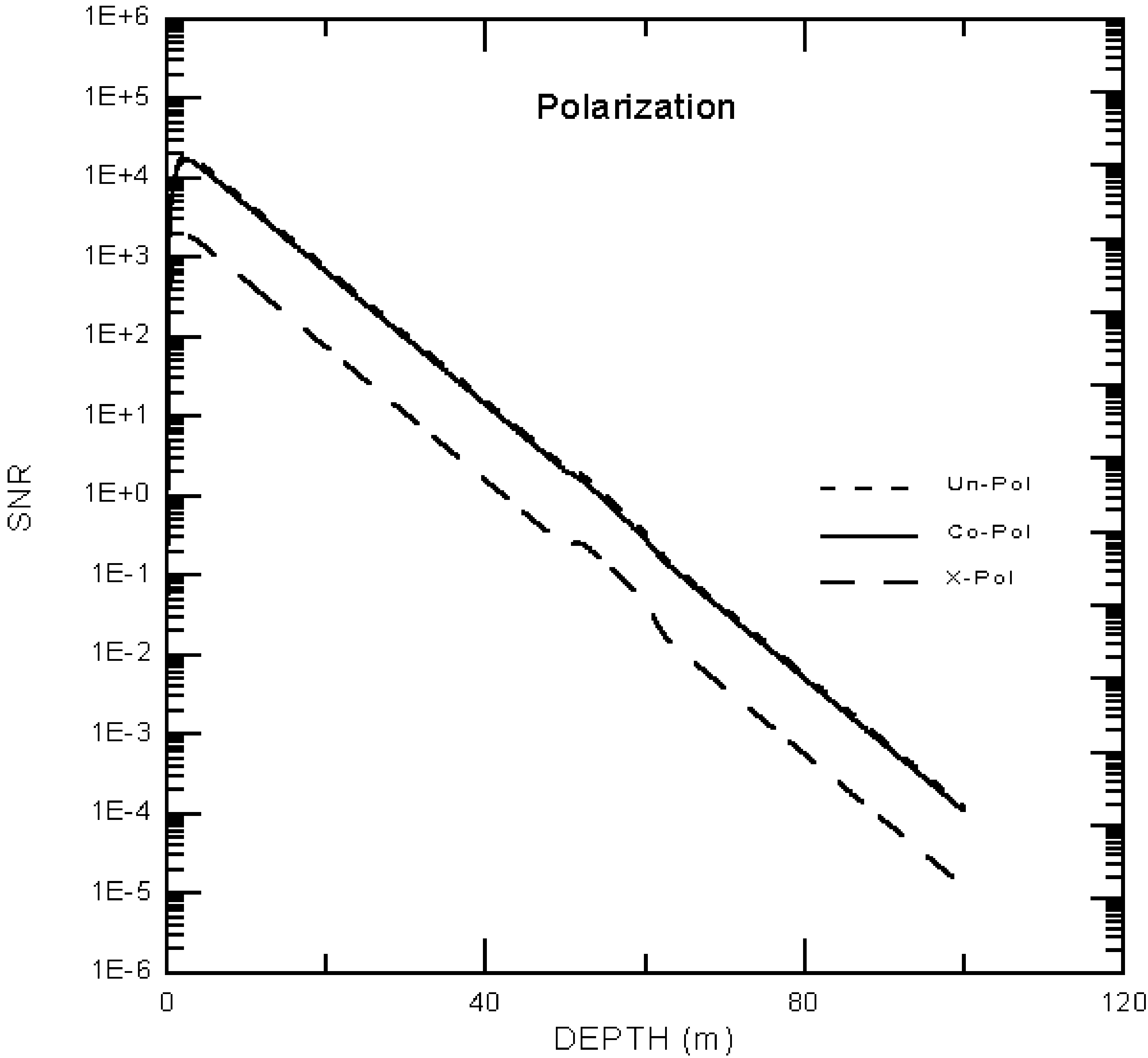


**Figure 13** SNR vs depth for different polarizations. Cross polarization gives about an order of magnitude less SNR than the co-polarized signal, but notice the hump in the line from the fish return. Compare the hump in the co-polarized signal with the hump in the cross-polarized signal. While you get less SNR with cross-polarization than you get with co-polarization you can detect the fish school better. This happens because the fish depolarize the laser more than the surrounding water.

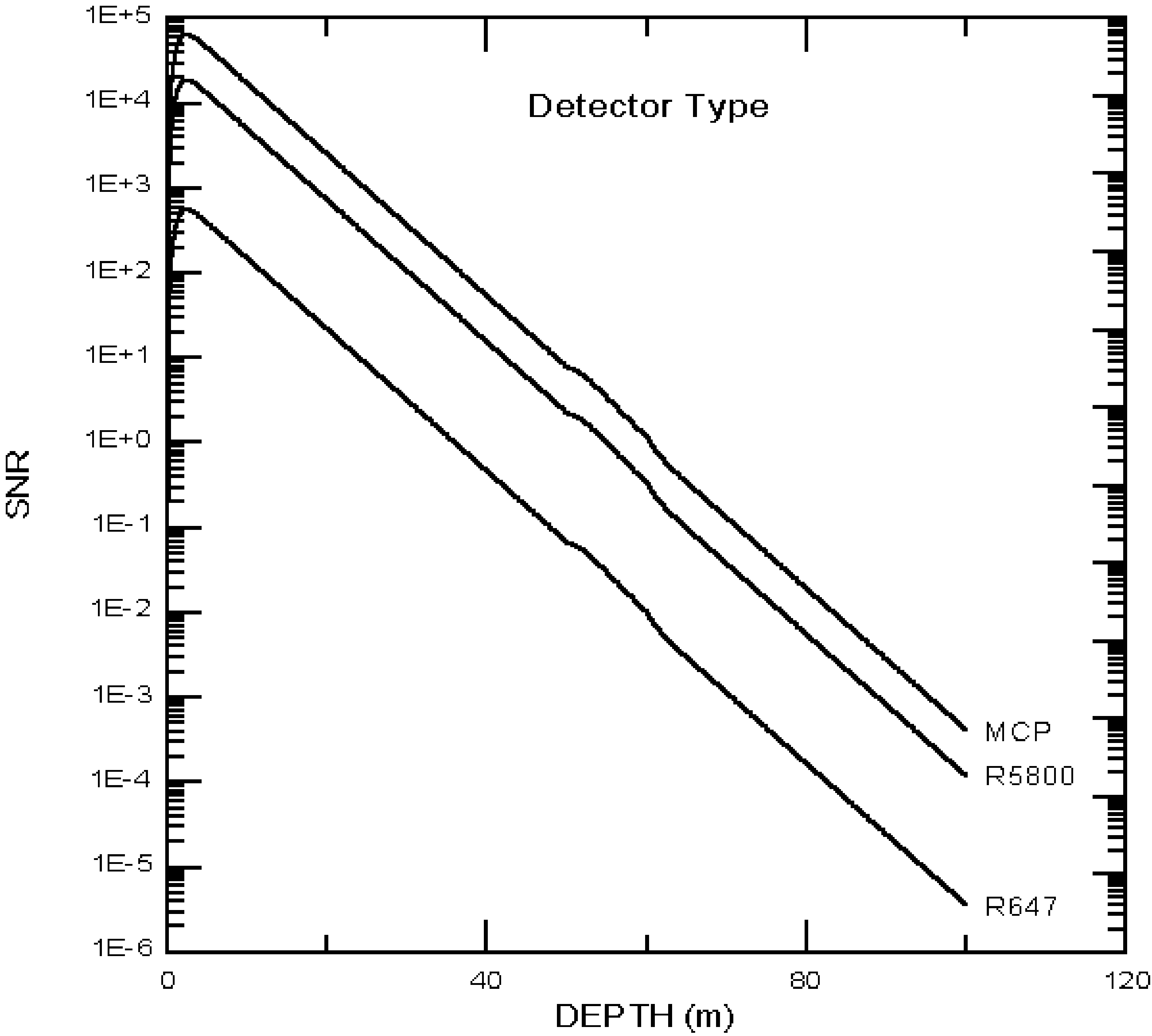


**Figure 14** SNR vs depth for different detectors. SNR can be affected by the choice of detector. There are several considerations to take into account in detector selection. In this plot, the micro channel plate MCP detector seems to be a slightly better choice than the R5800 photo multiplier tube PMT detector. The MCP can take a higher power light pulse without damage or loss of linearity than the R5800 PMT. When the laser pulse hits the water surface a portion of the light is reflected back toward the receiver and this reflected light is much greater than the light that is scattered back from the particles in the water. This reflected light temporarily saturates the detector and, if the saturation is great enough, the detector can be permanently damaged. To compensate for surface reflection the gain of the detector is turned down, sacrificing deeper detection of fish. Other considerations in detector selection are detector diameter, dark current and noise levels. The detector diameter affects the maximum FOV of the receiver. Dark current and noise levels affect the minimum detectable signal. The bandwidth is another important parameter with short pulse lasers. Also, the output voltages and dynamic range need to match the logarithmic amplifier or analog to digital converter that follow the detector.

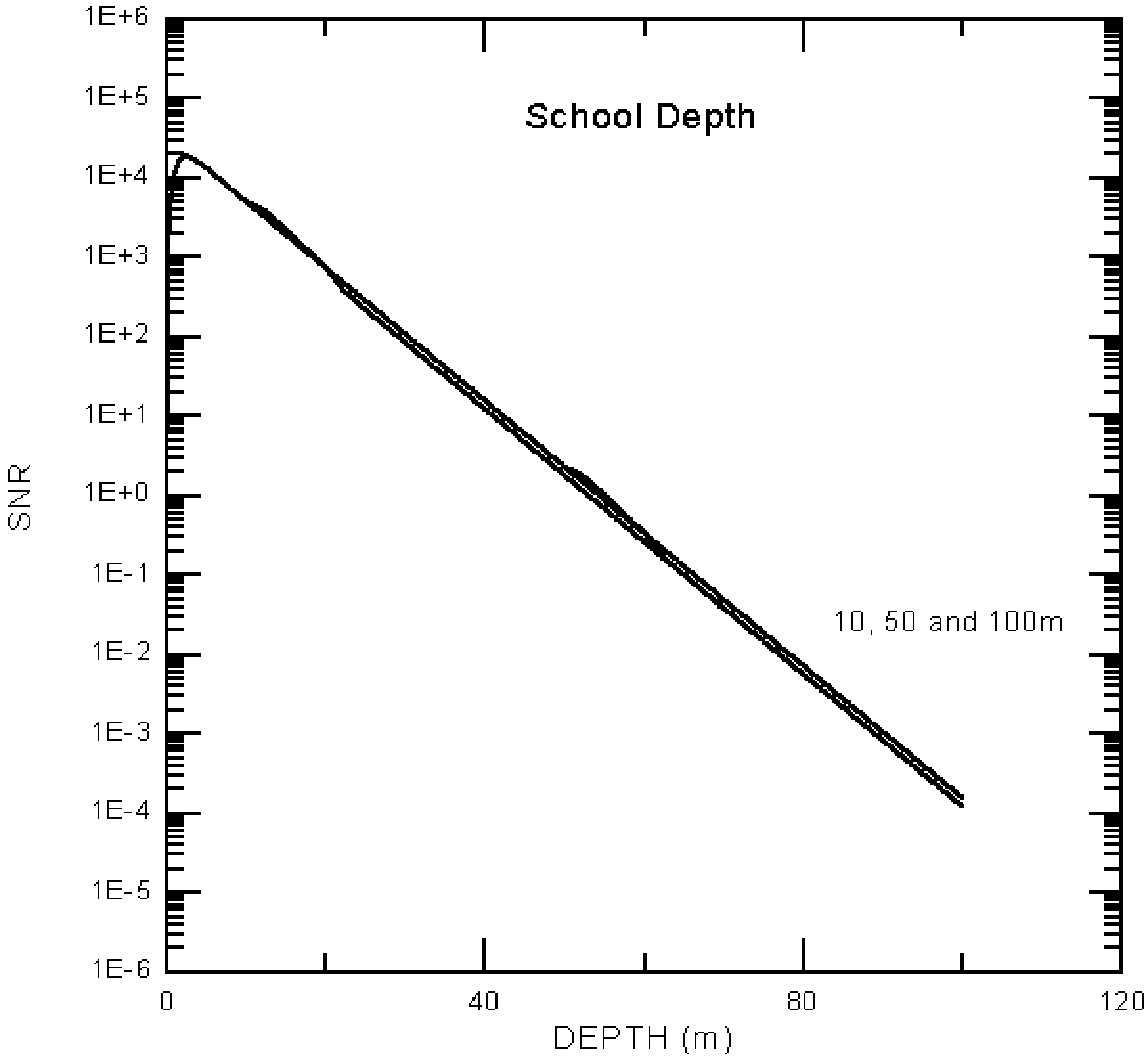


**Figure 15** SNR vs depth with fish schools at 10 m and 50 m. The 100 m school was so far down in SNR that there is no hope of seeing it and was cut from the plot. The 10 and 50 m schools are observed as deviations from the straight line that is the clear water return.

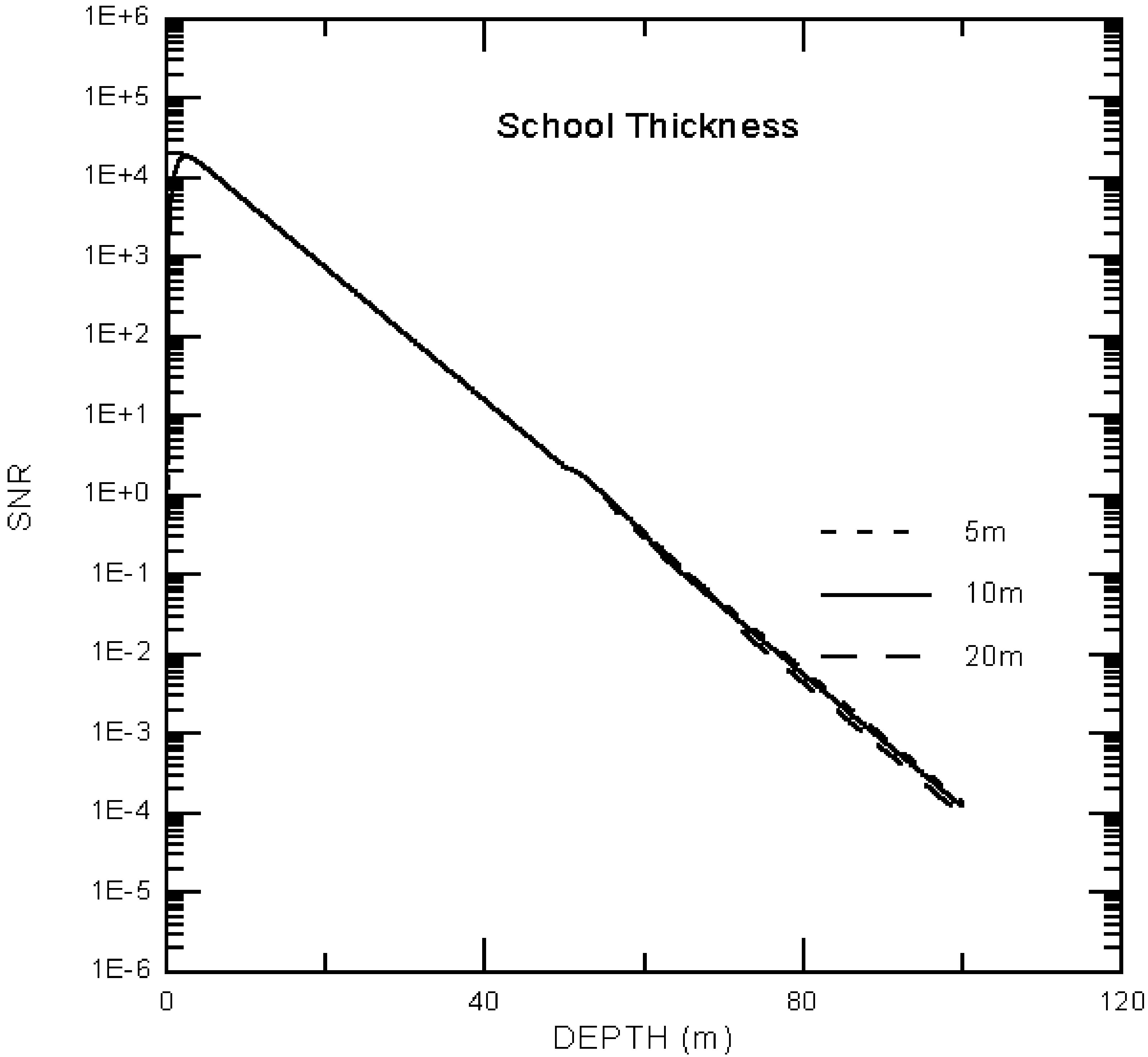


**Figure 16** SNR vs depth for different fish school thicknesses. As the schools get thicker, more light is attenuated by the school, and there is less light left below the school. This shows up as a decrease in SNR below the fish school.

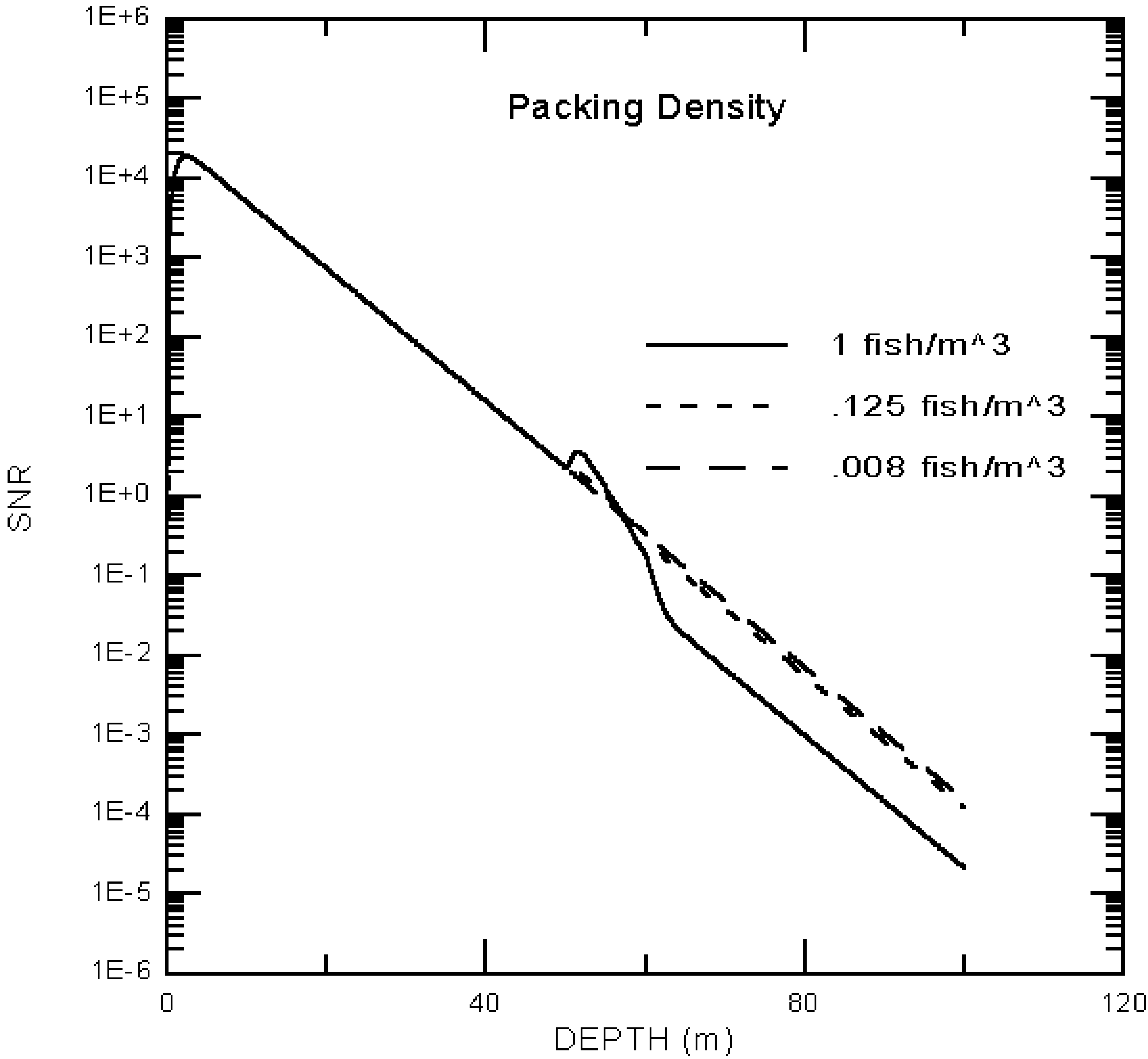


**Figure 17** SNR vs depth for different fish packing densities. One fish / $m^3$ is about a one body length spacing, based on an average 1 m long fish. 0.125 fish/ $m^3$ is about 2 body length spacing and 0.008 fish /$m^3$ is about a 5 body length spacing. The plot shows that the closer the fish are together, the more return signal there is and that there is less signal available below the school for detection of additional, deeper schools. With a greater packing density the fish are closer together so there are more fish in the laser beam, allowing more of the laser to be reflected back to the receiver. The reflective area of the fish in the beam is the important point. Assuming the same reflectivity, 10 fish with a reflective area of 10 $cm^2$ each, produce the same reflected laser energy as 1 fish with a reflective area of 100 $cm^2$. More dense fish schools are more easily detected and can be detected deeper than less dense fish schools.

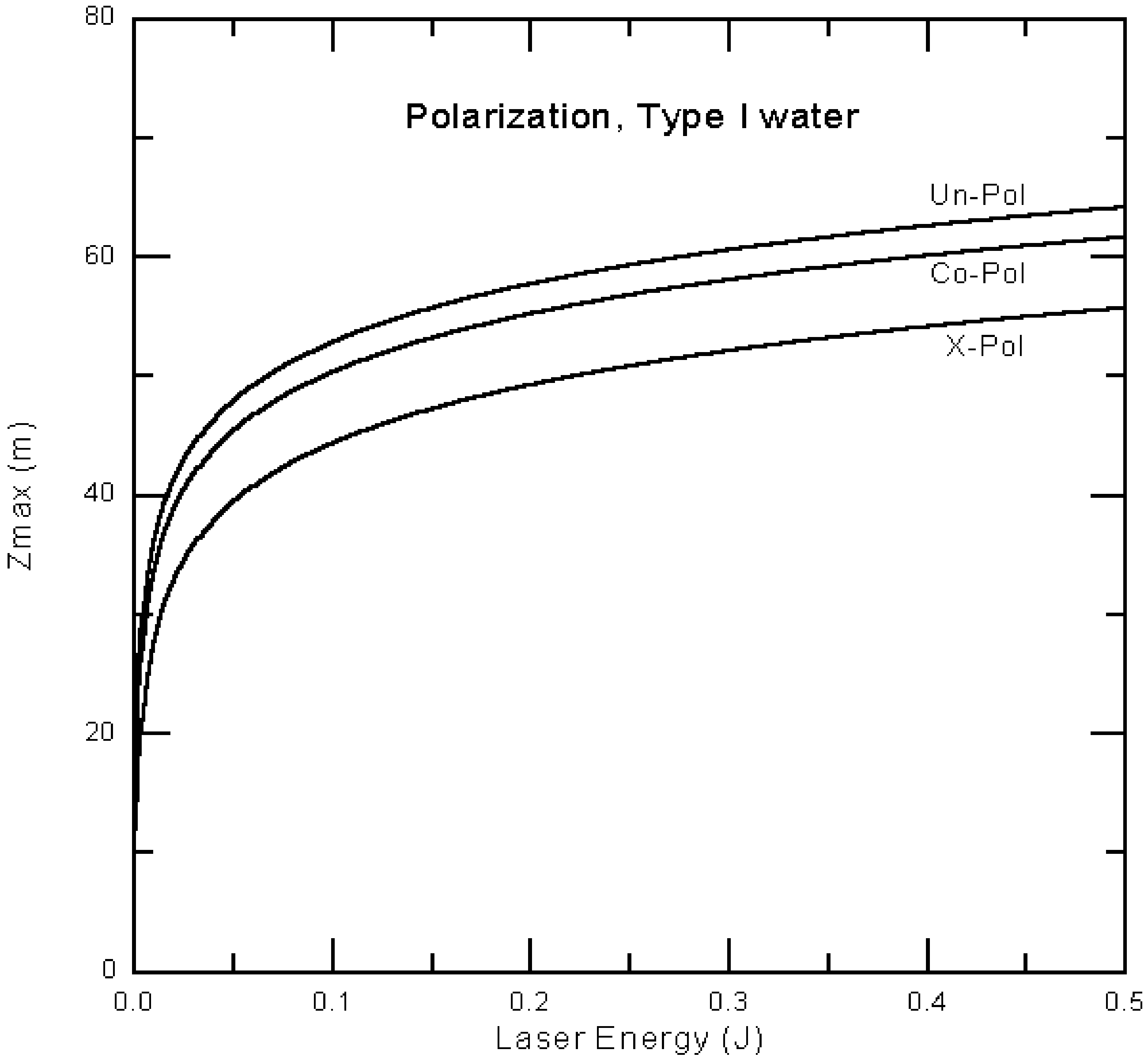


**Figure 18** $Z_{max}$ vs laser energy for different polarizations in type I water. Type I water is the cleanest. Cleaner water is better. Generally, you can see deeper using the unpolarized receiver as there is more energy available from both polarizations but this is not the only criteria. Fish tend to depolarize the light so the actual fish signal can be better discriminated from the water signal using cross-polarized light.

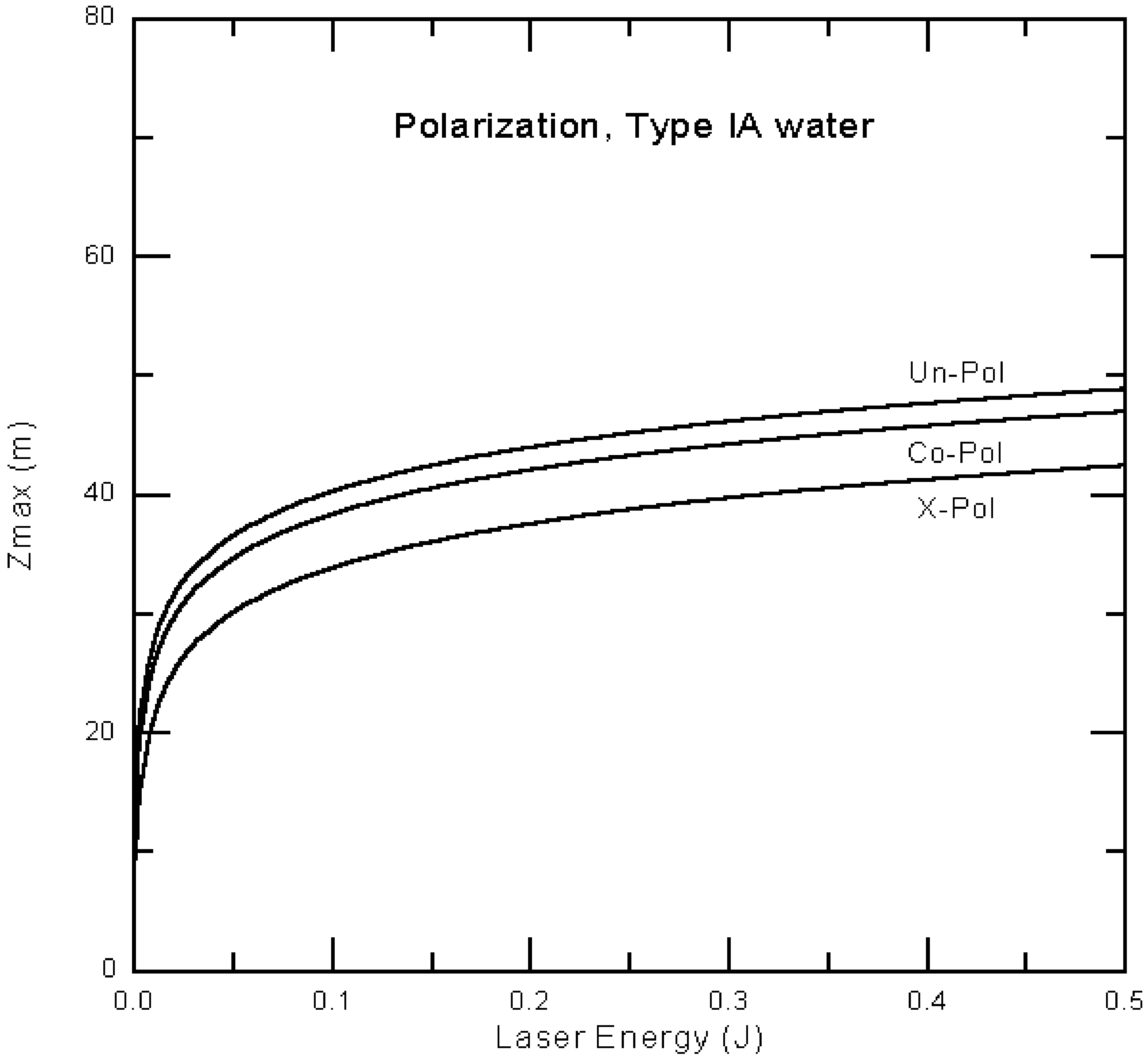


**Figure 19** $Z_{max}$ vs laser energy for different polarizations in type IA water.

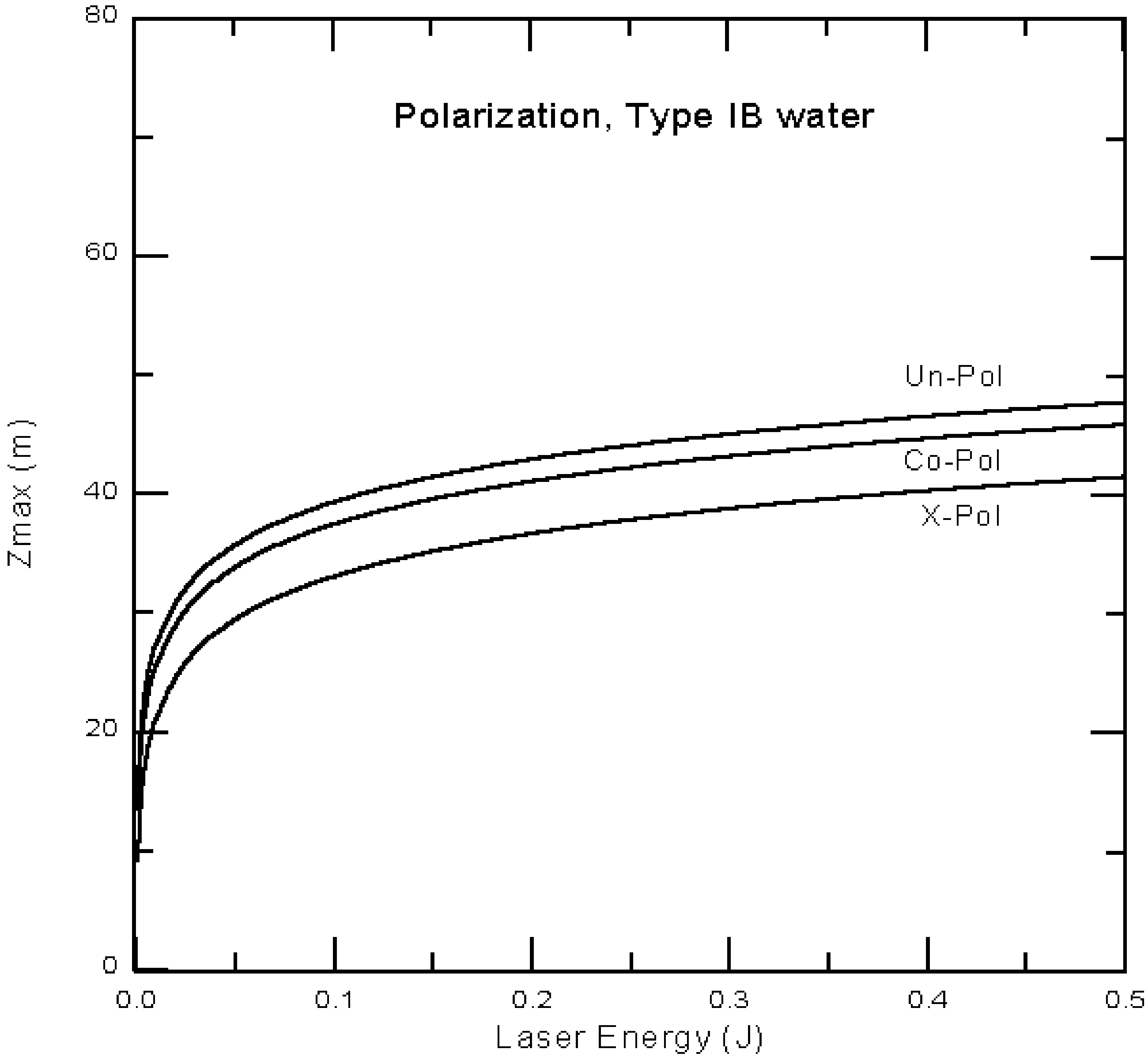


**Figure 20** $Z_{max}$ vs laser energy for different polarizations in type IB water. Type IB is the dirtiest water.

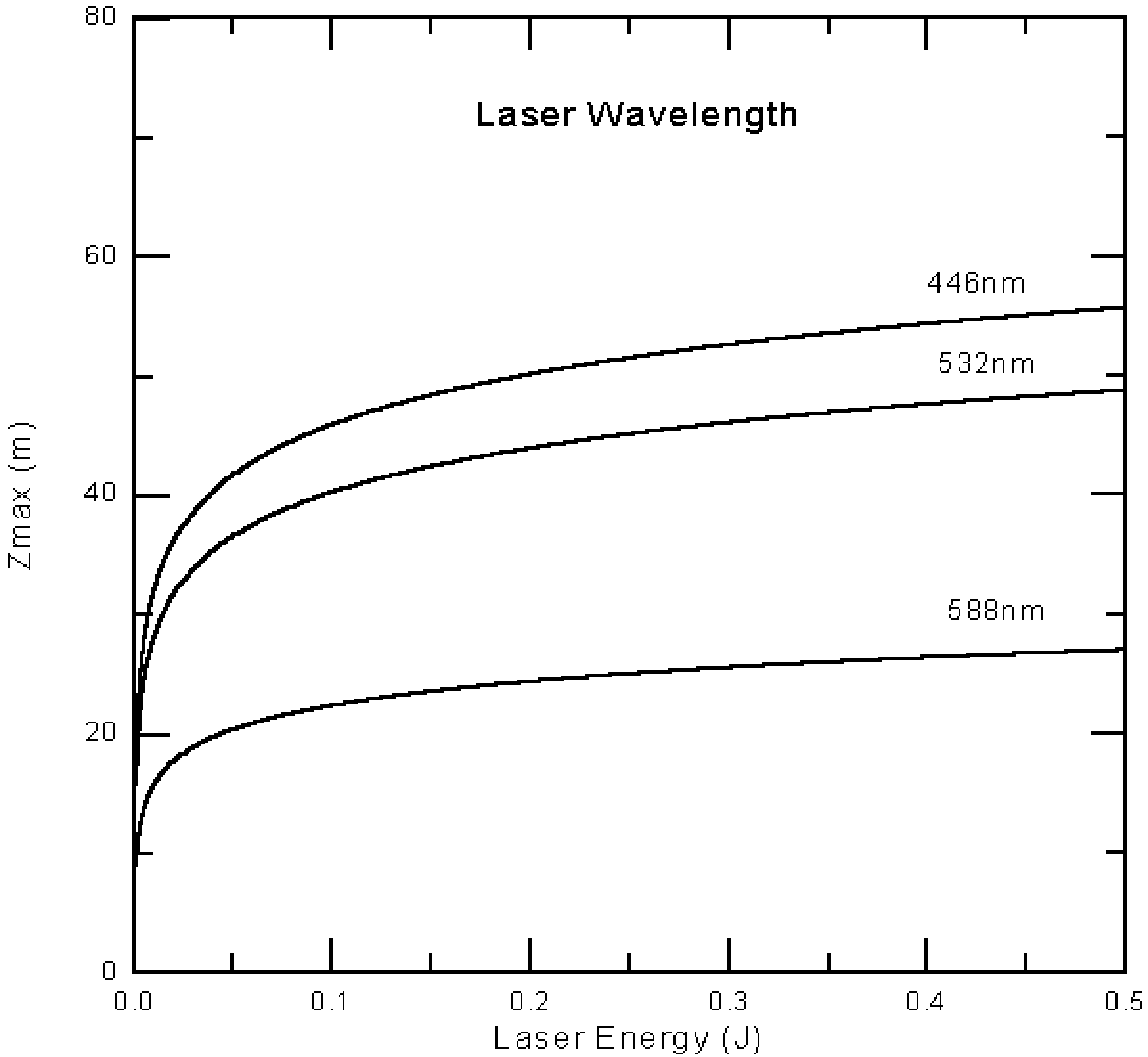


**Figure 21** $Z_{max}$ vs laser energy for three different laser wavelengths. A 446 nm wavelength laser produces the deepest $z_{max}$. The 532 nm wavelength produces a $z_{max}$ about 10 m less and the 588 nm wavelength produces a $z_{max}$ about 30 m less than the 488 nm wavelength.

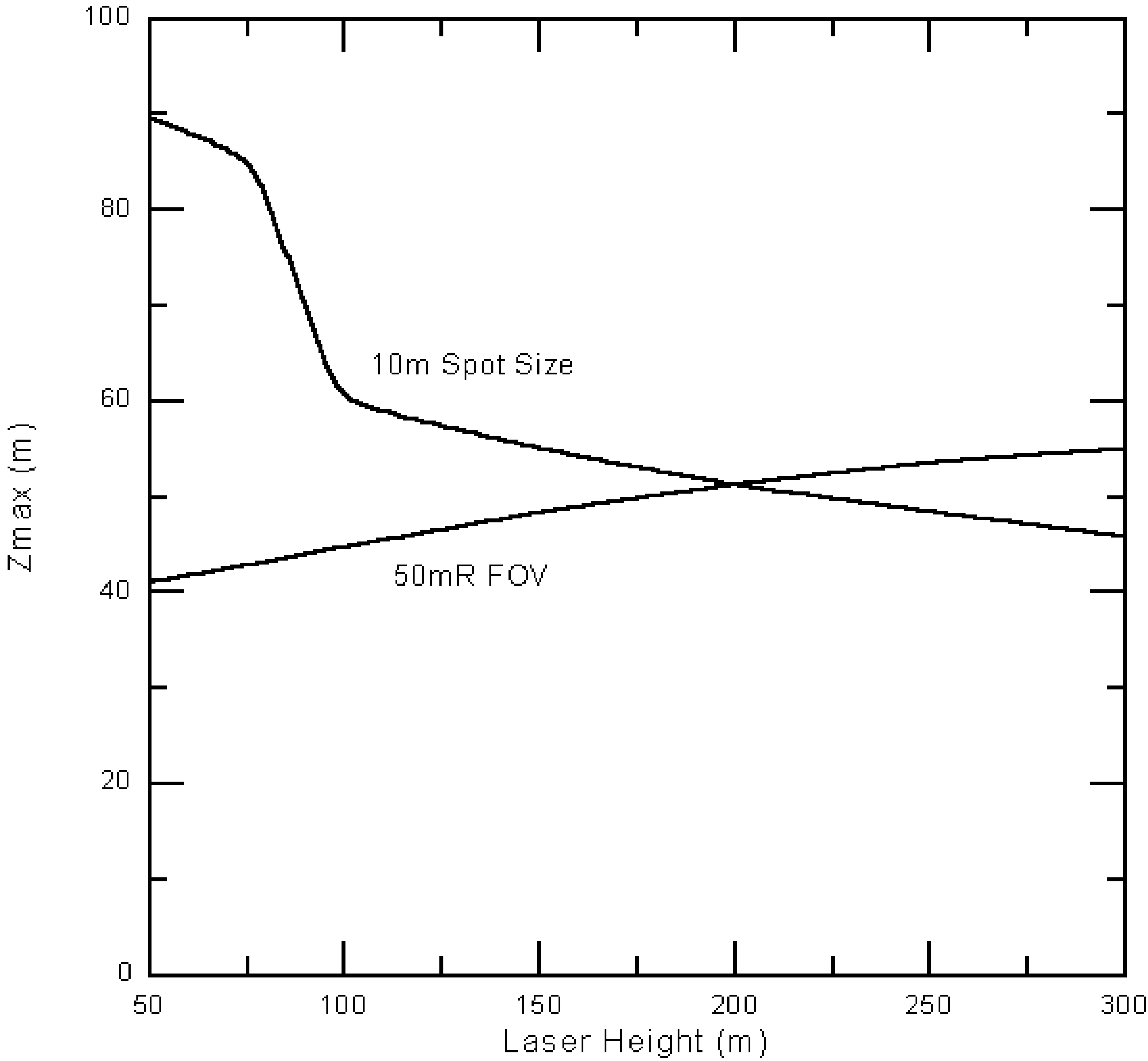


**Figure 22** $Z_{max}$ vs laser height for a constant 50 mR receiver FOV and for a constant 10 m surface spot size. This plot shows that below a laser height of 200 m, a fixed 10 m diameter spot size is better than a fixed 50 mR FOV and above 200 m the fixed FOV is better than the constant spot size. This is because the lidar attenuation coefficient is partially determined by the surface spot size. With a smaller spot size the attenuation increases and with a larger spot size the attenuation approaches the diffuse attenuation coefficient, which is the minimum attenuation. Physically what happens is this, light that enters the water is either scattered, absorbed or continues straight. In a narrow FOV the light that is scattered is mostly scattered outside the FOV and is lost. With a large FOV more of the scattered light is still in the FOV and is available to scatter back to the receiver.

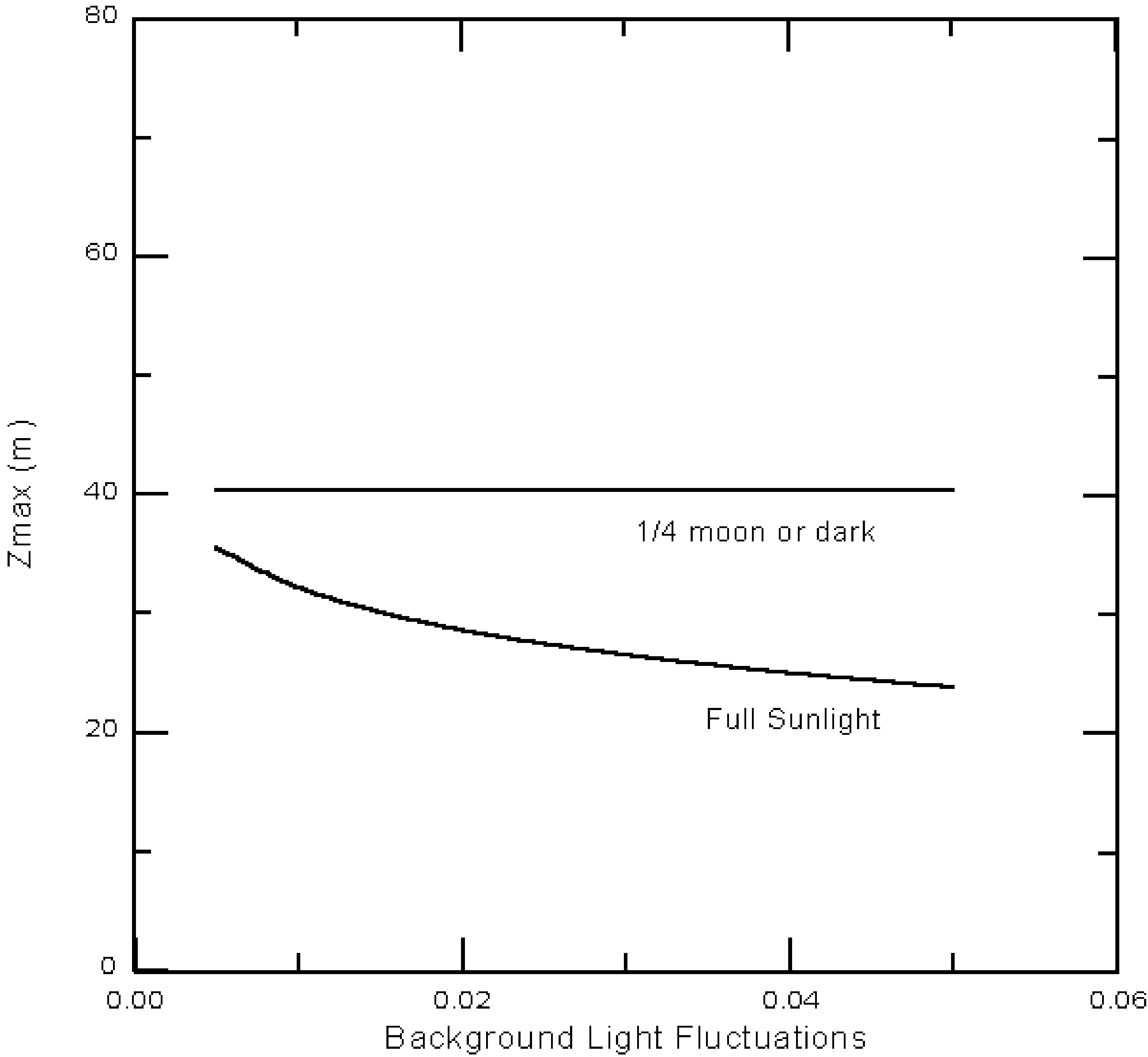


**Figure 23** $Z_{max}$ vs background light fluctuations for 1/4 moon or darker and full sunlight. Background light fluctuations are a source of noise and for large fluctuations will limit the maximum detection depth. The plot shows that for night time operations background light fluctuations are not a problem. During the day, in full sunlight, fluctuations are strong enough to contribute to the noise and affect the $z_{max}$

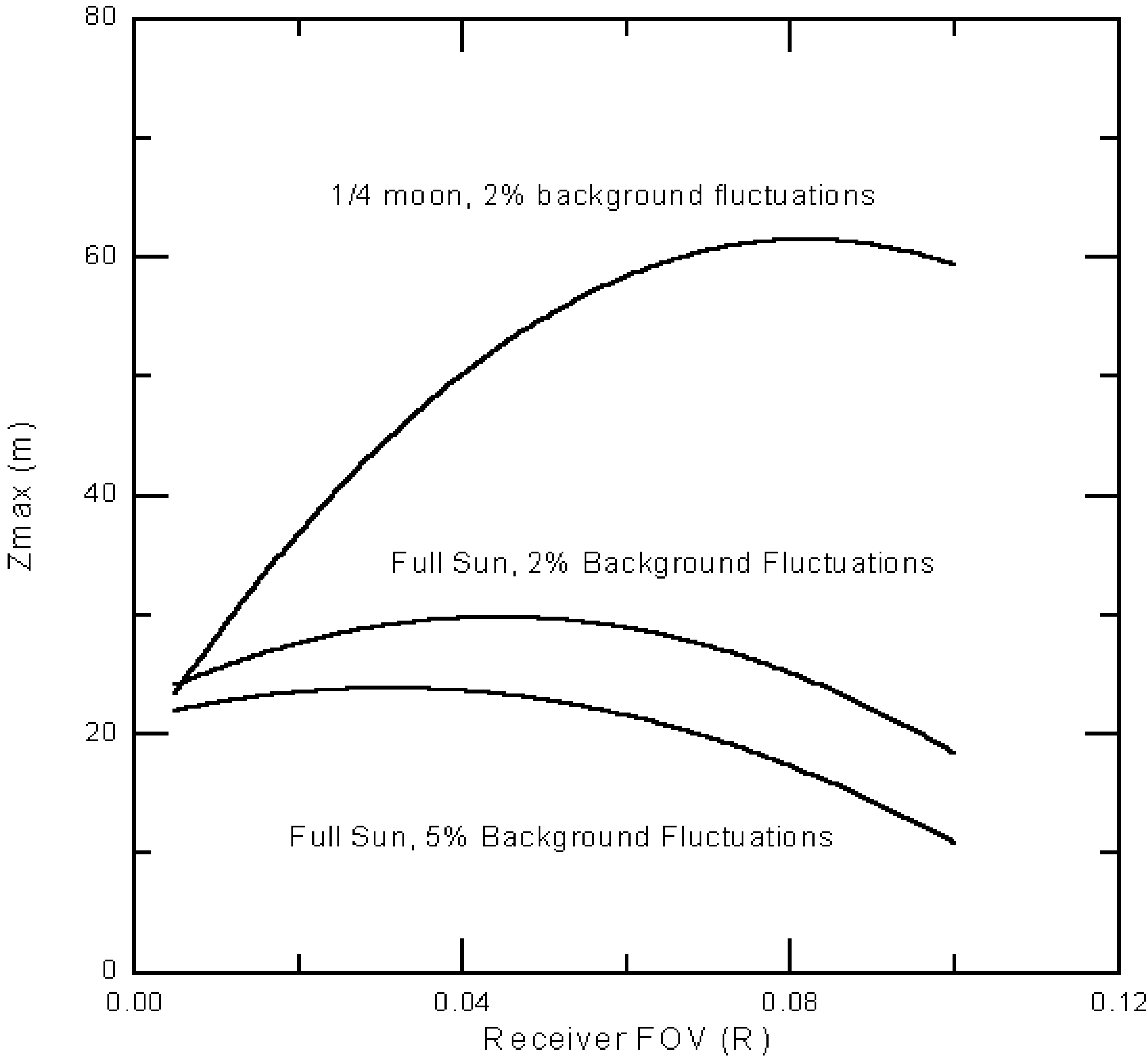


**Figure 24** $Z_{max}$ vs FOV for 1/4 moon, 2% background light fluctuations, full sun, 2% background light fluctuations and full sun, 5% background light fluctuations. The plot indicates that increasing the FOV during the day does not change the $z_{max}$ a lot. Increasing the FOV at night can significantly increase $z_{max}$ from a minimum of 24 m at 5 mR to a maximum of just over 60 m at a FOV of about 80 mR. This graph also indicates that there is an optimum FOV for a given background light level.

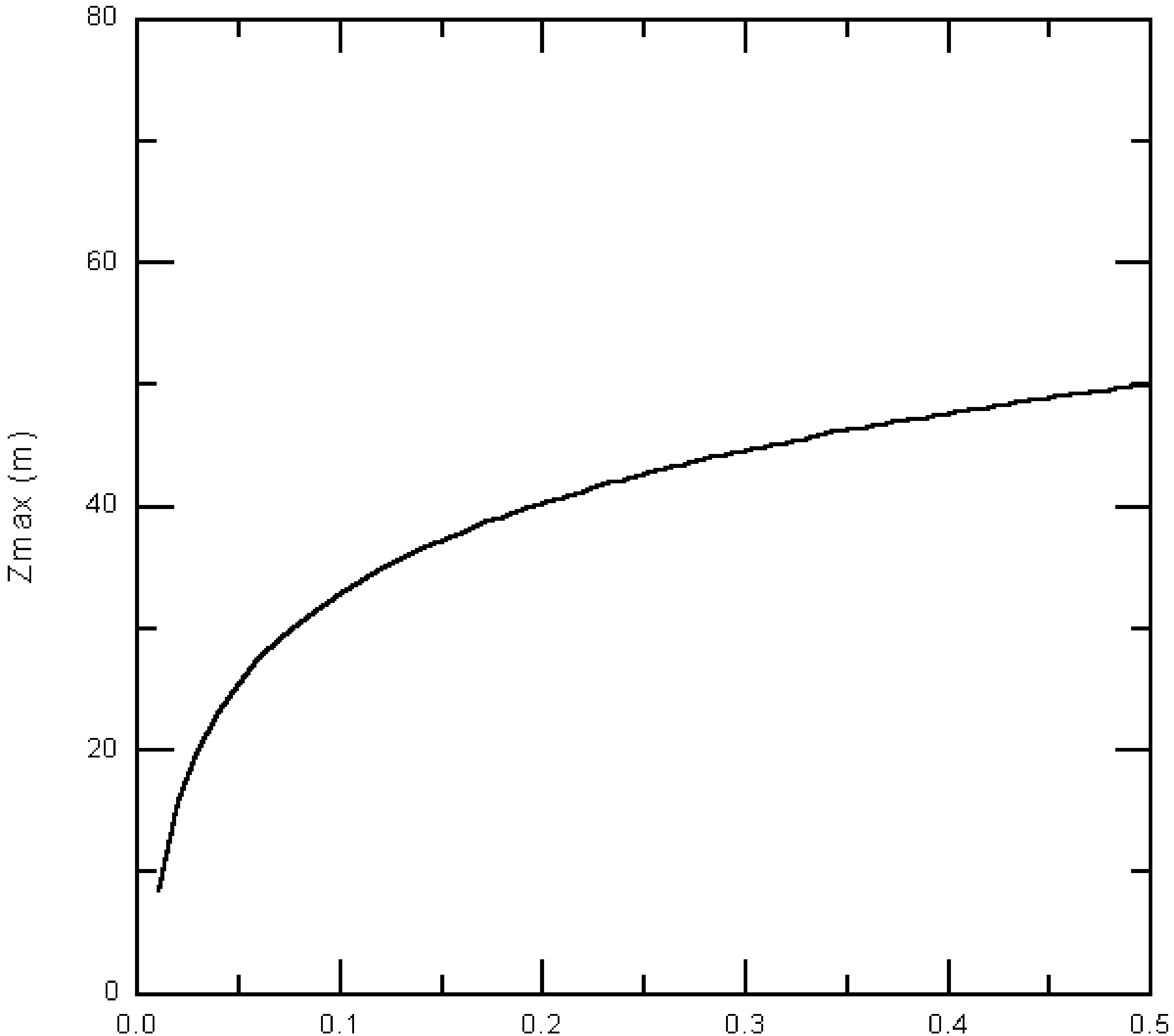


**Figure 25** $Z_{max}$ vs receiver diameter. This shows that a bigger diameter receiver is better but that increasing the diameter from 15 cm to 50 cm only increases $z_{max}$ another 10 m.

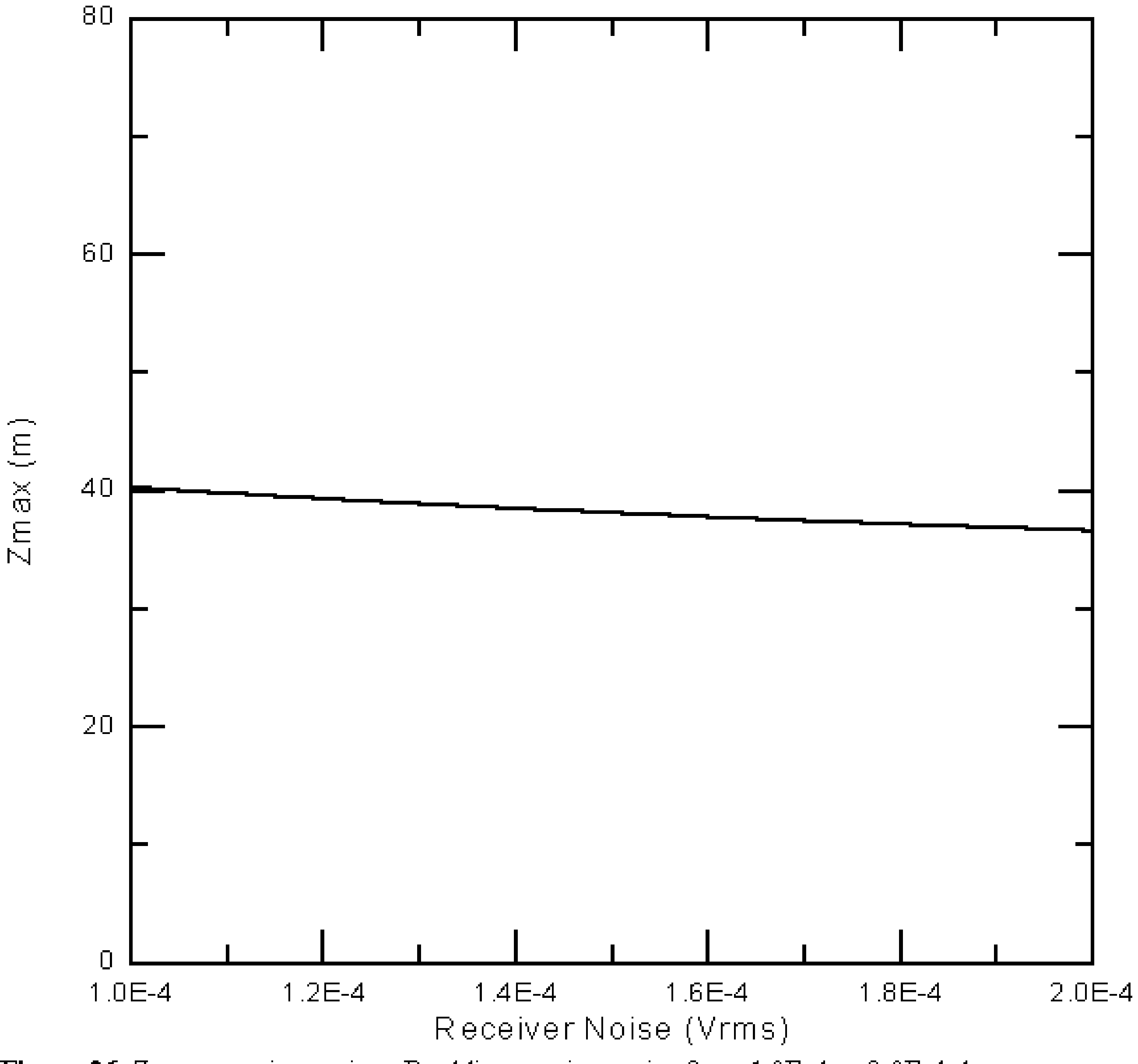


**Figure 26** $Z_{max}$ vs receiver noise. Doubling receiver noise from 1.0E-4 to 2.0E-4 decreases $z_{max}$ from 40 m to about 36 m.

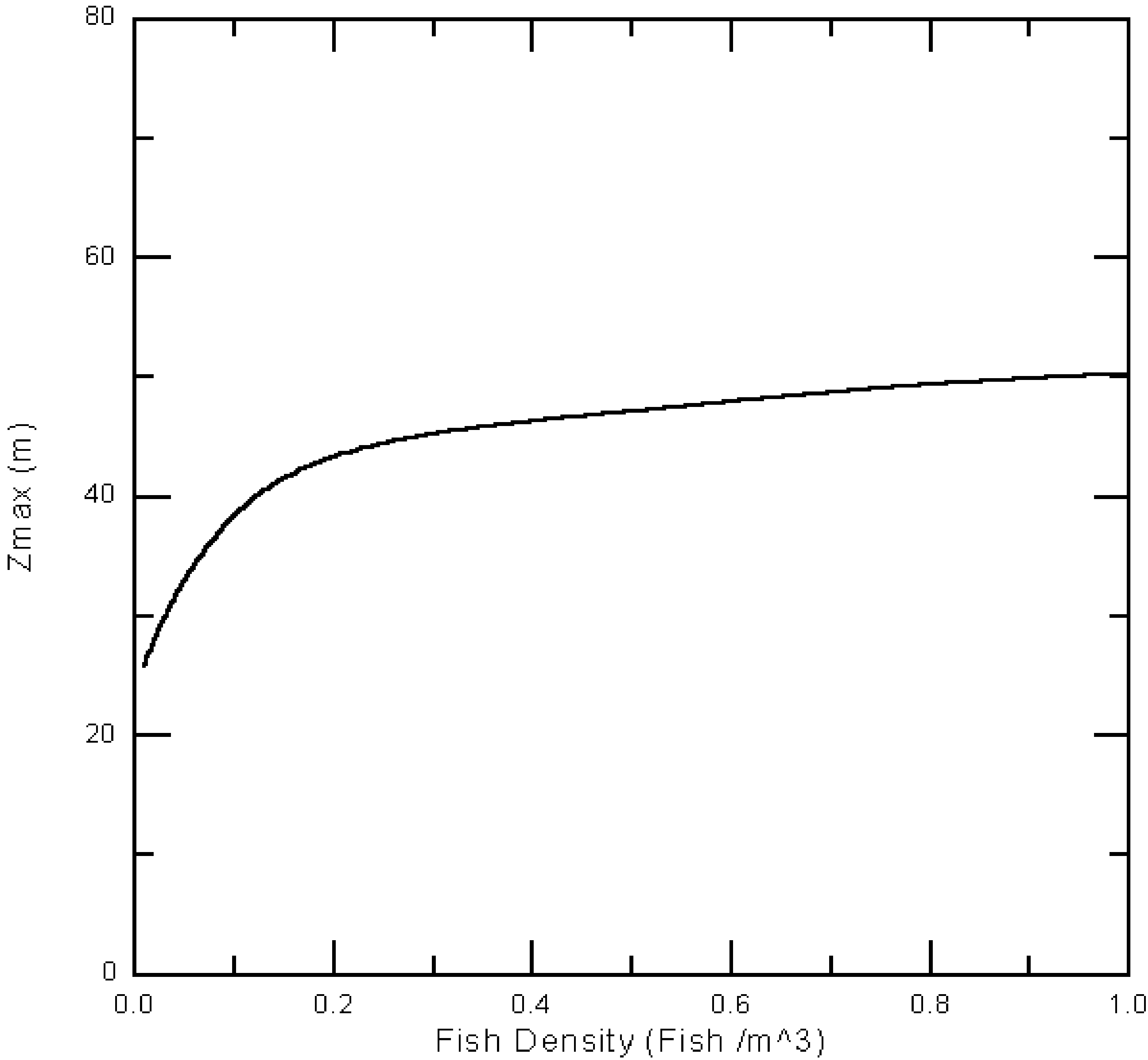


**Figure 27** $Z_{max}$ vs fish density. The formula for fish density is 1/(packing coefficient*fish length)$^3$ = fish density (fish/m^3), with the average fish length equal to 1 m. The packing coefficient is approximately the fish spacing in body lengths. A fish density of 1.0 is equal to 1 body length spacing. A 0.125 fish density is equal to 2 body length spacing and 0.008 fish density is equal to a 5 body lengths spacing.

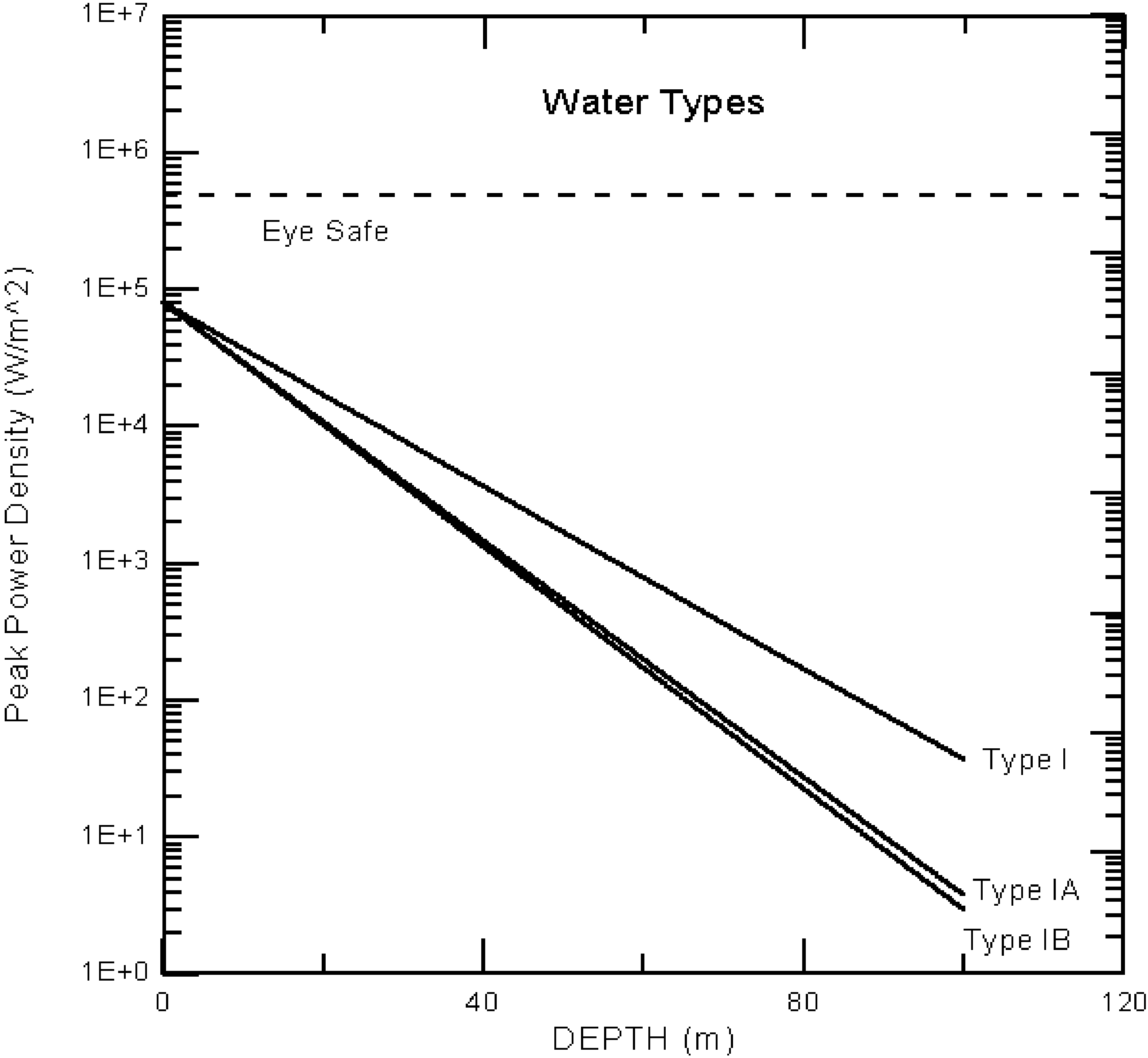


**Figure 28** Peak power density vs depth for the three Jerlov water types. Type I water is the cleanest and type IB is the dirtiest. Cleaner water allows more of the laser power to get deeper and possibly be scattered back from fish.

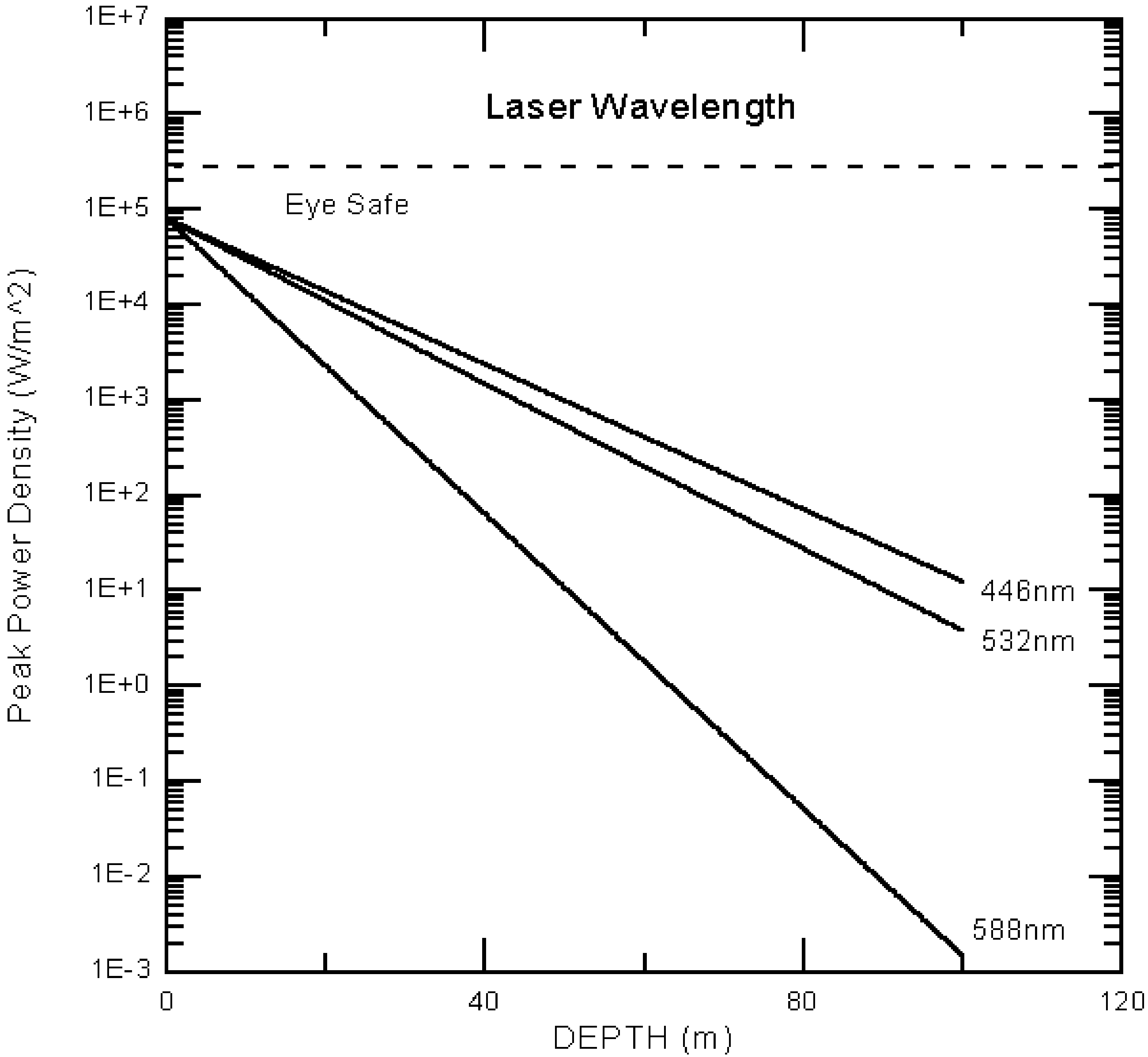


**Figure 29** Peak power density vs depth for the three different laser wavelengths. 588 nm is more strongly absorbed than either 532 nm or 446 nm with 446 nm being the least absorbed.

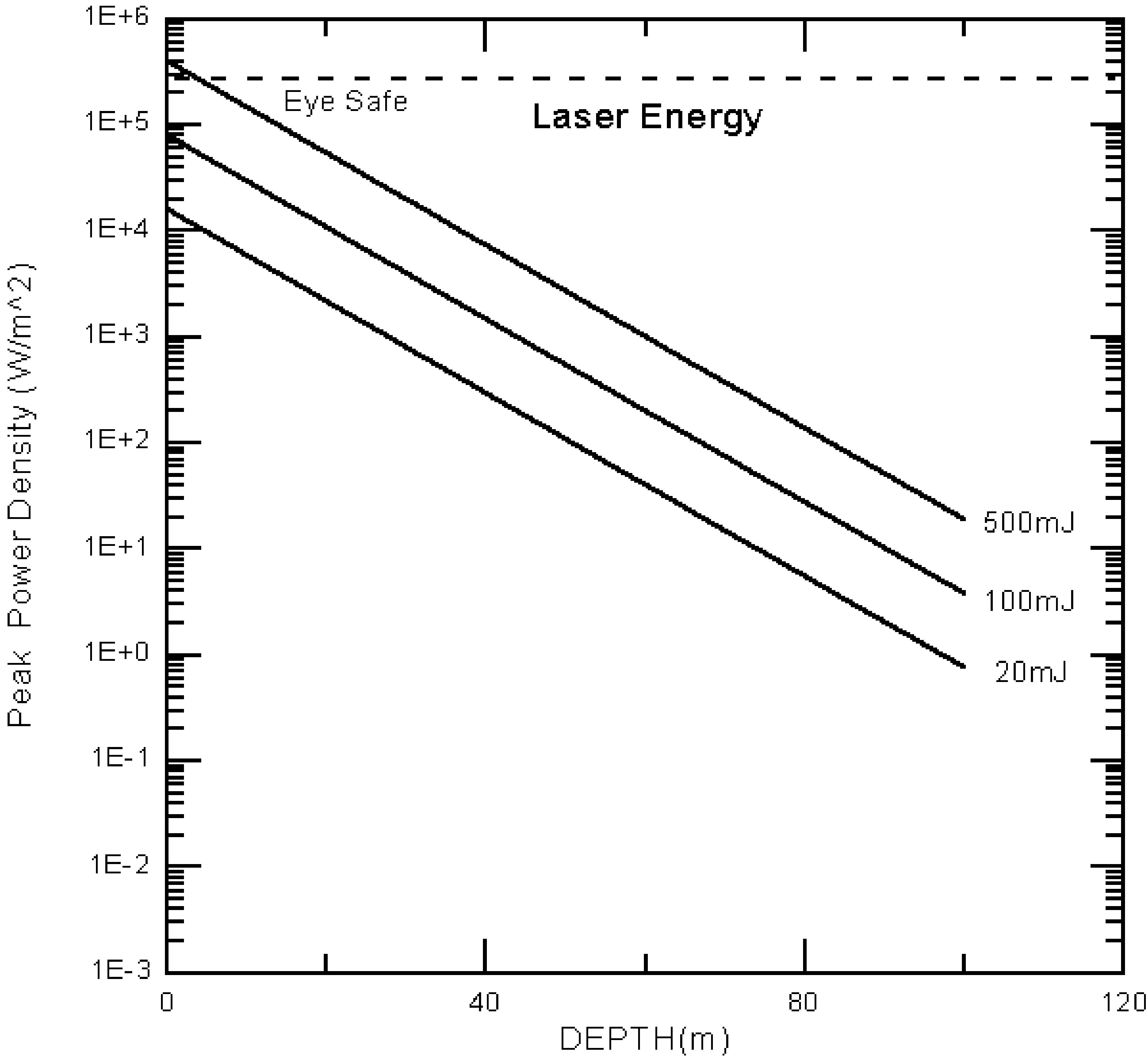


**Figure 30** Peak power density vs depth for three different laser energy levels. While the 20 mJ and 100 mJ energy pulses are eye-safe at the surface, the 500 mJ energy pulse doesn't become eye safe until 5 m below the surface.

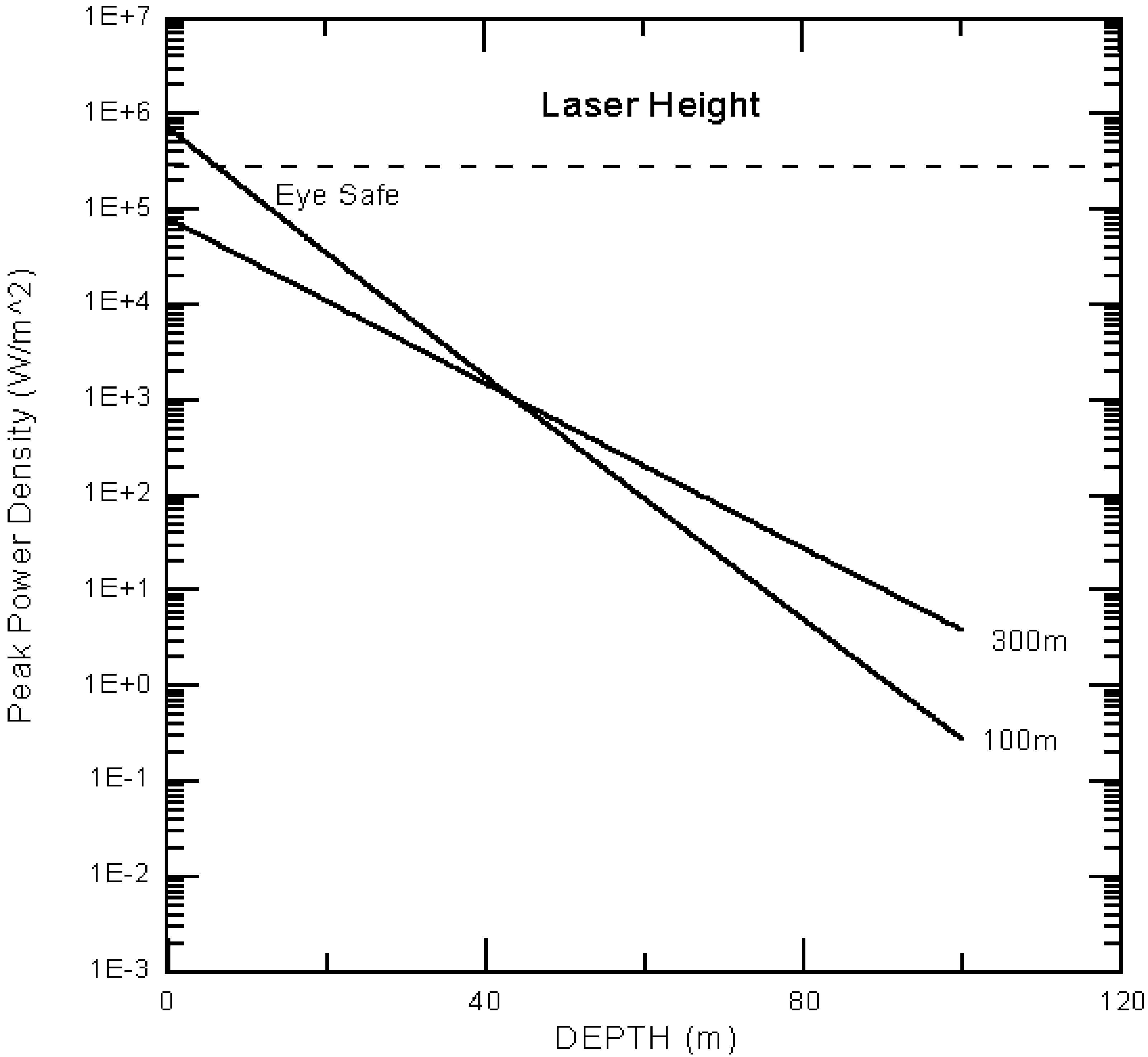


**Figure 31** Peak power density vs depth for two different laser heights. Flying at 100 m and using 100 mJ laser energy produces a non eye safe condition at the surface and does not become eye safe until about 10 m below the surface. Increasing the altitude to 300 m will produce an eye safe condition at the surface.

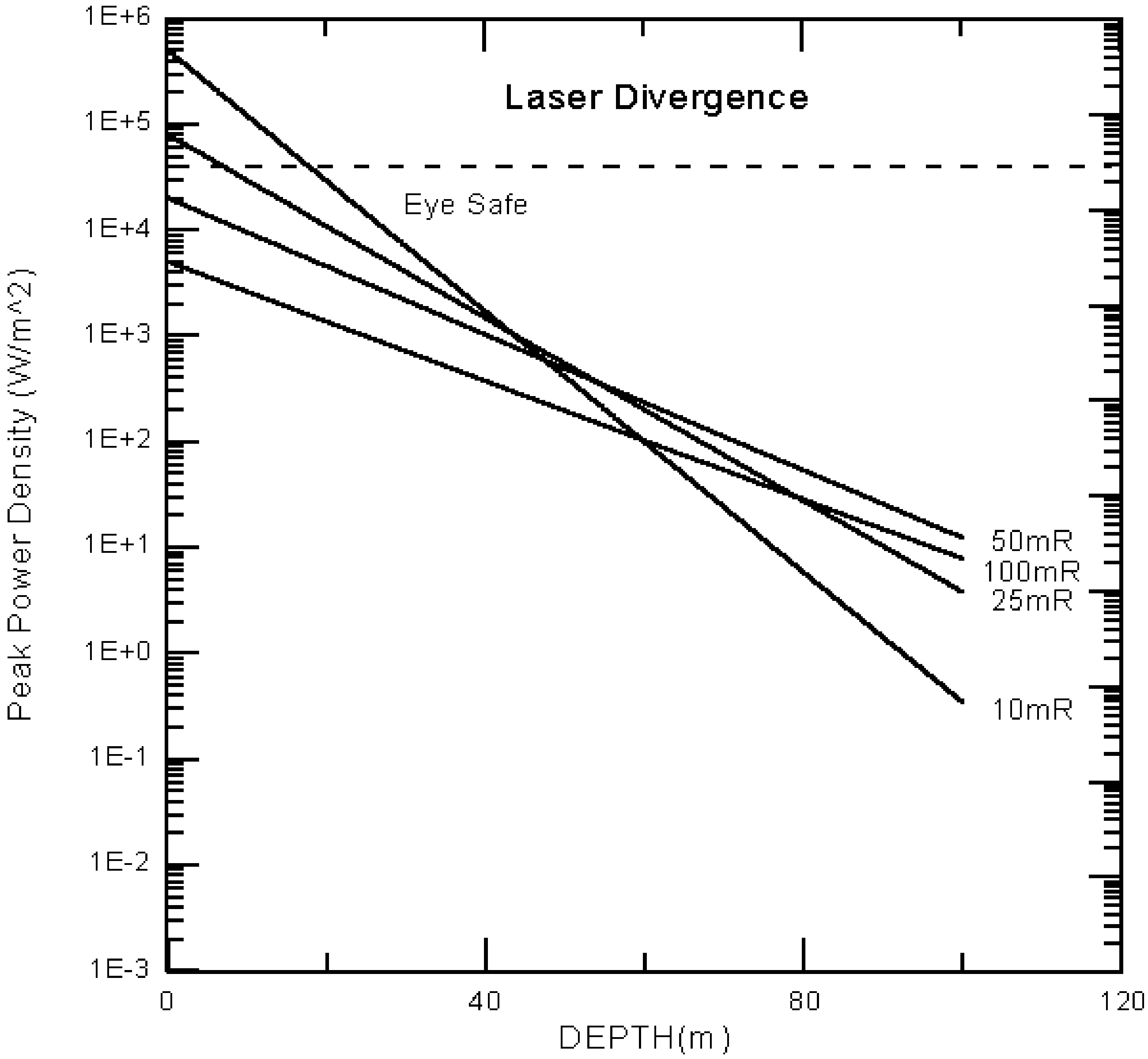


**Figure 32** Peak power density vs depth for four different laser divergences. The 100 mR and 50 mR divergences are eye safe at the surface while the 25 mR and the 10 mR are not.

| | | | | | | |
|---|---|---|---|---|---|---|
| TRANSMITTER | | | RECEIVER | | | |
| | | | Neutral Density (ND) | 0 | | |
| laser energy per pulse (E) | 0.1 | Joules | receiver diameter (D) | 0.2 | m | |
| beam divergence (DIV) | 0.025 | radians | Rx Aperture area (Ra) | 0.0314159 | m^2 | |
| laser height (H) | 300 | meters | receiver FOV(FOV) | 0.025 | radians | |
| pulse length (TAO) | 1.50E-09 | Seconds | receiver bandwidth (B) | 100000000 | Hz | |
| Sampling Interval (SI) | 1.00E-09 | Seconds | detector load (R) | 50 | ohms | |
| range element (DZ) | 0.112782 | meters | optical filter bandwidth (dlambda) | 10 | nm | |
| | | | receiver transmission (Tr) | 0.05 | | |
| | | | Rx water spot size (RxSS) | 44.178646691 | m^2 | |
| | | | TX,RX ANGLE MATCH | | | |
| SEAWATER CHARACTERISTICS | | | Tx,Rx angle match (Match) | 1 | | |
| diffuse attenuation (Kd) | 0.058 | per m | Angle Match (Am) | 1 | | |
| water backscatter (bb) | 0.00616 | per m | | | | |
| water scattering coef (b) | 0.136001 | per m | | | | |
| Lidar attenuation Coef (LAC) | 0.093861 | per m | LOG AMPLIFIER | | | |
| | | | Maximum output (LAmax) | -0.54 | Volts | |
| refractive index (Ri) | 1.33 | | Minimum output (LAmin) | 0 | Volts | |
| Water Backscatter coef(WBC) | 0.000695 | DZ | Output noise voltage (LAn) | 4E-03 | Volts rms | |
| Diffuse Attn coef contant (KDC) | 0.006541 | DZ | Minimum Input voltage (LAinmin) | -0.00015 | Volts | |
| Water Scattering Coef (Wb) | 0.015338 | DZ | Maximum Input voltage(LAinmax) | -2.5 | Volts | |
| Lidar attenuation Coef (LACC) | 0.010586 | DZ | LogAmp output noise converted to | 0.0001393157 | Volts rms | |
| | | | input noise (LAi) | | | |
| FLAGS AND VARIABLES | | | | | | |
| Water type flag (WTF) | | | | | | |
| 0 for type1, 1 for type 1A, | | | | | | |
| and 2 for type 1B | 1 | | | | | |
| on/off flag (fish) | 1 | | | | | |
| Fish Type Flag (FT) | | | | | | |
| 0 for Sardines,1 for Anchovies | 2 | | BACKGROUND | | | |
| 2 for Tuna | | | LIGHT LEVELS | | | |
| Detector flag (Df) | | | Watts/m^2*nm | Sun | Blue sky | total |
| 0 for MCP 1for R647 | 2 | | Direct sun | 1.12 | 0.28 | 1.4 |
| 2 for R5800, 3 for R980 | | | full daylight not direct | 0.112 | 0.028 | 0.14 |
| Detector responsivity (GD) | 194.5604 | | overcast | 0.0112 | 0.0028 | 0.014 |
| Detector dark Current (DC) | 1.5E-08 | | very dark day | 0.00112 | 0.00028 | 0.0014 |
| Detector current gain (DCG) | 7782.417 | | twilight | 0.000112 | 2.8E-05 | 0.00014 |
| | | | Deep Twilight | 1.12E-05 | 2.8E-06 | 1.4E-05 |
| | | | Full moon | 1.12E-06 | 2.8E-07 | 1.4E-06 |
| | | | Quarter moon | 1.12E-07 | 2.8E-08 | 1.4E-07 |
| Polarization Flag (PF) | | | Moonless, clear | 1.12E-08 | 2.8E-09 | 1.4E-08 |
| 0 for UnPol, 1 for CoPol, 2 for XPol | 0 | | Moonless, overcast | 1.12E-09 | 2.8E-10 | 1.4E-09 |
| | | | Light Level Sun (LLS) | 1.12E-07 | | |
| | | | Light Level Bluesky (LLB) | 2.80E-08 | | |
| ATMOSPHERIC PARAMETERS | | | BACKGROUND LIGHT VOLTAGES | | | |
| Atmospheric backscatter coef (ABC) | 1E-12 | per m | | | | |
| Surface Return (SR) | 2E-07 | | Sun Diffuse (BVSD) | 5.10721E-08 | Volts | |
| | | | Blue Sky Glint (BVBG) | 1.083784E-08 | Volts | |
| | | | Blue Sky Diffuse (BVBD) | 1.14993E-12 | Volts | |
| | | | Total Background voltage (VB) | 6.191109E-08 | Volts | |
| | | | Background Light Fluctuations(BLF) | | | |
| | | | from .01 to .1 | 2.000000E-02 | | |

**Figure 33** Columns A through G of the variables page.

| | | | | | |
|---|---|---|---|---|---|
| DETECTORS | | | | | |
| MCP (R5916U) | | | FISH CHARACTERISTICS | | |
| MCP responsivity (MCPga) | 674.333 | A/W | Sardines | | |
| MCP dark current (MCPdc) | 5E-10 | A | Sardine Length (SL) | 0.2 | m |
| MCP current gain (MCPg) | 22477.8 | | Sardine packing coef (SPC) | 2.44 | |
| Det dia (MCPdia) | 0.01 | meters | Sardine area coef (SAC) | 0.1 | |
| rise time (MCPrt) | 1.8E-10 | Seconds | Sardine laser reflection (SLR) | 0.126 | |
| Radiant Sensitivity (MCPrs) | 0.03 | A/W | Sardine Polarization Coef Xpol (SPCX) | 0.23 | |
| MCP Voltage (MCPV) | -2500 | Volts | Sardine Polarization Coef CoPol (SPCC) | 0.77 | |
| max supply voltage = -3400V | | | Sardine Height Coef (SHC) | 0.2 | |
| peak output current = 350ma @ | | | Anchovy | | |
| 10 Hz rep, 220 ma @ 30 Hz rep | | | Anchovy length (AL) | 0.1 | m |
| | | | Anchovy packing coef (APC) | 2.44 | |
| | | | Anchovy area coef (AAC) | 0.1 | |
| R647 1/2" | | | Anchovy Laser reflection (ALR) | 0.126 | |
| responsivity (R647ga) | 5.83984 | A/W | Anchovy Polarization Coef Xpol (APCX) | 0.23 | |
| dark current (R647dc) | 1.5E-08 | A | Anchovy Polarization Coef CoPol (APCC) | 0.77 | |
| current gain (R647g) | 224.609 | | Anchovy Height Coef (AHC) | 0.2 | |
| photocathode dia (R647dia) | 0.01 | meters | Yellowfin Tuna | | |
| rise time (R647rt) | 2.5E-09 | Seconds | Tuna length (TL) | 1 | m |
| cathode radiant sensitivity(R647rs) | 0.026 | A/W | Tuna packing coef (TPC) | 2 | 1=1fish/m^3, 2=1fish/8m^3, 5=1fish/125m^3 |
| R647 Voltage (R647V) | -320 | Volts | Tuna area coef (TAC) | 0.1 | |
| max supply voltage = -1200V | | | Tuna Laser reflection(TLR) | 0.13 | |
| Peak output current = 3 ma | | | Tuna Polarization Coef Xpol (TPCX) | 0.3 | |
| | | | Tuna Polarization Coef CoPol (TPCC) | 0.7 | |
| R5800HA 1" | | | Tuna Height Coef (THC) | 0.2 | Standard Fish School |
| Responsivity (R5800ga) | 194.56 | A/W | | | is 16.5 Tons = |
| dark current (R5800dc) | 1.5E-08 | A | FISH DENSITY CALCULATIONS | | 15,000 Kgms |
| current gain (R5800g) | 7782.42 | | length (L) | 1 | m |
| photo cathode dia | 0.021 | meters | Packing coef (PC) | 2 | |
| rise time | 1.7E-09 | S | Area Coef (AC) | 0.1 | |
| Radiant Sensitivity(calculated) | 0.025 | A/W | Laser Reflection (LR) | 0.13 | |
| R5800 Voltage (R5800V) | -600 | Volts | Height Coef(HC) | 0.2 | |
| max supply voltage = -1800V | | | Weight of 1 Fish(WF) | 20 | Kgms |
| max output current = 100 ma | | | Number of Fish in School (NFS) | 750 | |
| | | | Individual Fish area (FA) | 0.1 | m^2 |
| | | | School Reflective Area (SRA) | 75 | m^2 |
| R980 1.5" | | | Volume 1 fish occupies (FV) | 8 | m^3 Fish-- area around |
| Responsivity (R980ga) | 1.97826 | A/W | Fish School Volume (FSV) | 6000 | m^3 |
| dark current (R980dc) | 5E-09 | A | Fish School Diameter (FSD) | 27.6395 | meters |
| current gain (R980g) | 79.13 | | Number of fish in a range cell (FN) | 0.0141 | in 1m^2 of beam |
| photo cathode dia | 0.034 | meters | Area of fish in beam (FB) | 0.00141 | m^2 in 1 m^2 of beam |
| rise time | 2.8E-09 | S | Reflectivity coef (FR) | 0.00018 | in 1m^2 of beam |
| Radiant Sensitivity (R980rs) | 0.026 | A/W | Attenuation coef (FAC) | 0.00141 | |
| R980 Voltage (R980V) | -350 | Volts | | | |
| max supply voltage = -1200V | | | Fish Polarization Coef Xpol (FPCX) | 0.3 | |
| peak output current = 1 ma | | | Fish Polarization Coef CoPol (FPCC) | 0.7 | |
| | | | | | |
| | | | Water Polarization Coef Xpol (WPCX) | 0.1 | |
| | | | Water Polarization Coef CoPol (WPCC) | 0.9 | |
| | | | | | |
| | | | FISH SCHOOL PARAMETERS | | |
| | | | School Top (ST) | 50 | meters |
| | | | School Bottom (SB) | 60 | meters |

**Figure 34** Columns H through N of the variables page.

| TRANSMITTED PULSE POWER | | | |
|---|---|---|---|
| peak power per nanosecond | | | |
| Time in nanoseconds | Laser energy per nanosecond | Laser power (W) | Pulse |
| 0 | 0.000000E+00 | 0.000000E+00 | 12326 |
| 1 | 1.664085E-03 | 1.664085E+06 | 14670 |
| 2 | 4.201395E-03 | 4.201395E+06 | 17453 |
| 3 | 5.789512E-03 | 5.789512E+06 | 20755 |
| 4 | 6.684756E-03 | 6.684756E+06 | 24671 |
| 5 | 7.082483E-03 | 7.082483E+06 | 29310 |
| 6 | 7.130630E-03 | 7.130630E+06 | 34805 |
| 7 | 6.940373E-03 | 6.940373E+06 | 41307 |
| 8 | 6.594507E-03 | 6.594507E+06 | 48997 |
| 9 | 6.154000E-03 | 6.154000E+06 | 58086 |
| 10 | 5.663128E-03 | 5.663128E+06 | 68818 |
| 11 | 5.153469E-03 | 5.153469E+06 | 81480 |
| 12 | 4.647009E-03 | 4.647009E+06 | 96408 |
| 13 | 4.158547E-03 | 4.158547E+06 | 113988 |
| 14 | 3.697549E-03 | 3.697549E+06 | 134674 |
| 15 | 3.269574E-03 | 3.269574E+06 | 158987 |
| 16 | 2.877352E-03 | 2.877352E+06 | 187532 |
| 17 | 2.521621E-03 | 2.521621E+06 | 221004 |
| 18 | 2.201736E-03 | 2.201736E+06 | 260204 |
| 19 | 1.916141E-03 | 1.916141E+06 | 306047 |
| 20 | 1.662711E-03 | 1.662711E+06 | 359580 |
| 21 | 1.438999E-03 | 1.438999E+06 | 421991 |
| 22 | 1.242419E-03 | 1.242419E+06 | 494624 |
| 23 | 1.070369E-03 | 1.070369E+06 | 578991 |
| 24 | 9.203207E-04 | 9.203207E+05 | 676782 |
| 25 | 7.898717E-04 | 7.898717E+05 | 789872 |
| 26 | 6.767820E-04 | 6.767820E+05 | 920321 |
| 27 | 5.789911E-04 | 5.789911E+05 | 1070369 |
| 28 | 4.946241E-04 | 4.946241E+05 | 1242419 |
| 29 | 4.219911E-04 | 4.219911E+05 | 1438999 |
| 30 | 3.595802E-04 | 3.595802E+05 | 1662711 |
| 31 | 3.060471E-04 | 3.060471E+05 | 1916141 |
| 32 | 2.602036E-04 | 2.602036E+05 | 2201736 |
| 33 | 2.210039E-04 | 2.210039E+05 | 2521621 |
| 34 | 1.875317E-04 | 1.875317E+05 | 2877352 |
| 35 | 1.589871E-04 | 1.589871E+05 | 3269574 |
| 36 | 1.346740E-04 | 1.346740E+05 | 3697549 |
| 37 | 1.139884E-04 | 1.139884E+05 | 4158547 |
| 38 | 9.640758E-05 | 9.640758E+04 | 4647009 |
| 39 | 8.148027E-05 | 8.148027E+04 | 5153469 |
| 40 | 6.881773E-05 | 6.881773E+04 | 5663128 |
| 41 | 5.808575E-05 | 5.808575E+04 | 6154000 |
| 42 | 4.899748E-05 | 4.899748E+04 | 6594507 |
| 43 | 4.130717E-05 | 4.130717E+04 | 6940373 |
| 44 | 3.480459E-05 | 3.480459E+04 | 7130630 |
| 45 | 2.931014E-05 | 2.931014E+04 | 7082483 |
| 46 | 2.467059E-05 | 2.467059E+04 | 6684756 |
| 47 | 2.075541E-05 | 2.075541E+04 | 5789512 |
| 48 | 1.745348E-05 | 1.745348E+04 | 4201395 |
| 49 | 1.467034E-05 | 1.467034E+04 | 1664085 |
| 50 | 1.232576E-05 | 1.232576E+04 | 0 |
| | 0.0999360487 | | |

**Figure 35** Columns O through S of the variables page. This section contains the laser transmitter pulse information. The first column is the time in nanoseconds. The second column is the laser energy emitted at that time. The third column is the laser energy converted to power and the fourth column is the laser power inverted in time.

| Variable Names | Location | Variable Names | Location |
|---|---|---|---|
| Am | B:E14 | MCPV | B:I9 |
| APC | B:L13 | ND | B:E2 |
| APCC | B:L17 | NFS | B:L35 |
| APCX | B:L16 | PC | B:L30 |
| b | B:B16 | PF | B:B43 |
| BB | B:B15 | PMAX | B:Q11 |
| BLF | B:E56 | R | B:E7..E7 |
| BVBD | B:E52 | R5800dc | B:I28 |
| BVBG | B:E51 | R5800g | B:I29 |
| BVSD | B:E50 | R5800gd | B:I27 |
| C | E:L3 | R5800V | B:I33 |
| D | B:E3 | R647dc | B:I17 |
| DC | B:B37 | R647g | B:I18 |
| DCG | B:B38 | R647gd | B:I16 |
| Df | B:B34 | R647rs | B:I21 |
| DIV | B:B4 | R647rt | B:I20 |
| divide by | F:I377 | R647V | B:I22 |
| DLAMBDA | B:E8 | R980dc | B:I40 |
| DZ | B:B8 | R980g | B:I41 |
| E | B:B3 | R980gd | B:I39 |
| FA | B:L36 | R980rs | B:I44 |
| FAC | B:L44 | R980V | B:I45 |
| FB | B:L42 | Ra | B:E4 |
| FISH | B:B29 | Ri | B:B19 |
| FN | B:L41 | RxSS | B:E10 |
| FOV | B:E5 | S/N=1 | E:R3 |
| FPCC | B:L47 | SAC | B:L6 |
| FPCX | B:L46 | SB | B:L54 |
| FR | B:L43 | SHC | B:L10 |
| FSD | B:L40 | SI | B:B7 |
| FSV | B:L39 | SL | B:L4 |
| FT | B:B31 | SLR | B:L7 |
| FV | B:L38 | SPC | B:L5 |
| GD | B:B36 | SPCC | B:L9 |
| H | B:B5 | SPCX | B:L8 |
| HC | B:L33 | SR | B:B50 |
| KD | B:B14 | SRA | B:L37 |
| KDC | B:B21 | ST | B:L53 |
| L | B:L29..L29 | TAC | B:L22 |
| LAC | B:B17 | THC | B:L26 |
| LACC | B:B23 | TL | B:L20 |
| LAi | B:E23 | TLR | B:L23 |
| LAn | B:E20 | TPC | B:L21 |
| LLB | B:E46 | TPCC | B:L25 |
| LLS | B:E45 | TPCX | B:L24 |
| LR | B:L32 | TR | B:E9..E9 |
| Match | B:E13 | VB | B:E54 |
| MCPdc | B:I4 | Wb | B:B22 |
| MCPdia | B:I6 | WBC | B:B20 |
| MCPg | B:I5 | WF | B:L34 |
| MCPgd | B:I3 | WPCC | B:L50 |
| MCPrs | B:I8 | WPCX | B:L49 |
| MCPrt | B:I7 | WRC | E:I10 |
| | | WTF | B:B28 |

Figure 36. Columns A-D, rows 1-122 of the VARIABLE LOCATION page (D).

| | | | | | | | |
|---|---|---|---|---|---|---|---|
| | | Volume Scattering Function (m-1 sr-1) | | | | | |
| | | p.111 Light and Water | | | | | |
| | | | | | | | |
| | | | | | Case I | Case IA | Case IB |
| | Scattering | Scattering | Clear | | | Scaled | Scaled |
| | angle(Rad) | angle(deg) | Ocean | | b=.037 | for b=.136 | for b=.25 |
| | | 0 | | | | | |
| 0 | 0.001745329 | 0.1 | 53.18 | 0.092817 | 0.002362 | 0.00887 | 0.016305 |
| 0 | 0.002199115 | 0.126 | 40.42 | 0.088888 | 0.002778 | 0.0104318 | 0.019178 |
| 0 | 0.00275762 | 0.158 | 30.73 | 0.084742 | 0.00352 | 0.013217 | 0.024296 |
| 0 | 0.00349066 | 0.2 | 23.74 | 0.082868 | 0.00414 | 0.0155442 | 0.028574 |
| 0 | 0.004380776 | 0.251 | 18.14 | 0.079487 | 0.00502 | 0.0188518 | 0.034654 |
| 0 | 0.00551524 | 0.316 | 13.6 | 0.075007 | 0.00591 | 0.022193 | 0.040796 |
| 0 | 0.00694641 | 0.398 | 9.954 | 0.069144 | 0.006794 | 0.0255107 | 0.046895 |
| 0 | 0.0087441 | 0.501 | 7.179 | 0.062773 | 0.007738 | 0.0290571 | 0.053414 |
| 0 | 0.011013028 | 0.631 | 5.11 | 0.056275 | 0.008642 | 0.0324513 | 0.059653 |
| 1 | 0.013857914 | 0.794 | 3.591 | 0.049762 | 0.009616 | 0.0361081 | 0.066375 |
| 1 | 0.017453293 | 1 | 2.498 | 0.043596 | 0.010537 | 0.0395664 | 0.072732 |
| 1 | 0.021973895 | 1.259 | 1.719 | 0.03777 | 0.011436 | 0.0429426 | 0.078939 |
| 1 | 0.027663489 | 1.585 | 1.171 | 0.03239 | 0.012178 | 0.0457229 | 0.084049 |
| 1 | 0.034819019 | 1.995 | 0.7758 | 0.027007 | 0.012745 | 0.0478573 | 0.087973 |
| 1 | 0.043842671 | 2.512 | 0.5087 | 0.022296 | 0.013234 | 0.0496928 | 0.091347 |
| 1 | 0.055187311 | 3.162 | 0.334 | 0.018423 | 0.013787 | 0.0517726 | 0.09517 |
| 1 | 0.069481558 | 3.981 | 0.2196 | 0.015246 | 0.014372 | 0.0539666 | 0.099201 |
| 1 | 0.087475902 | 5.012 | 0.1446 | 0.012633 | 0.014991 | 0.056291 | 0.103476 |
| 1 | 0.110130276 | 6.31 | 0.09522 | 0.010465 | 0.015633 | 0.0587026 | 0.107909 |
| 1 | 0.138631302 | 7.943 | 0.06282 | 0.008681 | 0.016362 | 0.0614384 | 0.112936 |
| 1 | 0.174532925 | 10 | 0.04162 | 0.007227 | 0.031255 | 0.1173635 | 0.215742 |
| | | 15 | 0.02038 | 0.005275 | 0.022584 | 0.0848002 | 0.155886 |
| | | 20 | 0.01099 | 0.003759 | 0.015912 | 0.0597489 | 0.109833 |
| | | 25 | 0.006166 | 0.002606 | 0.011375 | 0.0427123 | 0.078515 |
| | | 30 | 0.003888 | 0.001944 | 0.008703 | 0.03268 | 0.060073 |
| | | 35 | 0.00268 | 0.001537 | 0.006895 | 0.0258895 | 0.047591 |
| | | 40 | 0.001899 | 0.001221 | 0.005477 | 0.0205664 | 0.037806 |
| | | 45 | 0.001372 | 0.00097 | 0.004379 | 0.0164425 | 0.030225 |
| | | 50 | 0.00102 | 0.000781 | 0.003527 | 0.0132433 | 0.024344 |
| | | 55 | 0.0007683 | 0.000629 | 0.002878 | 0.0108088 | 0.019869 |
| | | 60 | 0.0006028 | 0.000522 | 0.002411 | 0.0090552 | 0.016646 |
| | | 65 | 0.0004883 | 0.000443 | 0.002062 | 0.0077439 | 0.014235 |
| | | 70 | 0.0004069 | 0.000382 | 0.001791 | 0.0067242 | 0.012361 |
| | | 75 | 0.0003457 | 0.000334 | 0.001578 | 0.0059258 | 0.010893 |
| | | 80 | 0.0003019 | 0.000297 | 0.001411 | 0.0052983 | 0.00974 |
| | | 85 | 0.0002681 | 0.000267 | 0.001282 | 0.0048136 | 0.008852 |
| | | 90 | 0.0002459 | 0.000246 | 0.001191 | 0.0044734 | 0.008223 |
| | | 95 | 0.0002315 | 0.000231 | 0.001128 | 0.0042349 | 0.007785 |
| | | 100 | 0.0002239 | 0.00022 | 0.001089 | 0.0040875 | 0.007514 |
| | | 105 | 0.0002225 | 0.000215 | 0.001063 | 0.0039927 | 0.00734 |
| | | 110 | 0.0002239 | 0.00021 | 0.001039 | 0.0039022 | 0.007173 |
| | | 115 | 0.0002265 | 0.000205 | 0.00102 | 0.0038287 | 0.007038 |
| | | 120 | 0.0002339 | 0.000203 | 0.001019 | 0.0038279 | 0.007037 |
| | | 125 | 0.0002505 | 0.000205 | 0.001016 | 0.0038169 | 0.007016 |
| | | 130 | 0.0002629 | 0.000201 | 0.000974 | 0.0036576 | 0.006724 |
| | | 135 | 0.0002662 | 0.000188 | 0.000912 | 0.0034259 | 0.006298 |
| | | 140 | 0.0002749 | 0.000177 | 0.000857 | 0.0032182 | 0.005916 |
| | | 145 | 0.0002896 | 0.000166 | 0.000801 | 0.0030088 | 0.005531 |
| | | 150 | 0.0003088 | 0.000154 | 0.000735 | 0.0027603 | 0.005074 |
| | | 155 | 0.000334 | 0.00014 | 0.000659 | 0.0024754 | 0.00455 |
| | | 160 | 0.0003627 | 0.000124 | 0.000574 | 0.0021542 | 0.00396 |
| | | 165 | 0.0004073 | 0.000105 | 0.000466 | 0.0017511 | 0.003219 |
| | | 170 | 0.0004671 | 8.1E-05 | 0.000308 | 0.0011578 | 0.002128 |
| | | 175 | 0.0004845 | 4.2E-05 | 0.000106 | 0.0003964 | 0.000729 |
| | | 180 | 0.0005019 | 6.1E-20 | | | |
| | | | | | | | |
| | | | | 1.001539 | | | |
| | | | | | | | |
| | | | | blidar= | 0.000106 | | |
| | | | | 1/b= | 27.61043 | meters | |

**Figure 37** Page D columns D through K. This section describes the volume scattering function.

| | | | | | | | | | | |
|---|---|---|---|---|---|---|---|---|---|---|
| | Kd interpolated from table 3.15 p.130 Light and Water | | | | | | | | | |
| | | | | | | b calculated from volume scattering | | | | |
| **Jerlov Water Characteristics** | | | | | | including FOV | | | | LAC |
| | Kd | b | bb | a | c | | | new b | Klaser1 | Klaser2 |
| Case I | 0.054 | 0.036218 | 0.00164 | 0.05236 | 0.088578 | | 0.283366 | 0.031075 | 0.083075 | 0.072737 |
| Case IA | 0.058 | 0.136001 | 0.00616 | 0.05184 | 0.187841 | | 1.064051 | 0.116686 | 0.168686 | 0.093861 |
| Case IB | 0.063 | 0.250001 | 0.011323 | 0.051677 | 0.301678 | | 1.955977 | 0.214497 | 0.266497 | 0.092119 |

**Figure 38** Page D columns M through W. This section summarizes the water characteristics calculated from the volume scattering function.

| | | | | | | | | | | | |
|---|---|---|---|---|---|---|---|---|---|---|---|
| | | | | | | | | | | Constant (C) | 4.86400624 |
| | | | 1nS = | 0.112782 | m | | | | | | |
| | Depth (m) | Air/Water | Area of | Fish | Lidar | Fish | | reflection coeficients | | Laser Average | |
| | | Backscatter | Illumination | Backscatter | Sum LAC | Sum Kd | | WRC | FRC | Power | Normalized |
| time(nS) | | | m^2 | | | | | | | Density(W/m^2) | Signal |
| 0 | -300 | | | | | | | | | | |
| 1 | -299.8872 | 1E-12 | 6.2438E-06 | 0 | 0 | 0 | | 1E-12 | 0 | 2.855083E−11 | 3.824E-10 |
| 2 | -299.7744 | 1E-12 | 2.4975E-05 | 0 | 0 | 0 | | 1E-12 | 0 | 71377079662 | 9.5599E-11 |
| 3 | -299.6617 | 1E-12 | 5.6194E-05 | 0 | 0 | 0 | | 1E-12 | 0 | 31723146516 | 4.2489E-11 |
| 4 | -299.5489 | 1E-12 | 9.9901E-05 | 0 | 0 | 0 | | 1E-12 | 0 | 17844269916 | 2.39E-11 |
| 5 | -299.4361 | 1E-12 | 0.0001561 | 0 | 0 | 0 | | 1E-12 | 0 | 11420332746 | 1.5296E-11 |
| 6 | -299.3233 | 1E-12 | 0.00022478 | 0 | 0 | 0 | | 1E-12 | 0 | 7930786629.1 | 1.0622E-11 |
| 7 | -299.2105 | 1E-12 | 0.00030595 | 0 | 0 | 0 | | 1E-12 | 0 | 5826700380.6 | 7.804E-12 |
| 8 | -299.0977 | 1E-12 | 0.0003996 | 0 | 0 | 0 | | 1E-12 | 0 | 4461067478.9 | 5.975E-12 |
| 9 | -298.985 | 1E-12 | 0.00050575 | 0 | 0 | 0 | | 1E-12 | 0 | 3524794057.4 | 4.721E-12 |
| 10 | -298.8722 | 1E-12 | 0.00062438 | 0 | 0 | 0 | | 1E-12 | 0 | 2855083186.5 | 3.824E-12 |
| 11 | -298.7594 | 1E-12 | 0.0007555 | 0 | 0 | 0 | | 1E-12 | 0 | 2359572881.4 | 3.1603E-12 |
| 12 | -298.6466 | 1E-12 | 0.00089911 | 0 | 0 | 0 | | 1E-12 | 0 | 1982696657.3 | 2.6555E-12 |
| 13 | -298.5338 | 1E-12 | 0.0010552 | 0 | 0 | 0 | | 1E-12 | 0 | 1689398335.2 | 2.2627E-12 |
| 14 | -298.4211 | 1E-12 | 0.00122379 | 0 | 0 | 0 | | 1E-12 | 0 | 1456675095.1 | 1.951E-12 |
| 15 | -298.3083 | 1E-12 | 0.00140486 | 0 | 0 | 0 | | 1E-12 | 0 | 1268925860.7 | 1.6995E-12 |
| 16 | -298.1955 | 1E-12 | 0.00159841 | 0 | 0 | 0 | | 1E-12 | 0 | 1115266869.7 | 1.4937E-12 |
| 17 | -298.0827 | 1E-12 | 0.00180446 | 0 | 0 | 0 | | 1E-12 | 0 | 987918057.61 | 1.3232E-12 |
| 18 | -297.9699 | 1E-12 | 0.00202299 | 0 | 0 | 0 | | 1E-12 | 0 | 881198514.35 | 1.1802E-12 |
| 19 | -297.8571 | 1E-12 | 0.00225401 | 0 | 0 | 0 | | 1E-12 | 0 | 790881769.11 | 1.0593E-12 |
| 20 | -297.7444 | 1E-12 | 0.00249752 | 0 | 0 | 0 | | 1E-12 | 0 | 713770796.62 | 9.5599E-13 |
| 21 | -297.6316 | 1E-12 | 0.00275352 | 0 | 0 | 0 | | 1E-12 | 0 | 647411153.4 | 8.6711E-13 |
| 22 | -297.5188 | 1E-12 | 0.003022 | 0 | 0 | 0 | | 1E-12 | 0 | 589893220.35 | 7.9008E-13 |
| 23 | -297.406 | 1E-12 | 0.00330297 | 0 | 0 | 0 | | 1E-12 | 0 | 539713267.77 | 7.2287E-13 |
| 24 | -297.2932 | 1E-12 | 0.00359643 | 0 | 0 | 0 | | 1E-12 | 0 | 495674164.32 | 6.6388E-13 |
| 25 | -297.1805 | 1E-12 | 0.00390238 | 0 | 0 | 0 | | 1E-12 | 0 | 456813309.84 | 6.1184E-13 |
| 26 | -297.0677 | 1E-12 | 0.00422081 | 0 | 0 | 0 | | 1E-12 | 0 | 422340583.8 | 5.6568E-13 |
| 27 | -296.9549 | 1E-12 | 0.00455173 | 0 | 0 | 0 | | 1E-12 | 0 | 391643784.15 | 5.2455E-13 |
| 28 | -296.8421 | 1E-12 | 0.00489514 | 0 | 0 | 0 | | 1E-12 | 0 | 364168773.79 | 4.8775E-13 |
| 29 | -296.7293 | 1E-12 | 0.00525104 | 0 | 0 | 0 | | 1E-12 | 0 | 339486704.69 | 4.5469E-13 |
| 30 | -296.6165 | 1E-12 | 0.00561942 | 0 | 0 | 0 | | 1E-12 | 0 | 317231465.16 | 4.2489E-13 |
| 31 | -296.5038 | 1E-12 | 0.00600029 | 0 | 0 | 0 | | 1E-12 | 0 | 297095024.61 | 3.9792E-13 |
| 32 | -296.391 | 1E-12 | 0.00639365 | 0 | 0 | 0 | | 1E-12 | 0 | 278816717.43 | 3.7343E-13 |
| 33 | -296.2782 | 1E-12 | 0.0067995 | 0 | 0 | 0 | | 1E-12 | 0 | 262174764.6 | 3.5115E-13 |
| 34 | -296.1654 | 1E-12 | 0.00721784 | 0 | 0 | 0 | | 1E-12 | 0 | 246979514.4 | 3.3079E-13 |
| 35 | -296.0526 | 1E-12 | 0.00764866 | 0 | 0 | 0 | | 1E-12 | 0 | 233068015.22 | 3.1216E-13 |
| 36 | -295.9398 | 1E-12 | 0.00809197 | 0 | 0 | 0 | | 1E-12 | 0 | 220299628.59 | 2.9506E-13 |
| 37 | -295.8271 | 1E-12 | 0.00854777 | 0 | 0 | 0 | | 1E-12 | 0 | 208552460.66 | 2.7933E-13 |
| 38 | -295.7143 | 1E-12 | 0.00901606 | 0 | 0 | 0 | | 1E-12 | 0 | 197720442.28 | 2.6482E-13 |
| 39 | -295.6015 | 1E-12 | 0.00949682 | 0 | 0 | 0 | | 1E-12 | 0 | 187710926.13 | 2.5141E-13 |
| 40 | -295.4887 | 1E-12 | 0.00999008 | 0 | 0 | 0 | | 1E-12 | 0 | 178442699.16 | 2.39E-13 |
| 41 | -295.3759 | 1E-12 | 0.01049583 | 0 | 0 | 0 | | 1E-12 | 0 | 169844329.95 | 2.2748E-13 |
| 42 | -295.2632 | 1E-12 | 0.01101407 | 0 | 0 | 0 | | 1E-12 | 0 | 161852788.35 | 2.1678E-13 |
| 43 | -295.1504 | 1E-12 | 0.01154479 | 0 | 0 | 0 | | 1E-12 | 0 | 154412286.99 | 2.0681E-13 |
| 44 | -295.0376 | 1E-12 | 0.012088 | 0 | 0 | 0 | | 1E-12 | 0 | 147473305.09 | 1.9752E-13 |
| 45 | -294.9248 | 1E-12 | 0.0126437 | 0 | 0 | 0 | | 1E-12 | 0 | 140991762.3 | 1.8884E-13 |
| 46 | -294.812 | 1E-12 | 0.01321189 | 0 | 0 | 0 | | 1E-12 | 0 | 134928316.94 | 1.8072E-13 |
| 47 | -294.6992 | 1E-12 | 0.01379256 | 0 | 0 | 0 | | 1E-12 | 0 | 129247767.61 | 1.7311E-13 |
| 48 | -294.5865 | 1E-12 | 0.01438572 | 0 | 0 | 0 | | 1E-12 | 0 | 123918541.08 | 1.6597E-13 |
| 49 | -294.4737 | 1E-12 | 0.01499137 | 0 | 0 | 0 | | 1E-12 | 0 | 118912252.66 | 1.5927E-13 |
| 50 | -294.3609 | 1E-12 | 0.01560951 | 0 | 0 | 0 | | 1E-12 | 0 | 114203327.46 | 1.5296E-13 |
| 51 | -294.2481 | 1E-12 | 0.01624013 | 0 | 0 | 0 | | 1E-12 | 0 | 109768673.07 | 1.4702E-13 |

**Figure 39** Page E Columns A through L. Page E is the page where the receiver output calculations are done. This figure only shows the time for 50 ns after the pulse left the laser. This page goes on for over 4000 ns, so you only see the very first of the calculations for the whole pulse. Column A is time in nanoseconds since the laser pulse left the laser. Column B is Depth in meters. Negative numbers indicate distance above the waters surface and positive numbers indicate depth below the surface. Column C is the Air/Water backscatter coefficient. Column D is the area in $m^2$ of the laser beam. Column E contains the fish backscatter information. Columns F and G are sums of the lidar attenuation coefficient and Diffuse attenuation coefficient. Column H is not used. Columns I and J are the sums of the water and fish reflection coefficients. Column K is the average power density of the laser beam. Column L is the normalized signal output.

| | | | | | | | |
|---|---|---|---|---|---|---|---|
| | | | | | | | |
| | | | | | | | |
| max PMT | | | | S/N = 1 at | 55.280159 | | |
| Voltage = | 2.81902078 | | | | meters | | |
| | | | | | | | |
| | | Log Amp | negative | positive | | | Signal to |
| | Vout PMT | Limited | LOG out | Log out | | Detector | Noise |
| | Rx signal | signal | voltage | Voltage | | shot noise | Ratio (S/N) |
| | | | | | | | |
| | 8.1191E-07 | 0.00015 | -0.0080114 | 0.008011 | 0 | 1.1728E-10 | 1E-20 |
| | 0.00060715 | 0.000607 | -0.0865305 | 0.086531 | 0 | 3.2848E-09 | 4.587825 |
| | 0.0017865 | 0.001788 | -0.1418892 | 0.141889 | 0 | 5.4895E-09 | 12.87401 |
| | 0.00268706 | 0.002687 | -0.1648597 | 0.16486 | 0 | 6.7457E-09 | 19.28174 |
| | 0.0003288 | 0.003029 | -0.176286 | 0.176286 | 0 | 7.3081E-09 | 23.88812 |
| | 0.00072005 | 0.00072 | -0.1820186 | 0.182019 | 0 | 7.9071E-09 | 26.89648 |
| | 0.00090898 | 0.000909 | -0.1850077 | 0.185008 | 0 | 8.1061E-09 | 28.05247 |
| | 0.00094304 | 0.000943 | -0.185480 | 0.185480 | 0 | 8.1718E-09 | 28.29921 |
| | 0.00086475 | 0.000865 | -0.1840901 | 0.18409 | 0 | 8.09E-09 | 27.7351 |
| | 0.0007073 | 0.000707 | -0.1821320 | 0.182132 | 0 | 7.9235E-09 | 26.80499 |
| | 0.00049802 | 0.000498 | -0.1789778 | 0.178978 | 0 | 7.6968E-09 | 25.10276 |
| | 0.00025773 | 0.000258 | -0.1751144 | 0.175114 | 0 | 7.4275E-09 | 23.07798 |
| | 0.00000213 | 0.000002 | -0.1706787 | 0.170679 | 0 | 7.1302E-09 | 21.5430 |
| | 0.00274276 | 0.002743 | -0.1657734 | 0.165773 | 0 | 6.8152E-09 | 19.68152 |
| | 0.00248780 | 0.002488 | -0.1604777 | 0.160478 | 0 | 6.4908E-09 | 17.85171 |
| | 0.00224300 | 0.002243 | -0.1548540 | 0.154854 | 0 | 6.1632E-09 | 16.09449 |
| | 0.00201201 | 0.002012 | -0.1489539 | 0.148954 | 0 | 5.8072E-09 | 14.40829 |
| | 0.00179699 | 0.001797 | -0.1428181 | 0.142818 | 0 | 5.5165E-09 | 12.89280 |
| | 0.00159902 | 0.001599 | -0.1364818 | 0.136482 | 0 | 5.2007E-09 | 11.47187 |
| | 0.0014184 | 0.001418 | -0.129975 | 0.129975 | 0 | 4.901E-09 | 10.17509 |
| | 0.00125480 | 0.001255 | -0.1230230 | 0.123023 | 0 | 4.6098E-09 | 9.001298 |
| | 0.00110780 | 0.001108 | -0.1165494 | 0.116549 | 0 | 4.301E-09 | 7.944838 |
| | 0.00097598 | 0.000976 | -0.1098737 | 0.109874 | 0 | 4.0652E-09 | 6.998889 |
| | 0.00085845 | 0.000858 | -0.1027144 | 0.102714 | 0 | 3.8128E-09 | 6.158081 |
| | 0.00075424 | 0.000754 | -0.0958885 | 0.095889 | 0 | 3.5739E-09 | 5.408048 |
| | 0.00066205 | 0.000662 | -0.0886117 | 0.088612 | 0 | 3.3484E-09 | 4.748084 |
| | 0.00058075 | 0.000581 | -0.0814989 | 0.081499 | 0 | 3.1361E-09 | 4.162784 |
| | 0.00050923 | 0.000509 | -0.0743843 | 0.074384 | 0 | 2.9368E-09 | 3.649097 |
| | 0.00044645 | 0.000446 | -0.0672214 | 0.067221 | 0 | 2.7496E-09 | 3.198750 |
| | 0.00009144 | 0.000091 | -0.0600807 | 0.060084 | 0 | 2.5747E-09 | 2.800900 |
| | 0.00004300 | 0.000043 | -0.0529641 | 0.052964 | 0 | 2.4113E-09 | 2.45858 |
| | 0.0000013 | 0.000001 | -0.0458755 | 0.045875 | 0 | 2.2589E-09 | 2.158909 |
| | 0.00026483 | 0.000265 | -0.0388006 | 0.038801 | 0 | 2.1169E-09 | 1.890895 |
| | 0.00023267 | 0.000233 | -0.0318419 | 0.031842 | 0 | 1.985E-09 | 1.664245 |
| | 0.00020482 | 0.000205 | -0.024922 | 0.024922 | 0 | 1.8624E-09 | 1.46437 |
| | 0.00018058 | 0.000181 | -0.0180801 | 0.018080 | 0 | 1.7487E-09 | 1.29005 |
| | 0.00015948 | 0.000159 | -0.0113073 | 0.011307 | 0 | 1.6434E-09 | 1.13889 |
| | 0.00014111 | 0.00015 | -0.0080114 | 0.008011 | -295.71429 | 1.5459E-09 | 1.007084 |
| | 0.00012513 | 0.00015 | -0.0080114 | 0.008011 | 0 | 1.4557E-09 | 0.89238 |
| | 0.00011122 | 0.00015 | -0.0080114 | 0.008011 | 0 | 1.3724E-09 | 0.792537 |
| | 9.9113E-05 | 0.00015 | -0.0080114 | 0.008011 | 0 | 1.2955E-09 | 0.705597 |
| | 8.858E-05 | 0.00015 | -0.0080114 | 0.008011 | 0 | 1.2248E-09 | 0.62985 |

**Figure 40** Page E Columns M through T. Column M is not used. Column N is the voltage out of the detector. Column O is the log Amp limited signal. The signal out of the log amp cannot be less than it's noise or greater than it's maximum voltage. Column P is the voltage out of the log amp. This is the polarity that the log amp produces in real life. Column Q is the inverted voltage out of the log amp and is given because it is sometimes easier to work with positive voltages. Column R checks for a signal to noise ratio of 1 and prints out the depth it occurs at. This data is used as a diagnostic in the model. Column S is the shot noise of the detector. Column T is the signal to noise ratio.

| | | | | | | | | |
|---|---|---|---|---|---|---|---|---|
| | | | | | | | | |
| | | | note: to get true zmax you must | | | | | |
| | | | subtract the water return.  To do | | | | | |
| | | | this make Bb zero. B:B15 | | | | | |
| | | | | | | | | |
| S/N is approx 3 at fish school | | | 1358 for Height=100m | | | | | |
| Fish school must be at 50m to 60m | | | 3132 for Height=300m | | | | | |
| S(52) peak return from school | | | Note: S(52),S(0) and S/N at S(0) all have to be changed | | | | | |
| 0.000247045248 | | | | | | | | |
| S(0) | S/N at S(0) | Zmax | | | | | | |
| 4.466248834578 | 32058.479 | 49.4172 | | If Zmax is a negative number | | | | |
| | | | | there wasn't enough return  from the fish | | | | |
| | | | | | | | | |
| | | | | | | | | |
| | | | | | | | | |
| | | | | 40.3074 for no water return | | | | |
| | | | | 49.4172 with water return | | | | |
| | | | | 300m | | | | |

**Figure 41** Page E, columns V through AD. This section calculates the $z_{max}$

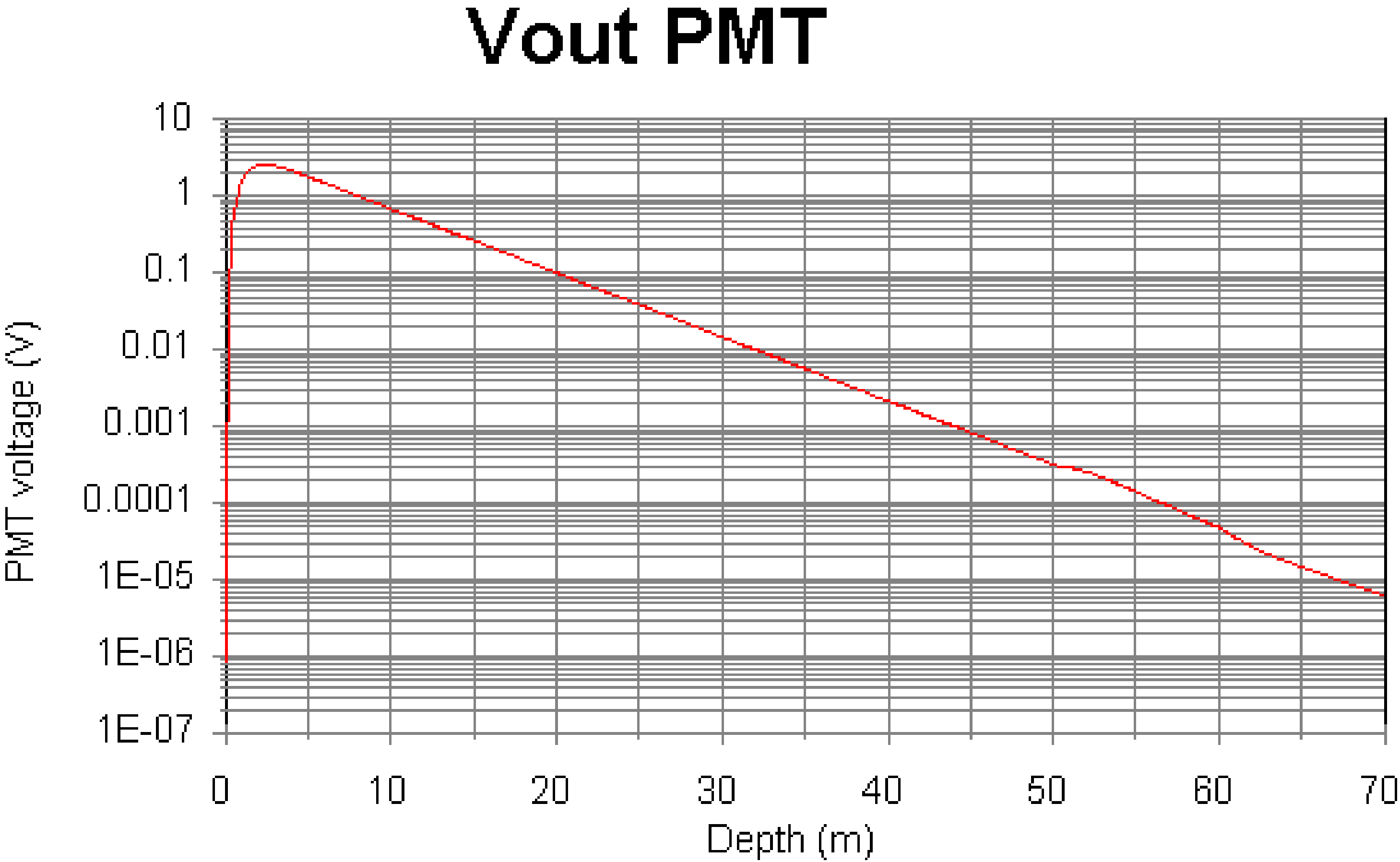


**Figure 42** Vout vs depth. This is one of the five graphs that are included in the model. Other graphs can be created in Quattro pro.

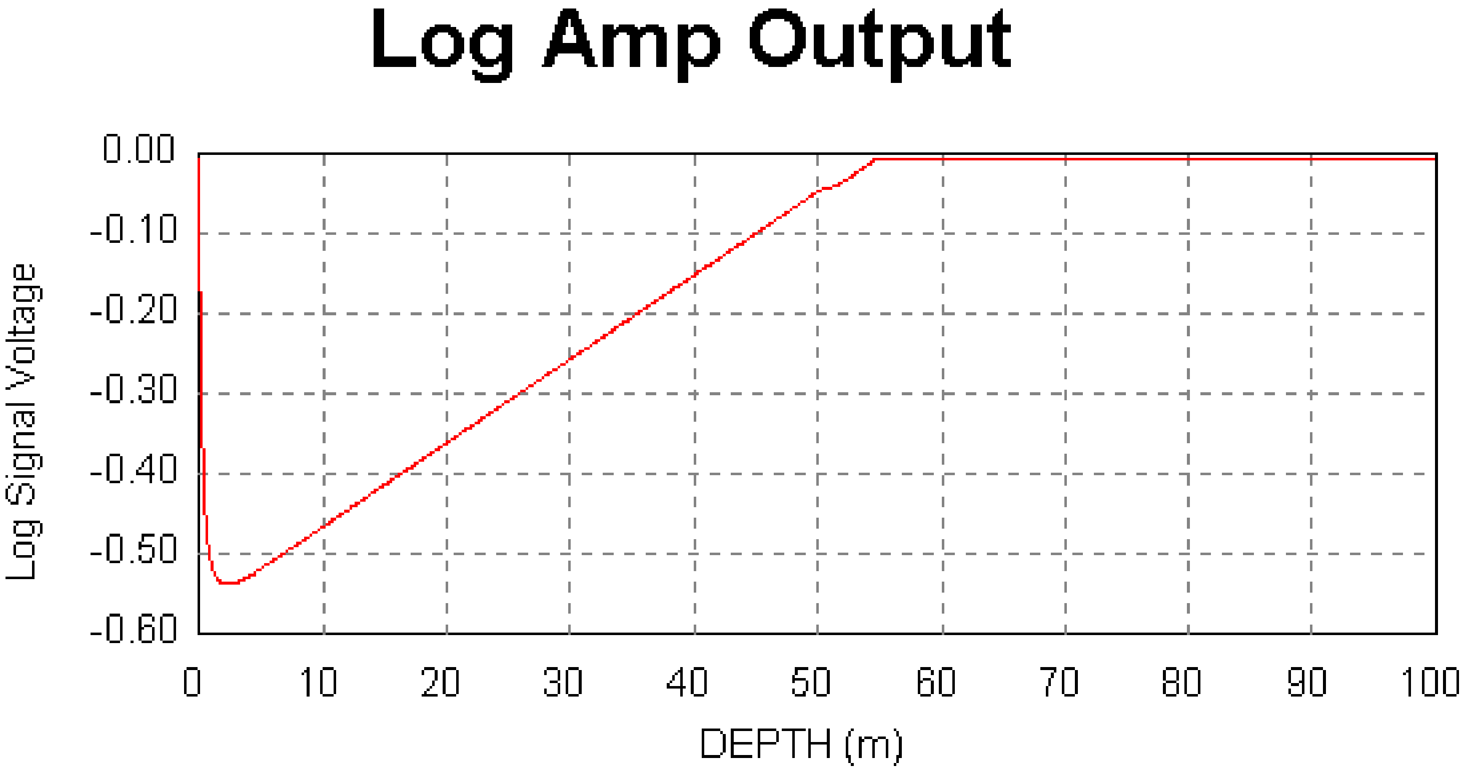


**Figure 43** Log amp output vs depth.

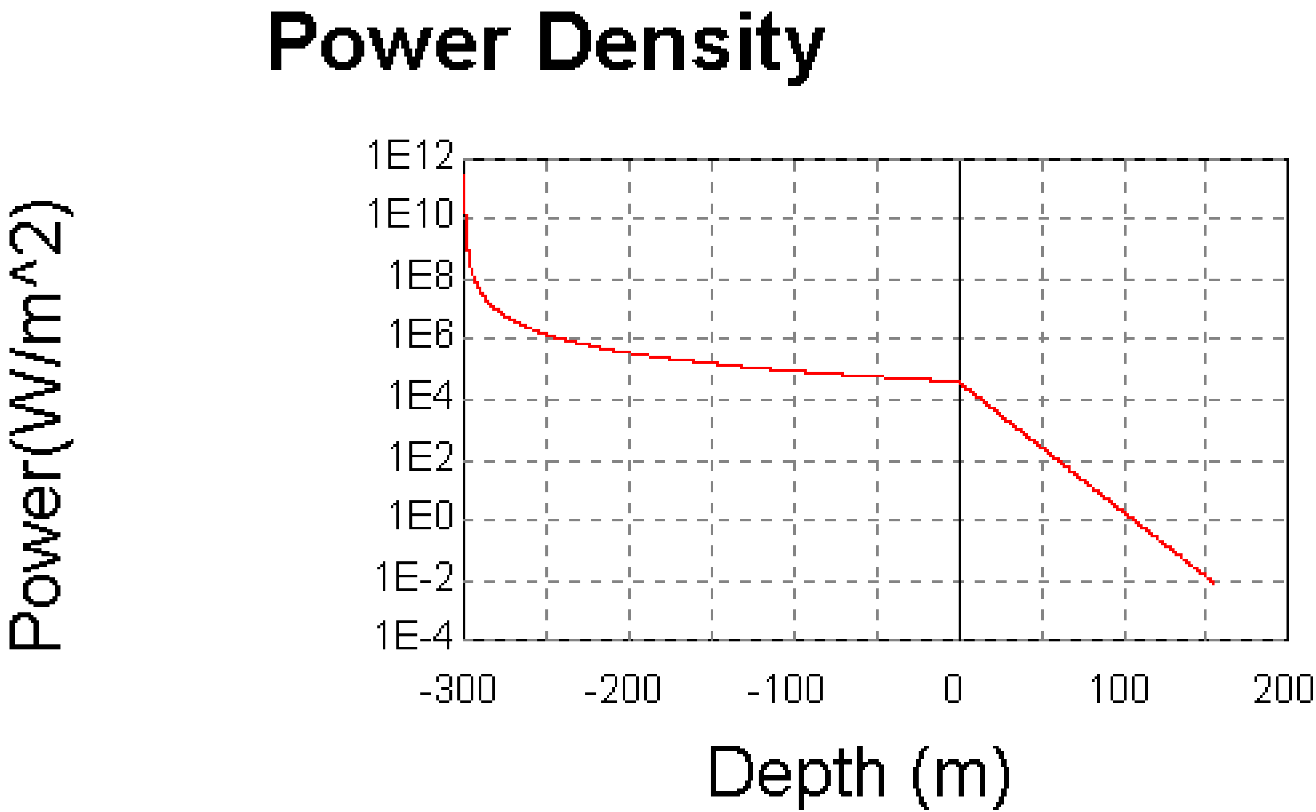


**Figure 44** Power density vs depth.

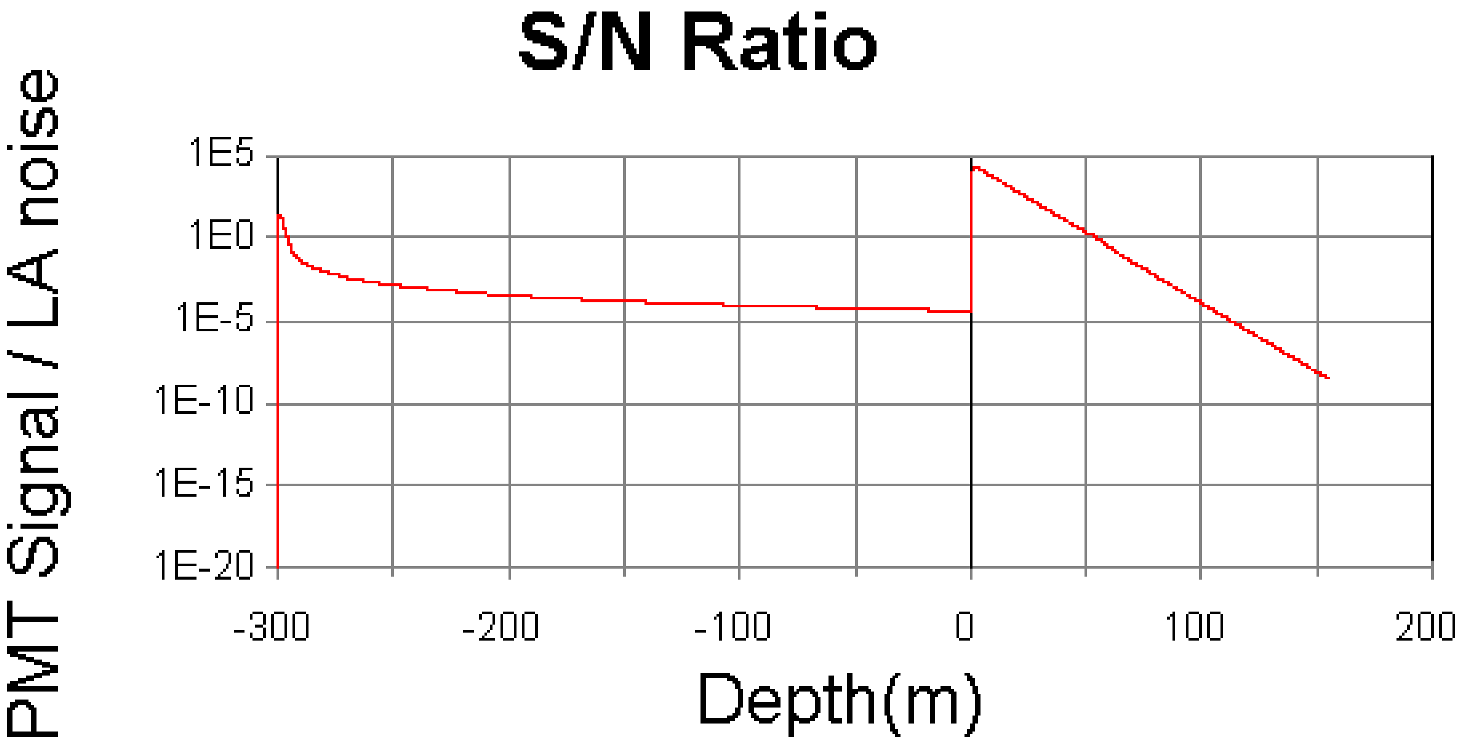


**Figure 45** S/N ratio vs depth.

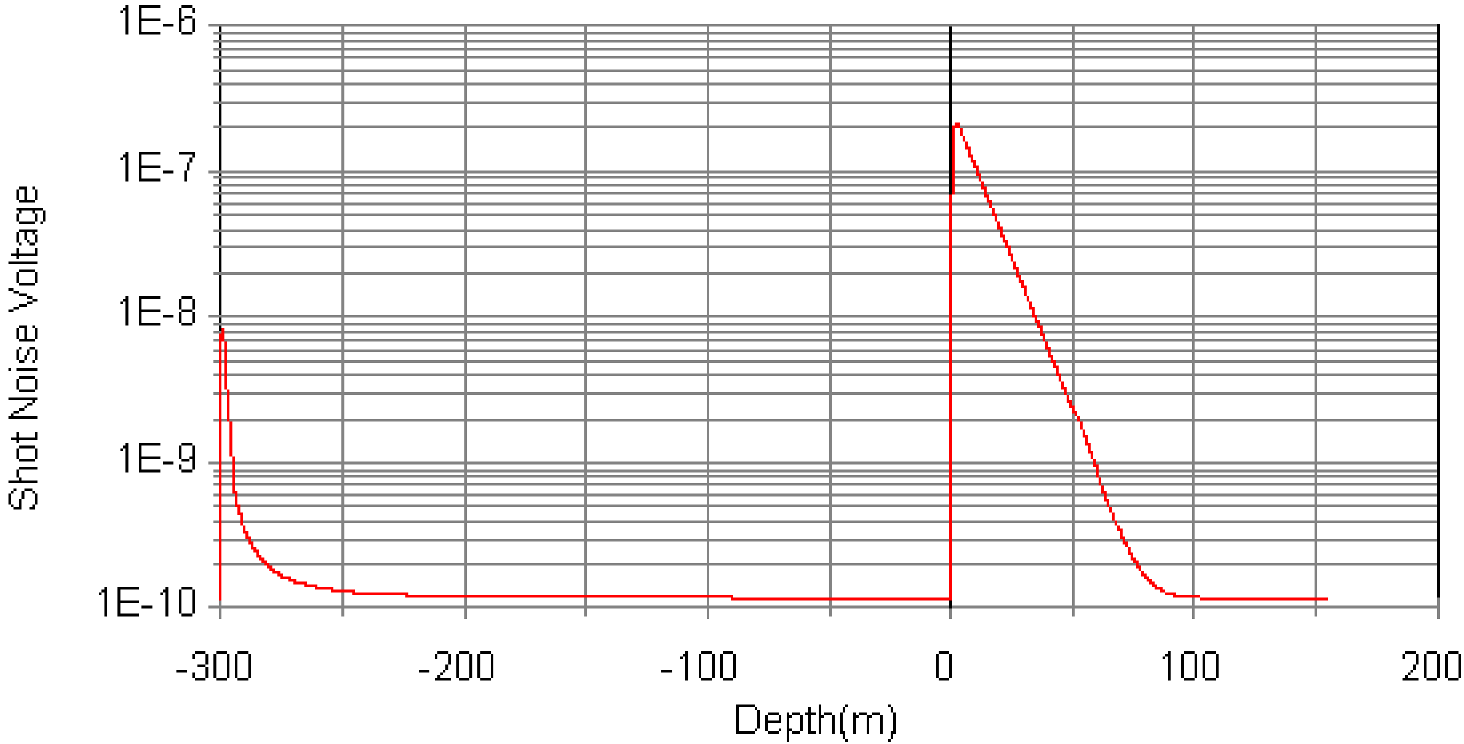


**Figure 46** Shot Noise vs depth.